

**SYNTHETIC CLAY FORMED BY EXTRUSION AND
SPHERONIZATION TECHNIQUES AND ITS USE
FOR LIQUID ADSORPTION**



**A Thesis Submitted in Partial Fulfillment of the Requirements for the
Degree of Doctor of Philosophy in Chemical Engineering
Suranaree University of Technology
Academic Year 2019**

ดินสังเคราะห์ที่ขึ้นรูปด้วยเทคนิคเอ็กทราซันและสเฟียโรไนเซชันและการใช้งาน
ในการดูดซับของเหลว

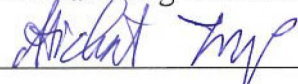


วิทยานิพนธ์นี้เป็นส่วนหนึ่งของการศึกษาตามหลักสูตรปริญญาวิศวกรรมศาสตรดุษฎีบัณฑิต
สาขาวิชาวิศวกรรมเคมี
มหาวิทยาลัยเทคโนโลยีสุรนารี
ปีการศึกษา 2562

**SYNTHETIC CLAY FORMED BY EXTRUSION AND
SPHERONIZATION TECHNIQUES AND ITS USE
FOR LIQUID ADSORPTION**

Suranaree University of Technology has approved this thesis submitted in partial fulfillment of the requirements for the Degree of Doctor of Philosophy.

Thesis Examining Committee



(Assoc. Prof. Dr. Atichat Wongkoblap)

Chairperson




(Asst. Prof. Dr. Panarat Rattanaphanee)

Member (Thesis Advisor)



(Prof. Dr. Chaiyot Tangsathitkulchai)

Member



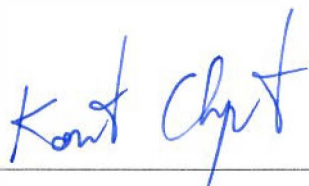
(Assoc. Prof. Dr. Sutham Srilomsak)

Member

SUPUNNEE J.

(Dr. Supunnee Junpirom)

Member



(Assoc. Prof. Flt. Lt. Dr. Kontorn Chamnirasart)

Vice Rector for Academic Affairs and
Internationalization



(Assoc. Prof. Dr. Pornsiri Jongkol)

Dean of Institute of Engineering

วิทยา จุลกลาง : ดินสังเคราะห์ที่ขึ้นรูปด้วยเทคนิคเอ็กทรูชันและสเฟียโรไนเซชันและการ
ใช้งานในการดูดซับของเหลว (SYNTHETIC CLAY FORMED BY EXTRUSION AND
SPHERONIZATION TECHNIQUES AND ITS USE FOR LIQUID ADSORPTION)
อาจารย์ที่ปรึกษา : ผู้ช่วยศาสตราจารย์ ดร.พนารัตน์ รัตนพานิ, 170 หน้า.

ในปัจจุบันการสังเคราะห์วัสดุชนิดใหม่ในระดับนาโนได้รับความนิยมกันอย่างแพร่หลาย
เนื่องจากเป็นวัสดุที่มีคุณสมบัติที่พิเศษ อย่างไรก็ตามการใช้งานวัสดุนาโน ไม่ว่าจะอยู่ในรูปของ
สารละลายนาโน หรือในรูปของผงแห้งขนาดนาโน หรือตลอดทั้งผงในระดับไมครอนก็ตาม
ยังไม่เหมาะสมที่จะนำไปใช้ในระดับอุตสาหกรรม การขึ้นรูปจากผงวัสดุสังเคราะห์เป็นโครงร่าง
ของวัสดุสังเคราะห์ที่สามารถใช้งานได้ในระดับอุตสาหกรรม จะสามารถดึงเอาความสามารถที่
พิเศษของวัสดุสังเคราะห์นั้นไปใช้งานได้ งานวิจัยนี้จึงศึกษาการขึ้นรูปของผงดินสังเคราะห์ให้อยู่
ในรูปของเม็ดกลมในระดับมิลลิเมตรเพื่อใช้งานในกระบวนการดูดซับของเหลวในเครื่องดูดซับ
แบบเบตนิ่ง ด้วยเทคนิคการขึ้นรูปแบบเอ็กทรูชันและสเฟียโรไนเซชัน ปัจจัยสำคัญในการขึ้นรูป
เม็ดกลมของผงดินสังเคราะห์ด้วยเทคนิคเอ็กทรูชันและสเฟียโรไนเซชัน ได้สำเร็จคือการตัดเม็ด
เอ็กซ์ทรูเดตและการให้ความร้อนกับผนังของเครื่องและสเฟียโรไนเซอร์ การขึ้นรูปด้วยวิธีการนี้
พื้นที่ผิวของเม็ดกลมที่ขึ้นรูปแล้วกับผงดินสังเคราะห์หลังจากผ่านกระบวนการเผาที่อุณหภูมิเท่ากัน
มีความใกล้เคียงกัน และเม็ดกลมที่เตรียมได้สามารถใช้ในการดูดซับสารได้เป็นอย่างดีในระบบการ
ดูดซับในสารอินทรีย์ สำหรับการดูดซับในระบบของสารอินทรีย์พบว่าเมื่อทำให้เม็ดที่ขึ้นรูปแล้ว
เสื่อมสภาพในระหว่างการดูดซับ

สาขาวิชาวิศวกรรมเคมี
ปีการศึกษา 2562

ลายมือชื่อนักศึกษา กฤษณา จุลกลาง
ลายมือชื่ออาจารย์ที่ปรึกษา Dr. Panart Rattanapani

WITTAYA JULKLANG : SYNTHETIC CLAY FORMED BY
EXTRUSION AND SPHERONIZATION TECHNIQUES AND ITS USE
FOR LIQUID ADSORPTION. THESIS ADVISOR : ASST. PROF.
PANARAT RATTANAPHANEE, Ph.D., 170 PP.

SYNTHETIC CLAY/POWDER FORMING/ LIQUID ADSORPTION

Synthesis of new materials in nanoscale has increased tremendously in recent years due to their superior properties. However, utilization liquid-based processing of nanoparticles and dry-phase of nanoparticles as well as intermediate powder are not suitable in industrial applications. Therefore, the knowledge of forming advanced synthetic powder into the technical body will allow extensive utilization of its superior function in the industrial application of synthetic material in industrial applications. This research study the shaping of synthetic clay intermediate powder into a millimeters size pellet of certain shapes for use in liquid fixed-bed adsorption by extrusion and spheronization technique. A key success in preparing spherical pellet of synthetic clay by extrusion and spheronization technique includes two critical steps, extrudate cutting and hot surface spheronization bowl. This forming technique is shown that the specific surface area of the calcinated pellets is equivalent to the calcination powder. The forming pellet is good in function when using in the liquid fixed-bed column for adsorption of organic adsorbate, but a malfunction in adsorption of the inorganic adsorbate.

School of Chemical Engineering

Academic Year 2019

Student's Signature Wittaya Julklang.

Advisor's Signature Panarat Rattanaphanee

ACKNOWLEDGEMENT

I am sincerely grateful to Assist. Prof. Dr. Panarat Ratanapanee, my thesis advisor, for her expert advice and never ending support throughout this research. Her direction, motivation, and patience contributed deeply to the completion of this thesis. Also, a special thanks to Assoc. Prof. Dr. Boris Golman for his consult and support during this thesis.

I would like to thank my thesis committee, Prof. Dr. Chaiyot Tangsathitkulchai, Assoc. Prof. Dr. Atichat Wongkoblaph, Assoc. Prof. Dr. Sutham Srilomsak and Dr. Supunnee Junpirom for their valuable time to serve on my committee and for their unconditional help and advice on the conduction of this thesis. I would also like to thank all of the lectures at the School of Chemical Engineering, Suranaree University of Technology, who led me to the world of Chemical Engineering. Special thanks to Mrs. Amporn Ladnongkhun for her skillful secretarial work and Mr. Saran Dokmaikun for his skillful technical work and assistance.

Nothing would be completed without showing my gratitude and love to those who brought me to this world, my beloved parents Jumnong and Songkla Julklang.

Finally, I would like to thank the National Research Council of Thailand for their funding of this research.

Wittaya Julklang

TABLE OF CONTENTS

	Page
ABSTRACT (THAI).....	I
ABSTRACT (ENGLISH).....	II
ACKNOWLEDGEMENTS.....	III
TABLE OF CONTENTS.....	IV
LIST OF TABLES.....	XI
LIST OF FIGURES.....	XIII
CHAPTER	
I INTRODUCTION	1
1.1 Background and significance of the study.....	1
1.2 Research objectives.....	4
1.3 Scope and limitation of the research.....	5
1.4. Thesis outline.....	6
1.5 References.....	7
II POWDER PREPARATION	10
2.1 Abstract.....	10
2.2 Introduction.....	10
2.3 Theory.....	12

TABLE OF CONTENTS (Continued)

	Page
2.4 Experimental	18
2.4.1 Clay powder preparation.....	18
2.4.2 Characterization of dry powder	23
2.5 Result and discussion	25
2.5.1 Oven-dried powder.....	25
2.5.2 Spray-dried powder	27
2.6 Conclusion.....	33
2.7 References	33
III PASTE PREPARATION	35
3.1 Abstract	35
3.2 Introduction	35
3.3 Theory	37
3.3.1 Paste definitions	37
3.3.2 Clay consistency	37
3.3.3 Methods for measurement of clay plasticity	40
3.4 Experimental.....	50
3.4.1 Paste and extrudate characterization.....	50

TABLE OF CONTENTS (Continued)

	Page
3.4.2 Experimental design and statistical analysis for paste preparation.....	50
3.4.3 Paste preparation	52
3.4.4 Cone penetration test.....	52
3.4.5 Ram extrusion and paste rheology	53
3.4.6 Paste kneading	54
3.5 Result and discussions	55
3.5.1 Cone penetration depth	55
3.5.2 Statistical analysis.....	56
3.5.2 Effect of process variables on cone penetration depth	58
3.5.3 Ram extrusion and paste rheology	62
3.5.4 Paste kneading	65
3.6 Conclusion	67
3.7 References.....	68
IV PELLETS PREPARATION BY EXTRUSION AND SPHERONIZATION	71
4.1 Abstract	71

TABLE OF CONTENTS (Continued)

	Page
4.2 Introduction	71
4.3 Theory	75
4.3.1. Equipment	76
4.3.2. Mechanics and mechanisms	82
4.4 Experimental	89
4.4.1 Extrudability and extrudate preparation	89
4.4.2 Extrudate cutting	90
4.4.3 Spheronization	90
4.4.4 Materials characterizations	91
4.4.5 Pellet drying and calcination	93
4.4.6 Experimental design and statistical analysis for spheronization	94
4.4.7 Pellets strength Improvement study	95
4.4.7.1 Additives utilization	95
4.4.7.2 Calcination temperature	96
4.4.7.3 Source of intermediate powder.....	96
4.5 Result and discussions	96

TABLE OF CONTENTS (Continued)

	Page
4.5.1 Paste flow analysis	96
4.5.2 Spheronization.....	104
4.5.3 Response surface design of spheronization process	107
4.5.4 Pellet morphology	107
4.5.5 Statistical analysis	109
4.5.6 Pellet specific surface area	117
4.5.7 Pellet improvement study	119
4.6 Conclusion.....	124
4.7 References	125
V PELLET UTILIZATION IN FIXED-BED LIQUID ADSORPTION.....	132
5.1 Abstract.....	132
5.2 Introduction.....	132
5.3 Theory	135
5.3.1 Characteristic of fixed-bed adsorption	135
5.3.2 Analysis of the breakthrough curve.....	139
5.3.2.1 Breakthrough curve modeling.....	139

TABLE OF CONTENTS (Continued)

	Page
5.3.2.1.1 Thomas Model.....	139
5.3.2.1.2 Bohart and Adams model	140
5.3.2.1.3 Yoon-Nelson model	140
5.3.3 Statistical test	141
5.4 Experimental	142
5.4.1 Pellets preparation.....	142
5.4.2 Adsorbate solution preparation.....	142
5.4.3 Adsorbent preparation.....	143
5.4.4 Fixed bed adsorption.....	144
5.4.5 Material characterization	145
5.5 Result and discussion.....	146
5.5.1 Adsorbent characterization	146
5.5.2 Synthetic clay pellets as adsorbent in fixed-bed adsorption of methyl orange	147
5.6 Conclusion	158
5.7 References.....	159

TABLE OF CONTENTS (Continued)

	Page
VI CONCLUSIONS AND RECOMMENDATIONS.....	163
6.1 Conclusion	163
6.2 Recommendation for future work.....	166
APPENDIX LIST OF PUBLICATIONS	168
BIOGRAPHY.....	170



LIST OF TABLES

Table	Page
2.1 Common methods for preparation of ceramic powder (Rahaman and Rahaman, 2006).....	11
2.2 Size reduction methods for different target sizes (Rhodes, 2008).	12
2.3 Median droplet size of different atomizers.....	14
2.4 Conditions for spray drying of syntheic slurry.....	27
2.5 Operating conditions for spray drying with additives.....	29
2.6 Effect of spray drying parameters on mean particle size of the received powder.....	28
3.1 Levels for independent variables.....	51
3.2 Experimental conditions of paste preparation generated by R software with cone penetration depth as the response variable.	51
3.3 Response on cone penetration depth.	56
3.4 Correlation coefficients from the quadratic regression analysis.	57
3.5 ANOVA analysis of quadratic regression.	57
3.6 Percentage of paste moisture before and after kneading process.....	66
4.1 Die geometry used in the extrudability analysis.....	90
4.2 Middle value of spheronization parameter for Box-Benhken method.	95
4.3 Apparent density, true density, and porosity of dried extrudate.....	103
4.4 Experimental design for spheronization and the process response data.....	107

LIST OF TABLES (Continued)

Table	Page
4.5 Statistical analysis of pellet shape	110
4.6 Statistical analysis of pellet crushing strength	110
4.7 Crushing strength of spheronized pellets	120
5.1 Adsorption parameter obtained from Adams–Bohart, Thomas, and Yoon–Nelson models for methyl orange adsorption in aqueous solution.....	151
5.2 Adsorption parameter from Adams–Bohart, Thomas, and Yoon–Nelson models for adsorption of methyl orange in non-aqueous solution.....	156

LIST OF FIGURES

Figure	Page
2.1 Schematic outline of spray drying systems: (a) open cycle and (b) closed-cycle (www.niro.com)	15
2.2 Schematic outline of spray drying systems: (a) two-fluid nozzle, (b) pressure nozzle and (c) rotary atomizer (www.niro.com).....	16
2.3 Schematic outline of spray-air contact modes: (a) co-current, (b) counter-current and (c) mixed flow chamber (www.spray-dryer.com)	18
2.4 Filter candle	19
2.5 Wet cake after second step filtration.....	19
2.6 Drying oven	20
2.7 Ultra centrifugal mill.....	21
2.8 Set up of the spray dryer	22
2.9 Homogenizer.....	23
2.10 Laser particle size analyzer.....	24
2.11 Belsorp mini ii apparatus	24
2.12 Scanning electron microscopy	25
2.13 Particle size distribution of synthetic clay sample.....	26
2.14 SEM image of oven-dried powder	27
2.15 Spray-dried powder obtained from SD1 experiment	28

LIST OF FIGURES (Continued)

Figure	Page
2.16 SEM image of spray-dried powder with (a) PVA1wt% with (b) PEG 1wt%	30
2.17 Spray-dried powder obtained from integrated spray drying- wet ball milling integrated process.....	31
2.18 Particle size distribution of spray-dried powder produced in SD6-SD10 experiment	32
3.1 Processing consistency states of mixture between dry powder with a wetting liquid or binder solution: $DPS < 1$ refer to granular stage, $DPS = 1$ refer to plastic stage and $DPS > 1$ refer to slurry stage.	38
3.2 More open particle packing due to transition from the (a) plastic body to (b) paste, with constant $DPS = 1$	40
3.3 Rolling method by (a) hand rolling and (b) rolling device	41
3.4 Pfefferkorn apparatus (Andrade et al., 2011).....	43
3.5 Torque rheometer (Andrade et al., 2011).....	44
3.6 Torque rheometer test (Sanchez et al., 1998)	45
3.7 Compression test of clay (Flores et al., 2010)	46
3.8 Stress-deformation compression curve (Ribeiro et al., 2005).....	47
3.9 Cone penetration apparatus.....	48
3.10 Experimental setup for a cone penetration test.	53

LIST OF FIGURES (Continued)

Figure	Page
3.11 Capillary rheometer (GÖTTFERT, RG20).....	54
3.12 Paste kneading equipment.....	55
3.13 Response surface plots of cone penetration depth; (a) effects of powder load and liquid to powder ratio, (b) effects of mixing time and liquid to powder ratio, (c) effects of mixing time and powder load.....	60
3.14 Percentage of moisture loss of fresh paste preparation.....	61
3.15 Paste resistance force during ram extrusion experiment; (a) experiment. 1, 6, 7, 12 and 14, and (b) experiment. 2-5, 8-11, 13 and 15.	63
3.16 Fresh paste after preparation; (a) semi-solid paste, (b) paste with plasticity.....	64
3.17 Extrudate moisture content during ram extrusion.....	65
3.18 Paste appearance after kneading	66
3.19 Extrusion profile of paste after kneading.....	67
4.1 The feed mechanism of the extrusion process (Wilson and Rough, 2007).....	78
4.2 Several extruder types used in extrusion spheronization process (Parikh, 2016)	79
4.3 Schematic of spheronizer (www.arcon-foodpharma.cz).	80

LIST OF FIGURES (Continued)

Figure	Page
4.4 Friction patterns: (a) a cross-hatched pattern and (b) a radial pattern (Parikh, 2016).....	81
4.5 An example of (a) good spheres produced (b) dumbbells shape (Parikh, 2016).	82
4.6 Terms used in the Benbow-Bridgwater analysis of ram extrusion.....	83
4.7 Ram extruder configurations.....	84
4.8 Surface fracture of extrudates (Rough and Wilson, 2005)	85
4.9 Ram extrusion profile with and without liquid migration (Benbow and Bridgwater, 1993a).....	87
4.10 Effect of wall slip on extrusion profile (Zhang et al., 2017).....	88
4.11 Models for evolution of extrudate pellets in spheronization (Bryan et al., 2015a).....	89
4.12 Design and construction of the spheronizer used in this thesis	91
4.13 Crushing strength experimental setup.....	92
4.14 Illustration of pellet's first crack during crushing strength test.....	93
4.15 TGA-DSC analysis of synthetic clay powder.....	94
4.16 Extrusion pressure profile for extrusion with die L/D ratio = 8 and different velocities: (a) V=0.5 mm/s, (b) V=0.7 mm/s, (c) V=1.0 mm/s, (d) V=1.2 mm/s, (e) V=1.5 mm/s, (f) V=5.0 mm/s, (g) V=10.0 mm/s, (h) V=20.0 mm/s.....	98
4.17 Wall slip effect on ram extrusion at high velocity	99

LIST OF FIGURES (Continued)

Figure	Page
4.18 Wall slip effect at different die geometry at (a) $L/D = 4$ and at (b) $L/D = 2$	100
4.19 Extrusion pressure profiles used for analysis extrudate porosity.....	102
4.20 Moisture content of green extrudate during drying at ambient temperature	103
4.21 Spheronized granules from the spheronization screening experiment	105
4.22 Spherical synthetic clay pellets obtained by extrusion and heated-wall.....	106
4.23 Shapes of pellets with different circularity (a) spheronized pellets with the highest circularity (b) spheronized pellets with the lowest circularity and (c) cut extrudates before being spheronized.....	108
4.24 Pellet size distribution after extrusion and spheronization	109
4.25 Crushing strength test with two-plane compression technique.....	111
4.26 Sensitivity of paste extrusion force during extrusion using the pastes with the same composition but prepared in different batches	112
4.27 Response surface plot of the effect of spheronization parameters.....	114

LIST OF FIGURES (Continued)

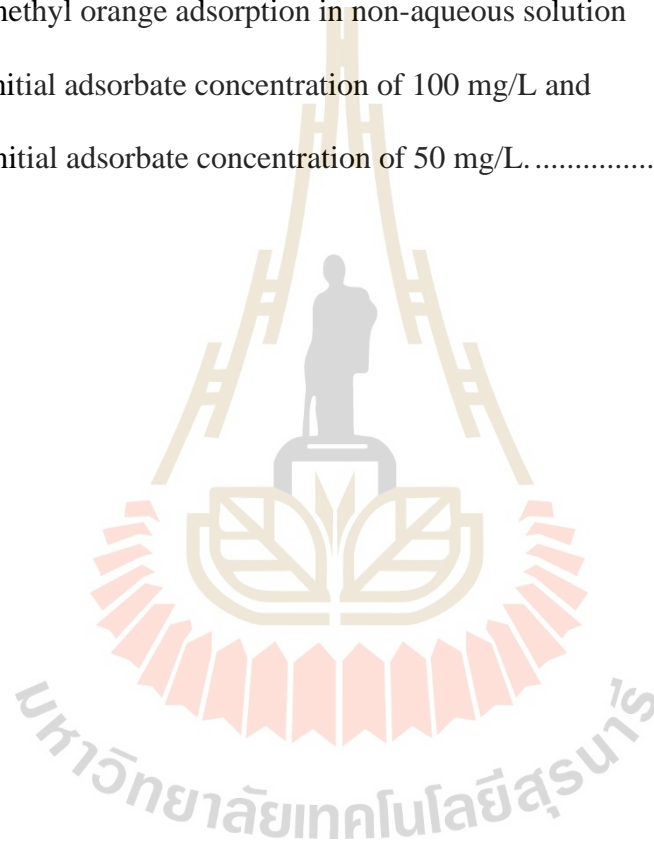
Figure	Page
4.28	Effect of spheronization parameter on pellet crushing strength and circularity 116
4.29	Effect of spheronization parameters on the specific surface area of the pellet 118
4.30	Extrusion force resistance of variation of paste composition 120
4.31	SEM image of spheronized pellets: (a) base case, (b) PVA 3% wt, (c) boehmite 5% wt, (d) calcination at 600°C, (e) spray-dried powder. 123
5.1	Concentration profile of adsorbate in fluid moving along the fixed-bed adsorption column. Mass transfer zone is depicted by the black diagonal line in each column 136
5.2	Schematic representation of saturated, mass transfer or adsorption, and unsaturated or fresh adsorbent zones in fixed-bed adsorption column (Chowdhury et al., 2014) 137
5.3	Breakthrough curve characteristics in the fixed-bed adsorption column (Chowdhury et al., 2014) 138
5.4	Molecular structure of methyl orange 143
5.5	Muffle furnace (Carbolite) 144
5.6	Fixed-bed adsorption process diagram adsorption 145
5.7	UV-VIS spectrometer (UV-Vis spectrophotometer, T80) 146
5.8	Size distribution of adsorbent's mesopores by BJH method 147

LIST OF FIGURES (Continued)

Figure	Page
5.9 Breakthrough curve of methyl orange adsorption in aqueous environment using synthetic clay adsorbent under ambient condition.....	148
5.10 Flow channeling in adsorption under aqueous environment of methyl orange at its initial concentration of 100 mg/L	149
5.11 Spent clay adsorbent from adsorption of methyl orange in aqueous solution.....	150
5.12 Experimental and simulated breakthrough curve from Adams–Bohart, Thomas, and Yoon–Nelson models for methyl orange adsorption in aqueous solution with (a) initial adsorbate concentration of 300 mg/L and (b) initial adsorbate concentration of 200 mg/L.....	152
5.13 Breakthrough curve for methyl orange adsorption using clay adsorbent in non-aqueous solution under ambient condition.....	154
5.14 Synthetic clay adsorbent in non-aqueous adsorption of methyl orange: (a) in the fixed-bed column, (b) after adsorption.	155

LIST OF FIGURES (Continued)

Figure	Page
5.15 Experimental and simulated breakthrough curve from Adams–Bohart, Thomas, and Yoon–Nelson models for methyl orange adsorption in non-aqueous solution (a) initial adsorbate concentration of 100 mg/L and (b) initial adsorbate concentration of 50 mg/L.....	157



CHAPTER I

INTRODUCTION

1.1 Background and significance of the study

Clay refers to a naturally occurring material, including primarily of fine-grained minerals. Superior clay properties, plasticity form, can be obtained when it mixed with an appropriate amount of water and solidity harden form when dried or fired (Moore et al., 1996). Due to the varieties of clay structure and its properties, such as high specific surface area, ion exchange capacity or hydration property, clay minerals are widely used in ceramics and building materials, pharmaceuticals, paper industries, and oil drilling industry, as well as foundry molds, catalyst, adsorbents, ion exchangers, and decolorizing agents (Konta, 1995; Murray, 2000; Ding et al., 2001; Carretero, 2002; Babel and Kurniawan, 2003; Bergaya and Lagaly, 2006; Brigatti et al., 2006; Choy et al., 2007).

Clay minerals are commonly phyllosilicates or layered silicates. It consists of two basic sheets: a sheet of corner-linked tetrahedra and a sheet of edge-sharing octahedra. The tetrahedrons sheet shares oxygen or hydroxyls to form layers. The space between layers is called interlayers, which include adsorbate cation and water. Clay normally contains both Brönsted and Lewis acid sites, the Brönsted sites mainly correlated with the interlamellar region and the Lewis sites mostly related to edge sites. Clay acidity is strongly influenced by the quantity of water in the interlayer. The acidic properties of clay can be changed by thermal treatment. Clay with strong Bronsted acidity can be produced by heating it to around 100°C to remove its water content.

Continuing supply of heat to the temperature around 200-300°C, where the water is completely removed, will result in the collapse of the clay interlayer. Bronsted acidity will be decreased at this state, while Lewis acidity will increase. Further heating of the clay to around 450°C will lead to the elimination of hydroxy group resulting in an entirely amorphous solid with retaining Lewis acidity. (Kaur and Kishore, 2012).

Even though clays naturally occur in enormous amount, natural clay composite has several drawbacks, such as the existence of impurities, random composition and morphology. These drawbacks limit utilization of clay minerals (Bergaya and Lagaly, 2006). Therefore, to control purity, composition, and morphology of clay, the synthesis method was adopted. Synthetic clay is usually prepared by coprecipitation method, which allows controlling the amounts of isomorphous substitutions in the synthetic clay. The technical knowledge from the synthesis will provided informative data for the establishment of new applications. Consequently, clay material with well-designed composition and structure can provide properties as advanced functional materials, which are now of great significance, industrially and academically (Zhang et al., 2009; Zhou, 2010).

Synthetic clay is mainly produced in a slurry phase. Liquid-base processing of nanoparticles requires a special technique for their separation from the final mixture (Chae et al., 2015). The dry-phase processing of nanoparticles has not been utilized at an industrial scale because these particles agglomerate uncontrollably. Furthermore, nanoparticles are known to have a noxious effect on humans and the ecosystem due to their unique combination of size, shape, and chemical composition (Schuster and Lomello, 2013). One of the alternative ways for safe handling of nanoparticles is to consolidate them into larger micron-sized agglomerates (Lindeløv and Wahlberg, 2011).

Utilization of an agglomerated powder has numerous advantages such as easy to handle agglomerates in dry phase and their good flowability, uniform particle size, and shape (Pal et al., 2014; Yousaf et al., 2015). Nevertheless, an industrial-scale application of agglomerated powder as adsorbents and catalysts is limited due to the relatively small size of the agglomerates.

Powder forming (granulation, palletization, or powder shaping) is a key to overcome the limitation of in utilizing powder properties on the industrial scale. Powder forming methods can be divided into two categories: wet methods, which use some form of liquid to incorporate the primary particles, and dry methods, which do not utilize any liquid. Dry granulation forming is normally used the mechanical compression or compaction to prepare the pellets, while the wet forming uses granulation liquid (binder/solvent) to prepare pellets via adhesively formation of wet mass by adhesion. The dry granulation is suitable for powders that are sensitive to moisture and heat. Among these two categories, the wet granulation forming is the most widespread granulation technique used even when it involves multiple unit processes such as wet massing, drying, and screening. These unit processes can be are complicated, time-consuming, expensive and may require large space and multiple types of equipment.

Industrial liquid adsorption is typically operated with the packed-bed column/reactor, in which the adsorbent/catalyst pellets are held stationary in a large packed bed and liquid are fed through this large column (or bed) of adsorbent/catalyst pellets. Several pellet shapes can be prepared by forming method depending on target applications. Cylindrical, rings, trilobed extrudate are used for application that requires low packing pressure drop and high surface-to-volume ratio, while the spherical pellet

is normally used in the application that required high bed packing density as the heterogeneous catalysis (Holt, 2004). More advantage of using spherical pellets in the packed bed/column is the uniform bed packing. When pellets of non-spherical particles are “loaded” or “packed” in these beds, they are known that the non-uniform bed packing appears in columns. The bed void fraction depends on the way the particles have been dumped into the column in the first place. This causes variations in flow pattern of the fluid, local packing density variations, wetting patterns, as well as the variations in regional fluid flow and transport and reaction of chemical species, resulting in variations in the exit conversion of chemical species. In some applications, these effects are small relative to the average performance of the reactor. Nevertheless, in several applications of great contemporary interest, these small variations in packing distribution can pose dramatic impact on overall reactor performance.

The aforementioned issues lead to the focus of this thesis, which is the coupling of techniques for synthesis of synthetic clay with powder forming method to produce spherical synthetic clay pellets. It is believed that this approach could be one of the ways to unlock superior utilization function of advanced material for industrial applications.

1.2 Research objectives

This thesis is intended to study formation of synthetic clay powder into a millimeter-sized pellets with desired shape, strength, and pellet properties using by extrusion and spheronization technique. The specific objectives are as follows.

1.2.1 To develop a simple method for preparation and characterization of synthetic clay paste for extrusion process.

1.2.2 To study rheology of the synthetic clay paste in ram extrusion at different die geometry and extrusion conditions.

1.2.3 To specify the extrusion condition for preparation of extrudate sample used in the spheronization step.

1.2.4 To evaluate the effect of spheronization parameters on pellet quality.

1.2.5 To observe and evaluate performance synthetic clay pellet as an adsorbent in fixed-bed liquid adsorption.

1.3 Scope and limitation of the research

1.3.1 Oven- and spray-drying techniques are adopted for preparation of synthetic clay powder from synthetic clay slurry.

1.3.1.1 The oven-dried powder is the leading powder used in the shaping process.

1.3.1.2 The spray-dried powder is prepared at the same mean particle size with oven-dried powder and is used to compare powder shape on pellet strength with its oven-dried counterpart.

1.3.2 Clay paste is prepared at plastic limit point.

1.3.3 Extrusion is carried out by a ram extrusion technique.

1.3.4 Extruded specimen are prepared without liquid migration and surface fracture.

1.3.5 A spheronizer is designed and constructed with one friction disk pattern to use in a spheronization step.

1.3.6 Spheronization parameters: extrudate loading, spheronization time and spheronization speed are utilized to produce a spherical form of synthetic clay pellet.

1.3.7 Pellet heat treatment is performed in two steps: drying at ambient temperature and calcination.

1.3.8 Characteristic of liquid adsorption on the prepared pellets is evaluated by breakthrough curve analysis in fixed-bed adsorption.

1.3.9 Improvement of mechanical properties of the prepared pellet is carried out by adding polyvinyl alcohol (PVA), alumina boehmite, powder shape, and calcination temperature.

1.4. Thesis outline

Powder shaping by extrusion and spheronization technique is a multi-step process. Therefore, this thesis is divided into 6 chapters. **Chapter I** gives a background and the significance of this thesis work to emphasize the major application of synthetic clay and importance of gaining knowledge about clay powder shaping. In **Chapter II**, procedure to prepare clay powder is described. Two different techniques for solvent elimination are used in this thesis: oven drying and spray drying. The oven-dried powder is used to study in the paste preparation step, which aims to evaluate whether the paste formulation is suitable to be used in the extrusion step. To analyze paste formulation, the cone penetration method equipped with rheology analysis is used for the first time in this work to characterize the paste before it is subjected to the extrusion process. This technique is simple but useful and flexible to use different powder types. Information on paste formulation is then used in **Chapter III**, where paste preparation at the plastic limit is performed for all extrusion step. Paste rheology during extrusion

is analyzed to determine suitable extrusion parameters that can be operated without liquid migration and surface fracture. Liquid migration in the paste is the dominant parameter dominant in the extrusion step. The high paste compaction of the longest die geometry and the extrusion velocity at the first steady-state compaction profile, which give extrudate without liquid migration and surface fracture, are selected to prepare extrudate samples for spheronization step. In **Chapter IV**, the spheronization parameters are used to transform the of extrudates into spherical pellets. Liquid migration is also the main control parameter in this step. Different hypothesis to improve pellet mechanical strength is proposed including addition of PVA into the paste to hinder liquid migration effect, utilizing alumina boehmite as a binder, using spherical shape powder from spray-drying method to decrease pore space in pellet, as well as calcination at a different temperature to increase contact point of clay layer sheet in the pellet. Pellets with desired shape and properties are used for liquid adsorption. to remove methyl orange from to adsorb liquid adsorbate in the next chapter. In **Chapter V**, the derived pellets are used as adsorbent in liquid adsorption for dye removal. The breakthrough curve and the breakthrough parameters are obtained for adsorption of the aqueous and non-aqueous solution of the dye. The conclusion and recommendation of this thesis work are summarized in **Chapter VI**.

1.5 Reference

Babel, S., and Kurniawan, T. A. 2003. Low-cost adsorbents for heavy metals uptake from contaminated water: a review. **Journal of Hazardous Materials** 97 (1–3):219-243.

- Bergaya, F., and Lagaly, G. 2006. Chapter 1 General Introduction: Clays, Clay Minerals, and Clay Science. **In Developments in Clay Science**, edited by Benny K. G. Theng Faïza Bergaya and Lagaly Gerhard: Elsevier, 1-18.
- Brigatti, M. F., Galan, E., and Theng, B. K. G. 2006. Chapter 2 Structures and Mineralogy of Clay Minerals. **In Developments in Clay Science**, 1:19-86.
- Carretero, M. I. 2002. Clay minerals and their beneficial effects upon human health. A review. **Applied Clay Science** 21 (3-4):155-163.
- Chae, S.-R., Noeiaghæi, T., Jang, H.-C., Sahebi, S., Jassby, D., Shon, H.-K., Park, P.-K., Kim, J.-O., and Park, J.-S. 2015. Effects of natural organic matter on separation of the hydroxylated fullerene nanoparticles by cross-flow ultrafiltration membranes from water. **Separation and Purification Technology** 140:61-68.
- Choy, J., Choi, S., Oh, J., and Park, T. 2007. Clay minerals and layered double hydroxides for novel biological applications. **Applied Clay Science** 36 (1-3):122-132.
- Ding, Z., Klopogge, J. T., Frost, R. L., Lu, G. Q., and Zhu, H. Y. 2001. Porous clays and pillared clays-based catalysts. Part 2: A review of the catalytic and molecular sieve applications. **Journal of Porous Materials** 8 (4):273-293.
- Holt, E. M. 2004. The properties and forming of catalysts and absorbents by granulation. **Powder Technology** 140 (3):194-202.
- Kaur, N., and Kishore, D. 2012. Montmorillonite: an efficient, heterogeneous and green catalyst for organic synthesis. **Journal of Chemical and Pharmaceutical Research** 4 (2):991-1015.
- Konta, J. 1995. Clay and man: clay raw materials in the service of man. **Applied Clay Science** 10 (4):275-335.

- Lindeløv, J. S., and Wahlberg, M. 2011. Consolidating nanoparticles in micron-sized granules using spray drying. **Journal of Physics: Conference Series** 304:012083.
- Moore, D. M., Guggenheim, S., and Martin, R. T. 1996. Definition of clay and clay mineral; joint report of AIPEA nomenclature and CMS nomenclature committees; comment and reply. **Clays and Clay Minerals** 44 (5):710-715.
- Murray, H. H. 2000. Traditional and new applications for kaolin, smectite, and palygorskite: a general overview. **Applied Clay Science** 17 (5–6):207-221.
- Pal, S., Laera, A. M., Licciulli, A., Catalano, M., and Taurino, A. 2014. Biphasic TiO₂ microspheres with enhanced photocatalytic activity. **Industrial & Engineering Chemistry Research** 53 (19):7931-7938.
- Schuster, F., and Lomello, F. 2013. From safe nanomanufacturing to nanosafe-by-design processes. **Journal of Physics: Conference Series** 429:012054.
- Yousaf, A. M., Kim, D. W., Kim, J. K., Kim, J. O., Yong, C. S., and Choi, H.-G. 2015. Novel fenofibrate-loaded gelatin microcapsules with enhanced solubility and excellent flowability: Preparation and physicochemical characterization. **Powder Technology** 275:257-262.
- Zhang, Z. G., Rapaud, O., Allain, N., Mercs, D., Brien, V., Dong, C., and Coddet, C. 2009. Influence of Ni content on the structure and properties of Cr–Ni–N coatings prepared by direct current magnetron sputtering. **Thin Solid Films** 517 (11):3304-3309.
- Zhou, C. H. 2010. Emerging trends and challenges in synthetic clay-based materials and layered double hydroxides. **Applied Clay Science** 48 (1-2):1-4.

CHAPTER II

POWDER PREPARATION

2.1 Abstract

The two different drying methods were used to prepare clay powder from synthetic slurry: oven-drying and spray-drying method. The oven-dried powder was in flake shape with wide particle size distribution, while its spray-dried counterpart was rather spherical and came with narrower particle size distribution. Clay powder prepared by spray-drying method also possessed higher specific surface area than that obtained by oven drying. However, the spray-drying method was a more complex method and consumed more energy than the oven-drying method. In this work, the oven-drying method was the main method for preparation of clay powder to be used in pellet forming to prepare powder for the pellet preparation step. Effect of powder preparation techniques on characteristic of pellet forming and the final pellet properties are investigated and compared between process with oven-dried and spray-dried powder.

2.2 Introduction

Methods for powder preparation can be classified into two main categories: mechanical and chemical methods. Mechanical methods, usually done by size reduction or milling, are usually used to preparation powders from naturally occurring raw materials. The chemical methods are generally used to prepare advanced powders from synthetic materials. Mechanical milling may be required in chemical method to

breakdown powder agglomerates and acquire desired physical properties of the powder such as average particle size, powder density, and particle size distribution. Table 2.1 provides a summary common methods used in preparation of ceramic powder.

Table 2.1 Common methods for preparation of ceramic powder (Rahaman and Rahaman, 2006)

Powder preparation method	Advantages	Disadvantages
Mechanical		
Comminution	Inexpensive, wide applicability	Limited purity, limited homogeneity, large particle size
Mechanochemical synthesis	Fine particle size, good for nonoxides, low temperature route	Limited purity, limited homogeneity
Chemical		
Solid-state reaction Decomposition, reaction between solids	Simple apparatus, inexpensive	Agglomerated powder, limited homogeneity for multicomponent powders
Liquid solutions Precipitation or coprecipitation; solvent vaporization (spray drying, spray pyrolysis, freeze drying); gel routes (sol-gel, Pechini, citrate gel, glycine nitrate)	High purity, small particle size, composition control, chemical homogeneity	Expensive, poor for nonoxides, powder agglomeration commonly a problem
Nonaqueous liquid reaction	High purity, small particle size	Limited to nonoxides
Vapor-phase reaction Gas-solid reaction	Commonly inexpensive for large particle size	Commonly low purity, expensive for fine powders
Gas-liquid reaction	High purity, small particle size	Expensive, limited applicability
Reaction between gases	High purity, small particle size, inexpensive for oxides	Expensive for nonoxides, agglomeration commonly a problem

This chapter describes methods to prepare intermediate powder, which will be used in pellet formation step, with different morphologies and shapes from the same synthetic slurry. The chemical method is used to prepare nano-sized clay primary particles. The mechanical method is used to reduce size of agglomerated nanoparticles after solvent evaporation by oven-drying, where flaky-shaped powder is received. Spray drying technique is applied to prepare a microspheres from the clay nanoparticles.

2.3 Theory

Solvent evaporation and powder size reduction by mechanical milling were conventional methods for the preparation of intermediate powder. Most of the liquid solvent in the slurry is removed by filtration, and oven drying is normally employed for complete solvent evaporation before the dried solid is finally received. Based on the required powder size, the dried powder will be reduced into target size by size-reduction methods. The powder size-reduction methods corresponding to the target size are shown in Table 2.2. However, this preparation method gives an irregular shape of powder leading to low powder flowability.

Table 2.2 Size reduction methods for different target sizes (Rhodes, 2008).

Size range of product	Methods
1–0.1m	Coarse crushing
0.1m	Crushing
1 cm	Fine crushing, coarse grinding
1mm	Intermediate grinding, milling
100 μ m	Fine grinding
10 μ m	Ultrafine grinding

The more advanced method used to prepare intermediate powder is spray drying, which is one of the well-known techniques that have been widely applied for the production of microspheres from nano-sized particles. This technique makes it possible to control the size distributions as well as the shape of spray-dried agglomerates (Nandiyanto and Okuyama, 2011). Spray drying is a complex process involving heat and mass transfer between droplets and drying medium (Julklang and Golman, 2013). The size, shape, and morphology of spray-dried agglomerates depend to a great extent on the process parameters (Wang et al., 2009). This technique also demonstrates superior ability than the conventional drying method in enhancement of ability to enhance the specific surface area of particles (Urruchurto et al., 2013; Sarawade et al., 2011; Chen et al., 2015).

Spray-drying system consists of feed preparation unit, atomizer, drying medium heater and distributor, drying chamber, and the system for powder recovery and exhaust drying medium cleaning. It can be operated in both open-cycle and closed-cycle mode, as illustrated in Figure 2.1 (Masters, 1979). Typically, the industrial spray dryers use open-cycle mode for drying of water-based feeds. Air for drying is drawn from the atmosphere and the exhaust air is discharged to the atmosphere. The product agglomerates are recovered in a cyclone, and the dust is removed from the exhaust air using combinations of bag filters, electrostatic precipitators and scrubbers. Direct and indirect heating are applied for heating the drying gas. Closed cycle spray dryers are utilized for evaporation of flammable solvents and drying of toxic or oxygen-sensitive products in order to recover the evaporated solvent and to avoid atmospheric pollution. An inert gas such as nitrogen is usually used in such a system. The closed-cycle systems

are equipped with the indirect heaters of drying medium and condenser for solvent vapor condensation in addition to the cyclone, bag filter, and wet scrubbers.

Spray-drying process normally consists of four stages: atomization, spray-air contact, drying and agglomerate formation, and separation of product agglomerate separation from the drying air. In the first stage, the liquid feed is atomized into a spray of droplets. There are three basic designs of atomizers classified by the source of energy used in the droplet formation process: centrifugal energy in the rotating wheel or disc atomizers, kinetic energy in the pneumatic nozzle, and pressure energy in pressure nozzle atomizers. Atomizers are selected according to the desired droplet sizes and throughput, as summarized in Table 2.3.

Table 2.3 Median droplet size of different atomizers

Atomization device	Median droplet size (μm)
Rotary atomizer(wheel)	10 - 200
Pressure nozzle	30 - 350
Pneumatic nozzle (two/three-fluid)	5 - 100

The rotary atomizer is illustrated in Figure 2.2 (c). The liquid feed enters the center, accelerates across the vanes forming a thin film of liquid that is ejected at the wheel rotating speed and rapidly disintegrates into droplets forming a wide jet with an umbrella shape (Masters, 1979). The droplet size distribution depends on the speed and the geometry of the rotary atomizer, and on the flow rate and physical properties of the liquid.

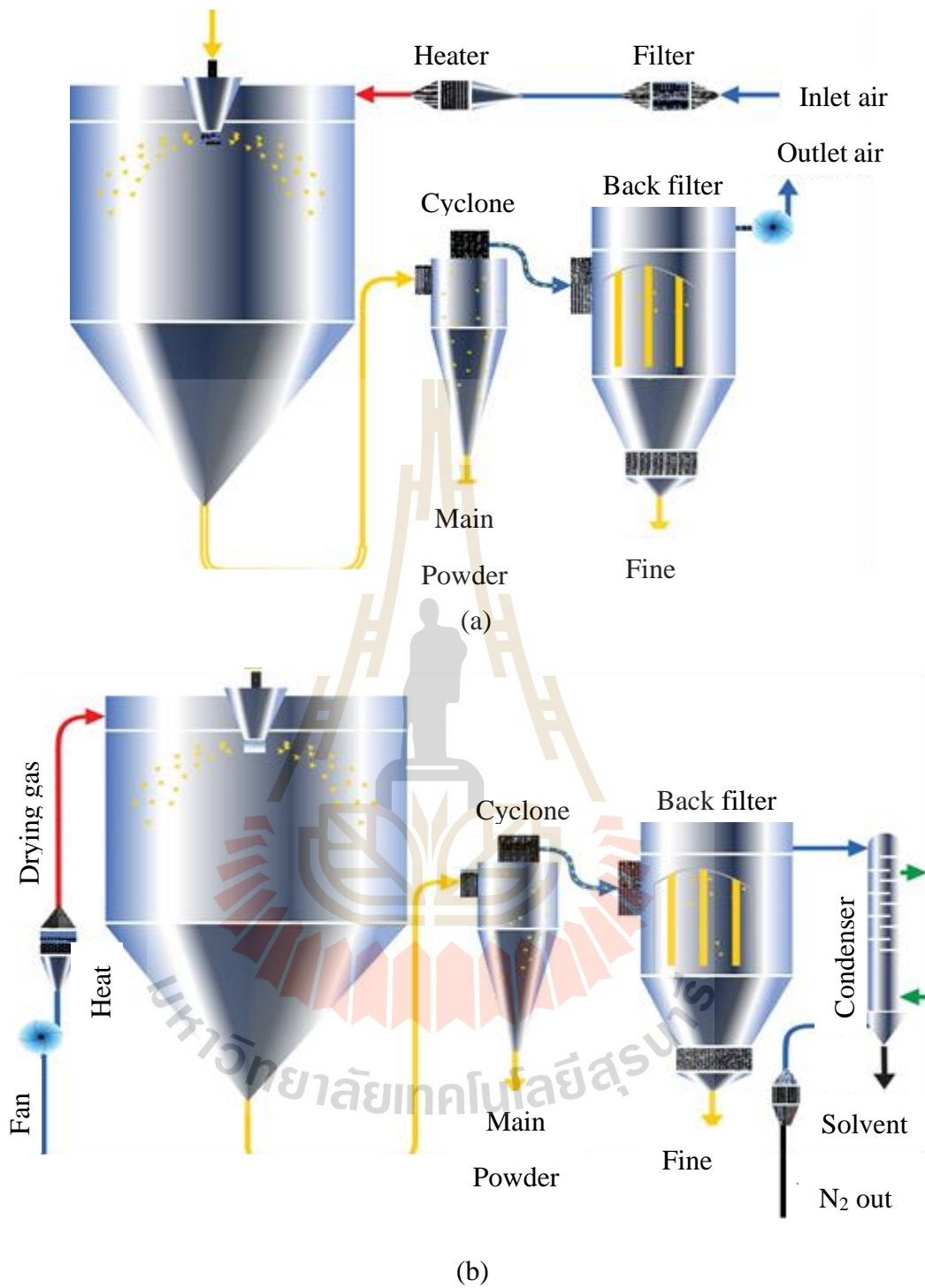


Figure 2.1 Schematic outline of spray drying systems: open-cycle (a) and closed-cycle

(b). (www.niro.com)

With two-fluid nozzles, it is possible to maintain the same droplet size distribution for different liquid flow rates by adjusting the compressed air flow rate. The main disadvantages of this kind of atomizer are the high cost of compressed air and the relatively low liquid throughput.

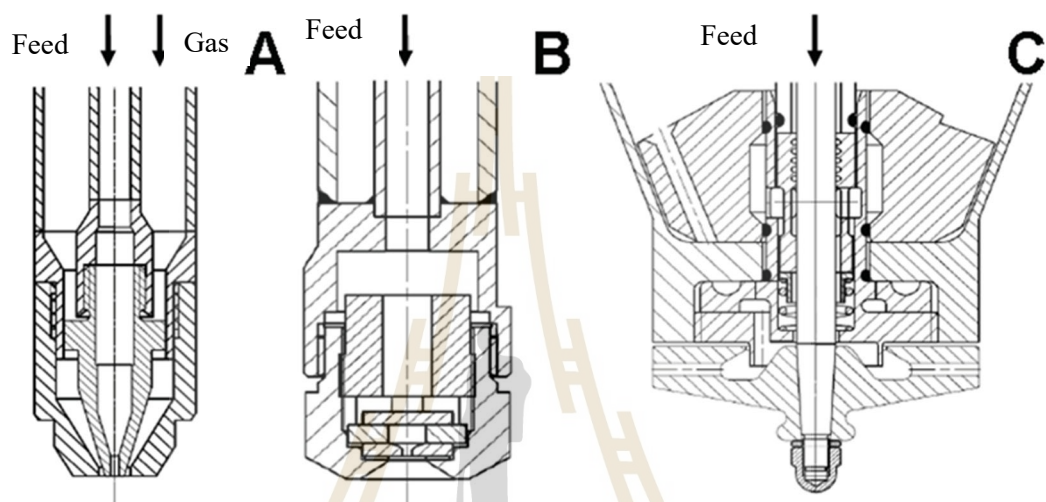


Figure 2.2 Schematic outline of spray drying systems: (a) two-fluid nozzle, (b) pressure nozzle and (c) rotary atomizer (www.niro.com)

The second process stage of spray drying involves the contact of spray droplets and drying air. The mode of contact between spray droplets and drying air controls the rate of evaporation, the final moisture content, the droplet residence time, and even the product quality.

In a co-current flow, the feed is sprayed in the same direction as the flow of the heated drying medium in the drying chamber, as shown in Figure 2.3 (a). The droplets of high moisture content contact with the hot drying medium resulting in optimal solvent evaporation for spray drying of heat-sensitive materials (Masters, 1979; Huang et al., 2003) such as enzymes, peptides and proteins.

In a counter-current flow design, the atomized feed and drying medium move in the opposite direction through the drying chamber, as illustrated in Figure 2.3 (b). The agglomerates, which are almost dried contact with hot air yielding in a product with low moisture content and consequently of good flowability. This contact mode is suitable for the drying of non-heat-sensitive products (Masters, 1979).

Spray dryer designs that combine co-current and counter-current flow modes are classified as mixed flow spray dryers, as shown in Figure 2.3 (c). The coarse free-flowing spray dried agglomerates can be produced in such systems using the drying chambers of relatively small dimensions. In mixed flow systems, partially dried particles contact with hot drying medium near the distributor.

The third process stage of spray drying is the drying combined with particle formation. Solvent in the droplets start to evaporate immediately after contact between spray droplets and the drying air. Initially, the evaporation occurs at the droplet surface and drying proceeds at a constant rate until the dry layer starts to form at the droplet surface. Then, the drying rate decreases as the evaporation interface move inside the droplet.

The fourth, and final, process step of spray drying includes the product separation from the drying air and the exhaust gas cleaning before discharge using the particle collection systems, i.e. cyclone, filter bag, scrubber, etc.

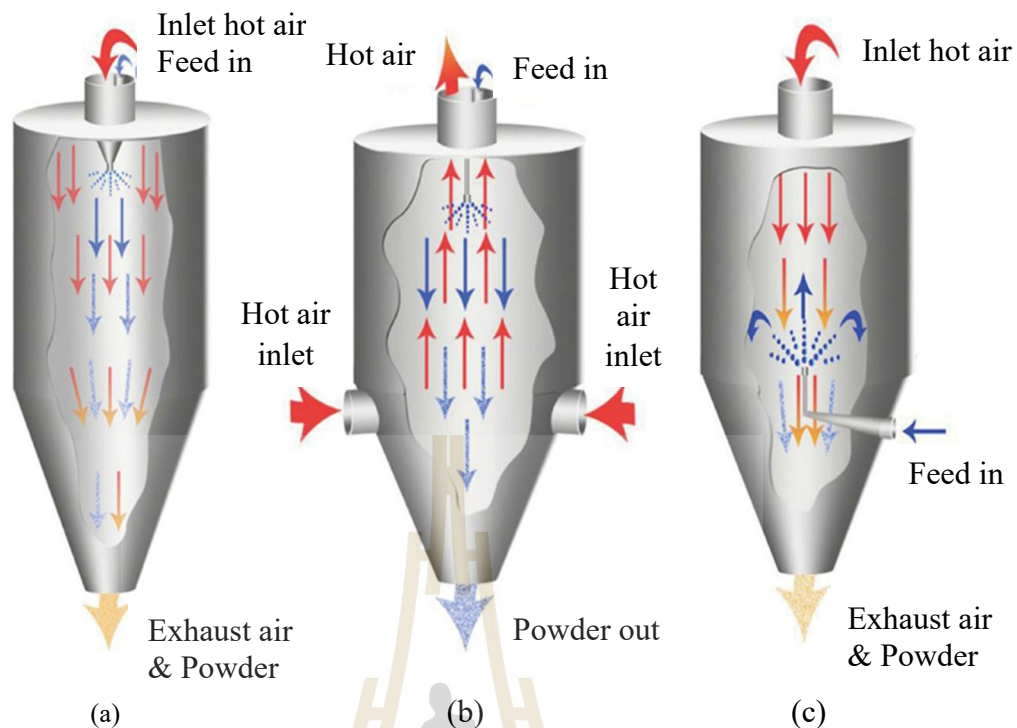


Figure 2.3 Schematic outline of spray-air contact modes: (a) co-current, (b) counter-current and (c) mixed flow chamber (www.spray-dryer.com)

2.4 Experimental

2.4.1 Clay powder preparation

2.4.1.1 Oven drying method

The synthetic clay slurry of initial solid concentration at 20%wt was concentrated in two filtration steps. The liquid was firstly removed from the slurry by filtration through a filter candle as illustrated in Figure 2.4 with a screen size of 5 microns. Then, the concentrated slurry was again filtrated through a 0.25 microns filtration paper. The wet powder collected after this double filtration is called a wet cake, as shown in Figure 2.5.



Figure 2.4 Filter candle



Figure 2.5 Wet cake after double filtration

The double-filtered wet cake was then dried in the drying oven at 110°C for 24 h. After that, the dried powder was milled by using the Ultra Centrifugal Mill (Ultra Centrifugal Mill, ZM 200) as shown in Figure 2.6 and Figure 2.7, respectively.

The rotation speed was kept constant at 10,000 rpm, and the milling screen was fixed at 80 μm . The milled prepared by the oven drying method was marked as OD-powder.



Figure 2.6 Drying oven



Figure 2.7 Ultra Centrifugal Mill

2.4.1.2 Spray drying method

The spray drying experiments were carried out in a laboratory-scale spray dryer (Mini Spray Dryer B-290, Buchi), as shown in Figure 2.8. The slurry was fed to the nozzle via a peristaltic pump at a specified feed flow rate. The slurry introduced in a two-fluid nozzle (1.4 mm in diameter) was sprayed by means of a flow of compressed air, which flow rate was controlled with a needle valve and measured with a rotameter. Droplets were dried in contact with air heated to the specified temperature using an electrical heater. The spray dryer was operated in a suction mode. An aspirator was used to draw air through the chamber. The flow rate of the drying gas was controlled by setting an aspirator ratio, which indicates the percent of flow. In the present experiment, the aspirator ratio was kept constant at 100%. The solid microspheres formed in the drying chamber were separated from the exhaust gas

in a cyclone and collected in a product collection vessel. The agglomerate collected in the spray dryer was marked as SD-powder. The spray drying parameters: drying gas temperature, spraying gas flowrate, slurry feed rate and slurry concentration were adjusted in order to achieve the powder mean particle size closed to that prepared by oven-drying method. The objective for this protocol was to compare effect of both preparation methods on the powder morphology and pellet strength.



Figure 2.8 Set up of the spray dryer.

Initial experimental conditions for spray drying process to prepare larger-sized dried powder were designed based on our experience with the spray drying clay material (Julklang et al., 2017). The synthesis clay slurry as received was diluted in the water at designed concentration and homogenized by homogenizer (Electrolux, model: ESTM54175) as illustrated in Figure 2.9 at the highest speed of 12000 rpm for 5 minutes.



Figure 2.9 Homogenizer

2.4.2 Characterization of dry powder

The particle size of the dried powder was analyzed by a laser particle size analyzer (Horiba partica, LA-950V2) as illustrated in Figure 2.10 using the dry method. The nitrogen adsorption-desorption isotherms were measured at 77K with a BelSorp mini II apparatus (Bel Japan) as illustrated in Figure 2.11. Before analysis, samples were degassed overnight at 110°C under vacuum. The specific surface area of spray-dried agglomerates was determined by the Brunauer-Emmett-Teller (BET) method. The morphology of powder was characterized by a scanning electron microscopy (SEM, Neo-Scope, JEOL) as shown in Figure 2.12.



Figure 2.10 Laser particle size analyzer



Figure 2.11 BelSorp mini II apparatus



Figure 2.12 Scanning electron microscopy

2.5 Result and discussions

2.5.1 Oven-dried powder

The size distribution of synthetic clay particles after milling is shown in Figure 2.13. The size distribution was bimodal, with the main peak located at $8.26 \mu\text{m}$ and a small peak at $124.6 \mu\text{m}$. Mean diameter of the milled powder was $14.05 \mu\text{m}$. The particles larger than the mill screen size of $80 \mu\text{m}$ were obtained during measurements of particle sizes in the dry phase. The particles were supplied to the measuring cell using a vibrating powder feeder. The fine clay particles readily absorb water vapor from the atmosphere. The water vapor then condenses and forms a liquid film on the outer particle surface. Vibration and displacement of particles in the feeder induce particle collisions and formation of particle agglomerates with water film acting as a binder. The specific surface area and total pore volume of particles were $72.87 \text{ m}^2/\text{g}$ and $0.4636 \text{ cm}^3/\text{g}$,

respectively. The morphology of oven-dried powder is shown in Figure 2.14. The SEM image illustrates flake shape of the milling powder with the wide size distribution as expected.

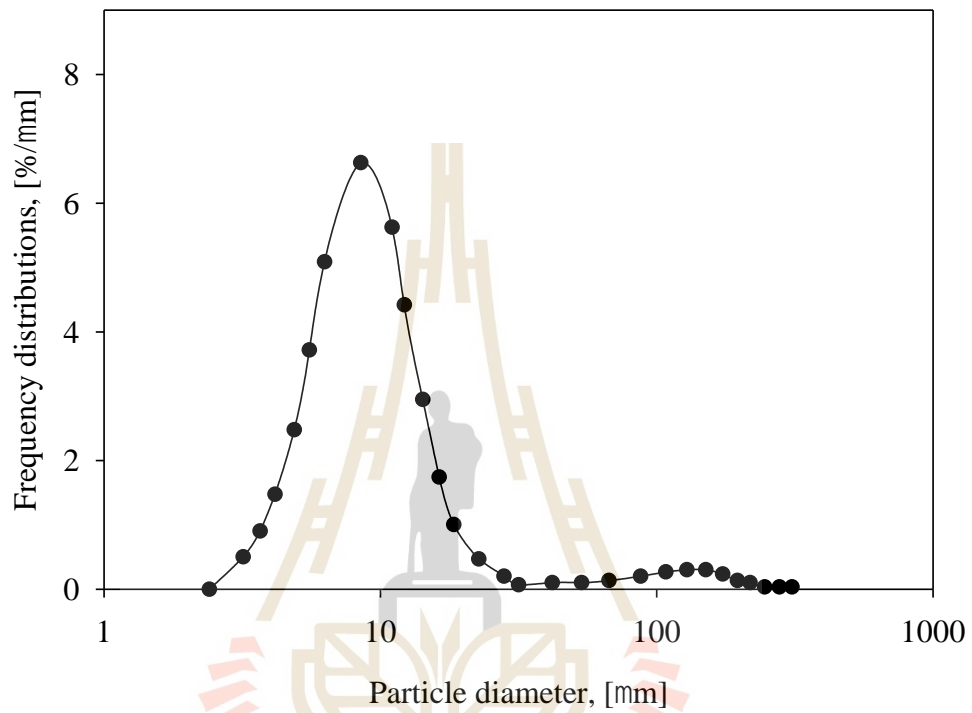


Figure 2.13 Particle size distribution of synthetic clay sample.

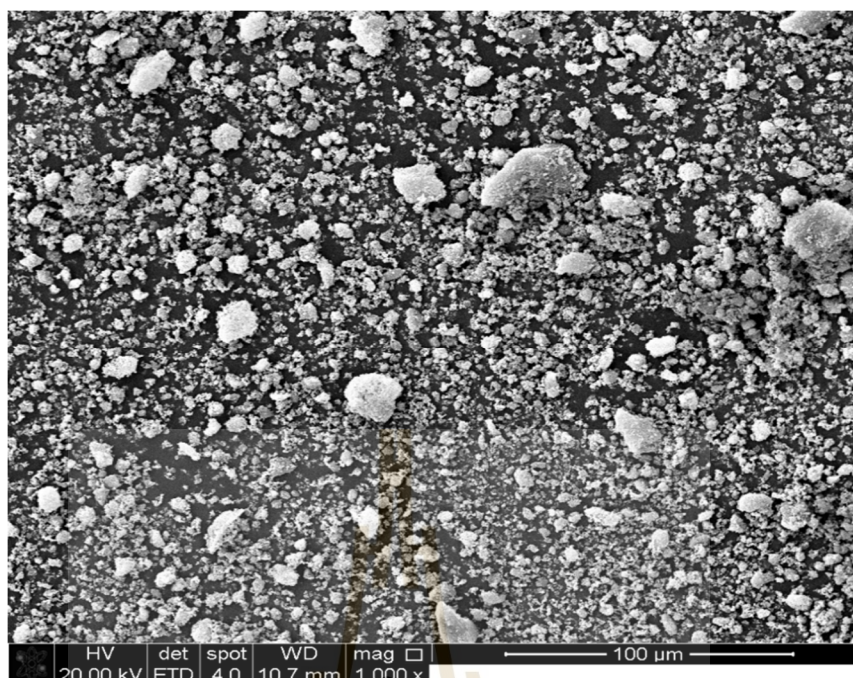


Figure 2.14 SEM image of oven-dried powder

2.5.2 Spray-dried powder

The first set of experimental conditions for the spray drying are illustrated in Table 2.4. Due to the swelling of synthetic clay in water, the maximum slurry concentration that can be prepared was only at 10wt%. The slurry with concentration higher than 10%wt was also difficult to be pumped through the spray drying nozzle.

Table 2.4 Conditions for spray drying of synthetic slurry.

Code	Drying air temperature (°C)	Spray air flow rate (L/h)	Slurry concentration (wt%)	Slurry feed rate (ml/min)	Aspirator ratio (%)
SD1	150	473	10	30	100
SD2	170	473	10	30	100
SD3	190	473	10	30	100

The mean particle size of the spray-dried powder obtained from SD1, SD2 and SD3 experiment were 20.4, 20.3, and 21.4 microns, respectively. However, all the spray-dried powder obtained from these experiments was not as expectably spherical.

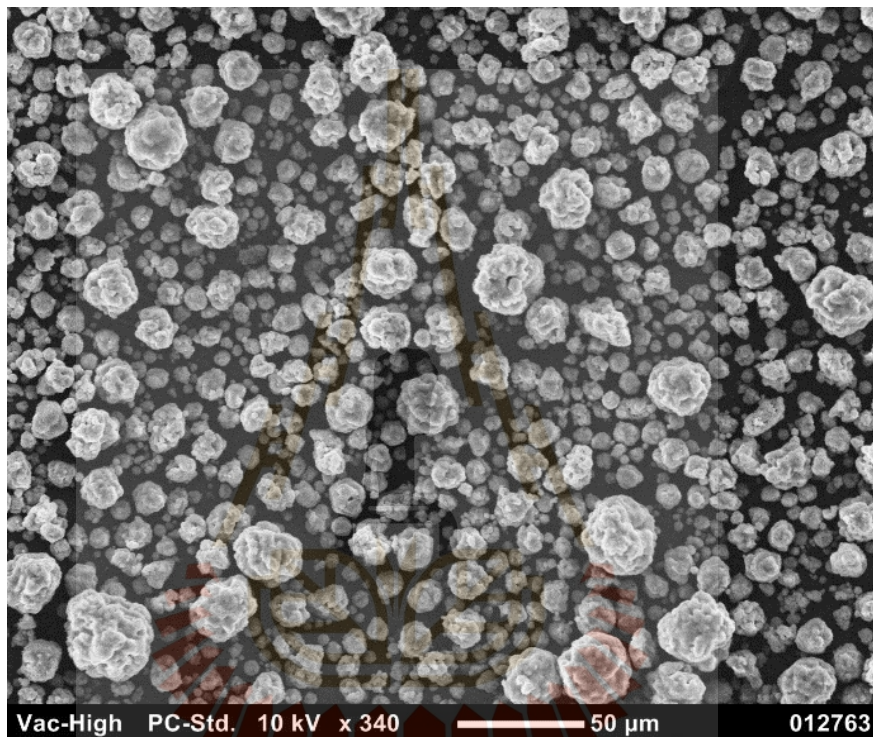


Figure 2.15 Spray-dried powder obtained from SD1 experiment

As shown in Figure 2.15, the obtained spray-dried powder appeared to be round, but its external surface was rough. It also seemed like the powder was formed by agglomeration of some undispersed materials during the drying. These results were likely an indicator of poor solid dispersion in the slurry. To improve the solid dispersion, two additives were utilized in order to modify the slurry interaction surface, polyvinyl alcohol (PVA) and polyethylene glycol (PEG) (Chiangka et al., 2017;

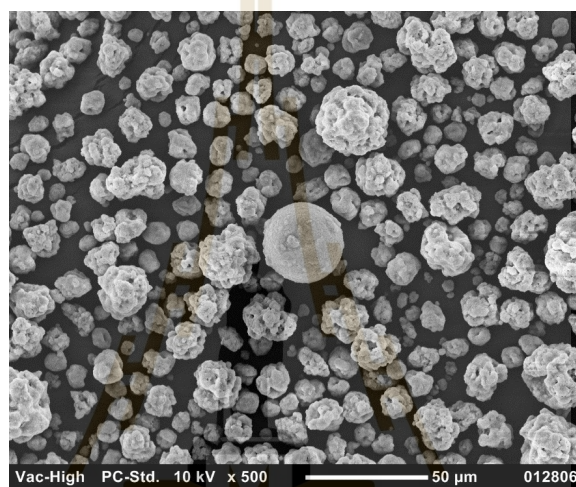
Sukaraseranee et al., 2017). Experimental conditions for spray drying with use of additives are shown in Table 2.5. The two additives were found to increase the slurry viscosity, so the maximum slurry concentration that can be prepared was down to 5% wt for these experiments.

Table 2.5 Operating conditions for spray drying with additives.

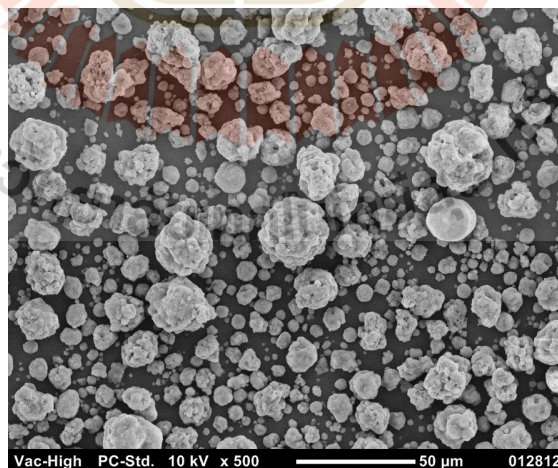
Code	Drying air temperature (°C)	Spray air flow rate (L/h)	Slurry concentration (wt%)	Slurry feed rate (ml/min)	Aspirator ratio (%)	PVA content (wt%)	PEG content (wt%)
SD4	150	473	5	30	100	1	0
SD5	150	473	5	30	100	0	1

The mean particle size of sample from SD4 and SD5 experiment were 18.6 and 17.4 microns respectively. The powder produced from SD4 and SD5 experiment, shown in Figure 2.16, appeared to have smoother surface and was more spherical than that obtained from the spray drying without additives. This observation supported the hypothesis of inhomogeneous when no additives were added in spray drying process. Addition of these two additives, however, seemed to be insufficient to improve the process and bring about the spherical powder as the final product. To further improve the spray drying performance, wet ball milling technique was utilized. The slurry and the 3-mm ceramic ball were filled in the plastic bottle at 50 %vol and 30% vol, respectively. Slurry with designed concentration was homogenized in a ball mill for 4 hr before it is fed to the spray dryer. Operating conditions of the ball mill-integrated spray drying, denoted as SD7 experiment, were similar to those of SD1 experiment. Morphology of the resulted spray-dried powder, clearly with spherical shape and smooth surface, is shown in Figure 2.17.

Therefore, it can be concluded that the dispersion of slurry before feeding to spray dryer was the most crucial factor in achieving the final powder with spherical shape and smooth surface. Based on this method, the spray drying condition that can produce the mean size of spray-dried powder closed to the oven drying technique was then determined.



(a)



(b)

Figure 2.16 SEM image of spray-dried powder with (a) PVA 1wt% with (b) PEG 1wt%

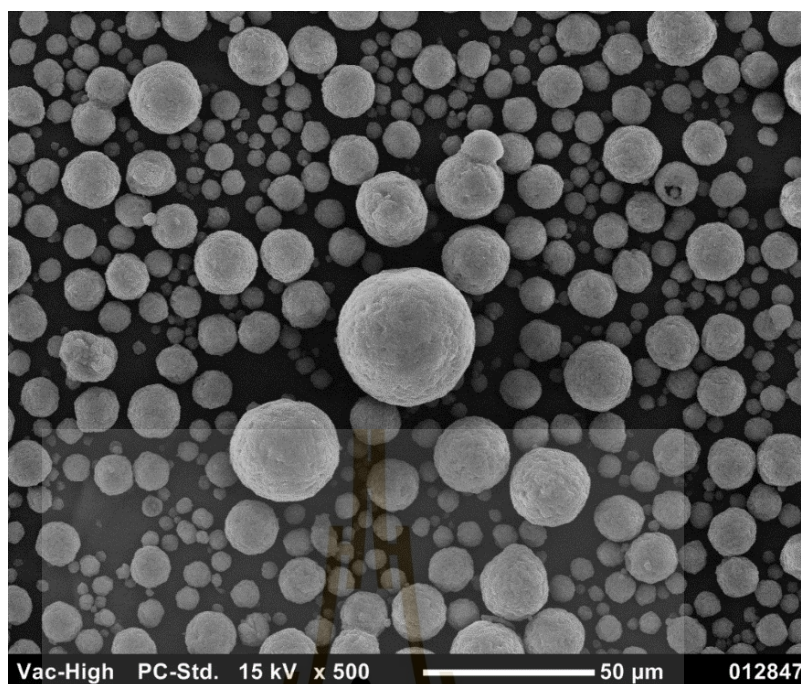


Figure 2.17 Spray-dried powder obtained from integrated spray drying-wet ball milling integrated process.

Investigation of three significant spray drying parameters was carried out with the target in production of spray-dried powder with mean particle size distribution close to its oven-dried counterpart. Results from those experiments are shown in Table 2.6. The slurry concentration and the aspirator ratio were kept constant at 10 wt% and 100% respectively. The particle size distribution of a spray-dried powder in Figure 2.18, appeared to be quite was narrow size with the powder's specific surface area of spray-dried powder is $111.44 \text{ m}^2/\text{g}$ and the total pore volume is $0.8493 \text{ cm}^3/\text{g}$. The spray-dried powder also appeared to have higher surface area and larger pore volume than the oven-dried one.

The spray drying condition for SD7 experiment yielded the final spray-dried powder with the particle size distribution close to that obtained in oven-drying

method, so it is used for preparing the powder for the study of pellet strength improvement.

Table 2.6 Effect of spray drying parameters on mean particle size of the received powder.

Code	Spray air flow rate (L/h)	Drying air temperature (°C)	Slurry feed rate (ml/min)	Mean particle size, d_{50} (μm)
SD6	473	140	8	15.37
SD7	473	150	8	14.31
SD8	473	160	8	15.36
SD9	473	150	6	15.78
SD10	357	150	8	22.97

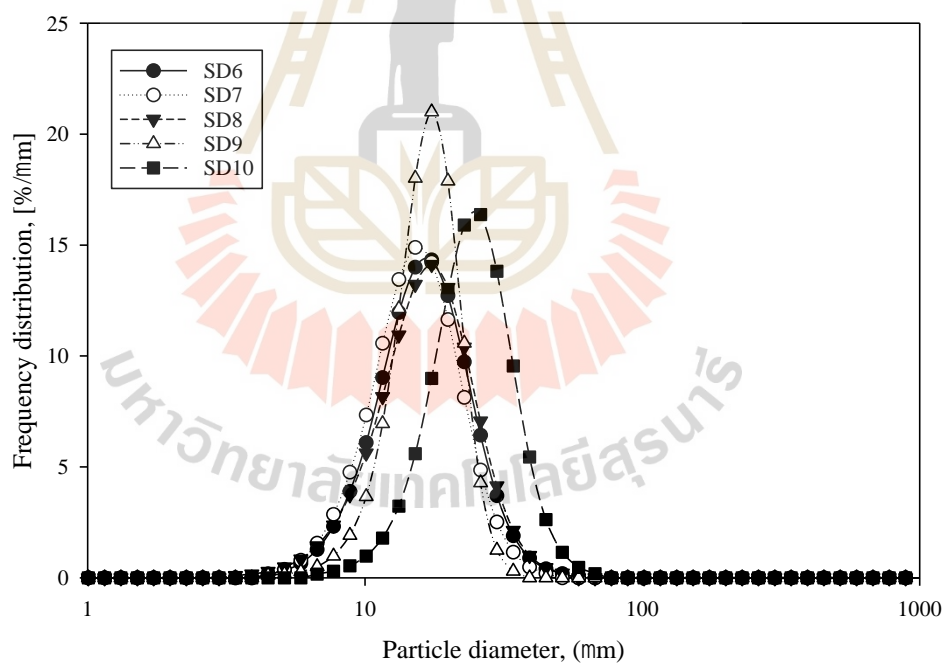


Figure 2.18 Particle size distribution of spray-dried powder produced in SD6-SD10 experiment

2.6 Conclusion

The intermediate powder was successfully prepared using oven-drying and spray-drying technique. The oven drying gave bimodal powder with broad particle size distribution. The spray-dried powder showed narrower single-peak particle size distribution. The key success to prepare spherical-shaped and smooth-surface spray-dried powder was well-homogenization of the slurry before feeding it to the spray dryer. The specific surface area of the prepared and oven-dried powder were 111.44 m²/g and 72.87 m²/g, respectively.

2.7 Reference

- Chen, C., Wangriya, A., Buffet, J.-C., and O'Hare, D. 2015. Tuneable ultra high specific surface area Mg/Al-CO₃layered double hydroxides. **Dalton Transactions**. 44 (37):16392-16398.
- Chiangka, S., Watcharamaisakul, D. S., and Golman, B. 2017. Influence of spray drying conditions on particle size and morphology of Al₂O₃/ZrO₂(3Y) composite particles. **Key Engineering Materials** 728:172-177.
- Huang, L., Kumar, K., and Mujumdar, A. S. 2003. Use of computational fluid dynamics to evaluate alternative spray dryer chamber configurations. **Drying Technology** 21 (3):385-412.
- Julklang, W., and Golman, B. 2013. analysis of slurry drying in a spray dryer. **International Journal of Engineering & Technology** 5 (6):5178.
- Julklang, W., Wangriya, A., and Golman, B. 2017. Fabrication of layered double hydroxide microspheres by spray drying of nanoparticles: Effects of process conditions. **Materials Letters** 209 (Supplement C):429-432.

- Masters, K. 1979. **Spray drying handbook**. London; New York: G. Godwin ; Halsted Press.
- Nandiyanto, A. B. D., and Okuyama, K. 2011. Progress in developing spray-drying methods for the production of controlled morphology particles: From the nanometer to submicrometer size ranges. **Advanced Powder Technology** 22 (1):1-19.
- Rahaman, M., and Rahaman, M. N. 2006. **Ceramic Processing**: Taylor & Francis.
- Rhodes, M. J. 2008. **Introduction to Particle Technology**: Wiley.
- Sarawade, P. B., Kim, J.-K., Hilonga, A., Quang, D. V., and Kim, H. T. 2011. Effect of drying technique on the physicochemical properties of sodium silicate-based mesoporous precipitated silica. **Applied Surface Science** 258 (2):955-961.
- Sukaraseranee, W., Watcharamaisakul, D. S., Golman, B., and Suwanprateeb, J. 2017. Effect of process parameters on characteristics of spray-dried hydroxyapatite granules. **Key Engineering Materials** 728:341-346.
- Urruchurto, C. M., Carriazo, J. G., Osorio, C., Moreno, S., and Molina, R. A. 2013. Spray-drying for the preparation of Al–Co–Cu pillared clays: A comparison with the conventional hot-drying method. **Powder Technology** 239:451-457.
- Wang, A.-j., Lu, Y.-p., Zhu, R.-f., Li, S.-t., and Ma, X.-l. 2009. Effect of process parameters on the performance of spray dried hydroxyapatite microspheres. **Powder Technology** 191 (1-2):1

CHAPTER III

PASTE PREPARATION

3.1 Abstract

Extrusion process has been widely used for transformation of powder into pellets with intended industrial applications like adsorption and heterogeneous catalytic reaction. The first and very important step of extrusion is paste preparation, where the fine, micron-sized powder is mixed with the liquid binding solution in the proper proportion. Rheological properties and consistency of the paste strongly affect quality of the extrudate formed by extrusion. This chapter describe utilization of a modified cone penetration method in characterization of the prepared synthetic clay paste preparation. The response surface methodology (RSM) is used to study effects of paste composition and operating parameters of the paste preparation on paste consistency. The paste extrudability and extrudate quality are determined by the ram extrusion technique. The paste with plasticity is found to yield lower force resistance and lower liquid migration during extrusion resulting in the production of extrudates of more uniform moisture content than the semi-solid paste.

3.2 Introduction

Synthesis of new nanoscale materials has increased tremendously in recent years due to their superior functional properties. However, industrial utilization of nano-sized materials is limited owing to poor flow properties of fine powders, spontaneous agglomeration during fluidization, high-pressure drop through packed bed of particles

in dry processes and difficulties in pumping and filtration in liquid processes. Therefore, nano-sized materials are frequently shaped into technical bodies of larger sizes for industrial applications. The shaping of millimeter-sized pellets from powder can be carried out using various particle processing technologies such as extrusion, granulation, tableting, etc. (Parikh, 2016). Extrusion is the simplest and most widely utilized powder shaping process. It is often used in the manufacturing of many products such as foods (Patil and Kaur, 2018), pharmaceuticals (Thiry et al., 2015), ceramics (Händle, 2009), adsorbents (Akhtar et al., 2014), and catalysts (Devyatkov et al., 2016). Recently, the paste extrusion has been applied in manufacturing of high-value products including metal and alloy components (Yan et al., 2017), ceramic composites (Feilden et al., 2017) and cementitious materials (Ma et al., 2018).

Solid content of the paste is one of the important parameters for paste extrusion process. Extrusion of paste with high solid content is beneficial due to the high mass rate of extrudate produced, low amount of liquid binding solution consumed, and low energy requirement for the extrudate drying (Azzolini et al., 2014). The plasticity of clay can be retained by addition of liquid beyond the plastic limit of the paste until it reaches its critical value and the clay becomes wet and sticky and can no longer maintain the molded shape. However, increasing of moisture content in the paste extrusion process can also have a negative effect on the extruded pellet quality. Salehi and Salem (2008) confirmed that an increase in moisture content of kaolinitic–illitic paste could cause a decrease in pellet’s compressive strength due to the larger number of defects and higher total of the pellet produced.

3.3 Theory

3.3.1 Paste definitions

Paste preparation is an essential step in the paste extrusion process (Benbow and Bridgwater, 1993). Paste is the material prepared by mixing solid and liquid components at proper relative amount. The mixture can be readily molded and can retain its molded shape without application of other forces. The paste can be referred to as single-phase liquid such as a molten polymer. According to Oxford English Dictionary, the word 'paste' was defined as any composition or mixture such as flour, dough, lard, or suet and the like used in making pastry, etc., which contains just enough moisture to render its softness and plasticity. Paste can also mean a mixture of clay and water, and/or other ingredients, of which earthenware or porcelain is made. Paste can be categorized as hard or soft paste according to its consistency and heat resistance.

3.3.2 Clay consistency

The term "consistency" refers to states of ceramic raw materials, namely dry powder, agglomerate, plastic body, paste and slurry which are dependent on the liquid content (Reed, 1995). These consistency states are indicated in Figure 3.1. A dry powder consisting of discrete particles and random agglomerates produced by attractive Van der Waals, electrostatic, or magnetic interparticle forces. Bulk density and flow resistance of the powder depend on random particle attraction and agglomeration. Both properties tend to decrease with particle size of the powder.

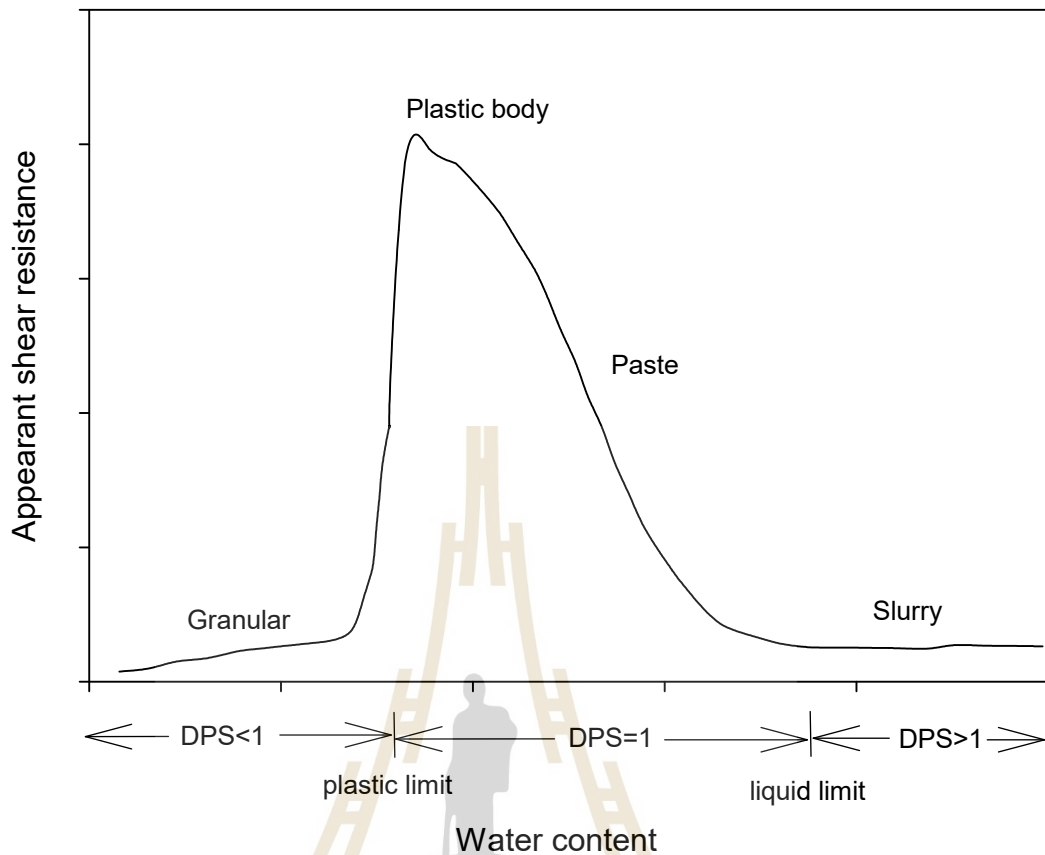


Figure 3.1 Processing consistency states of mixture between dry powder with a wetting liquid or binder solution: $DPS < 1$ refer to granular stage, $DPS = 1$ refer to plastic stage and $DPS > 1$ refer to slurry stage.

Bulky dry powders do not flow well when they are offer little flow resistance when stirred. Agglomerates are formed when a wetting liquid of low viscosity such as water is sprayed into a stirred dry powder. Agglomerates size are increased due to the adhering between dry particles and wet particle groups. Dry particles adhere to particle groups with wet surfaces and their size increases. Capillary forces of the wetting liquid and coagulation forces between particles are the bonding force in the agglomerates, as well as flocculation forces provided by an adsorbed binder.

The degree of pore saturation (DPS) is defined as the volume of liquid to the pore volume of agglomerates.

Within agglomerates, $DPS < 1$. Further spraying and stirring produce additional agglomerates at the expense of the dry powder. The resistance to stirring remains low. Purposefully-made powder agglomerates are commonly called granules and the free-flowing material is referred to granular. Upon increasing the liquid to some particular content, nearly all of the powder will have been transformed into discrete granules with dry surfaces. A small amount of additional liquid will now cause nearly total agglomeration of the agglomerates into a cohesive mass. The cohesive mass is very resistant to shearing and may have plastic-like properties if a significant fraction of the powder is submicron in size and the particles are coagulated. The minimum amount of water necessary to induce the plastic-like properties in clay is called the “plastic limit” (PL).

Upon addition of more liquid into the system with coagulated particles, the fully saturated material ($DPS = 1$) with a slightly open particle packing and moderate to low cohesive strength become more like a paste in consistency (Figure 3.2). The flow behavior of the paste depends on the content of colloidal particle sizes and coagulation forces. The presence of a flocculating binder can significantly increase its cohesion and resistance to shear. The apparent consistency is influenced by the powder dispersion produced during mixing and may change with time when the interparticle forces change. The compressibility of the paste is very low at moderate pressures because $DPS = 1$ and the particles are not able to arrange into a denser packing.

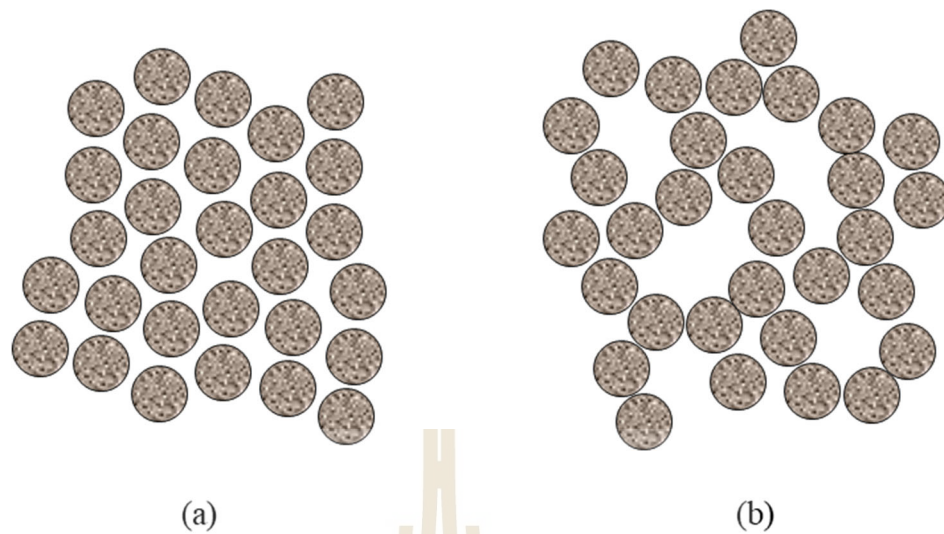


Figure 3.2 More open particle packing due to transition from the (a) plastic body to (b) paste, with constant $DPS = 1$.

Adding more liquid to a paste can lead to the decreasing of shear resistance to decrease and a change in consistency of the of a slurry. The water content which corresponds to this state is called “liquid limit” (LL). In the slurry state, coagulated/flocculated structure becomes discontinuous, particles are dispersed in the liquid, and $DPS > 1$. The material may flow under its own weight. The concentrated suspension that is relatively stable over time is called a slurry.

3.3.3 Methods for measurement of clay plasticity

Concept of plasticity is employed in many areas of engineering and science. Therefore, it is a hard task to choose a method that can be used for any type of raw material or processing condition. In the processing of clay-based material, the plasticity is a fundamental property, since it defines the technical parameters to convert a clay mass into a given shape by application of pressure (Andrade et al., 2011). Experimental determination of plasticity in some cases may observe different results

when using different measuring methods. There are several methods for measurement and characterization of the clay plasticity such as rolling, Pfefferkorn, torque rheometer, stress-strain curves and penetration methods.

3.3.3.1 Rolling Method

The standard method for determining the plastic limit is widely known as a rolling method. In this test, a small mass of clay with lower moisture contents than the liquid limit is rolled into a cylindrical shape with 1/8-inch diameter by either an operator's hands or a rolling device as shown in Figure 3.3. Normally, the rolling by hand is less accurate than using the rolling device, even though hand rolling allows more time for the sample to slowly dry. It is also difficult to measure an exact 1/8-inch length and to ensure constant and even pressure while rolling with one's hands.

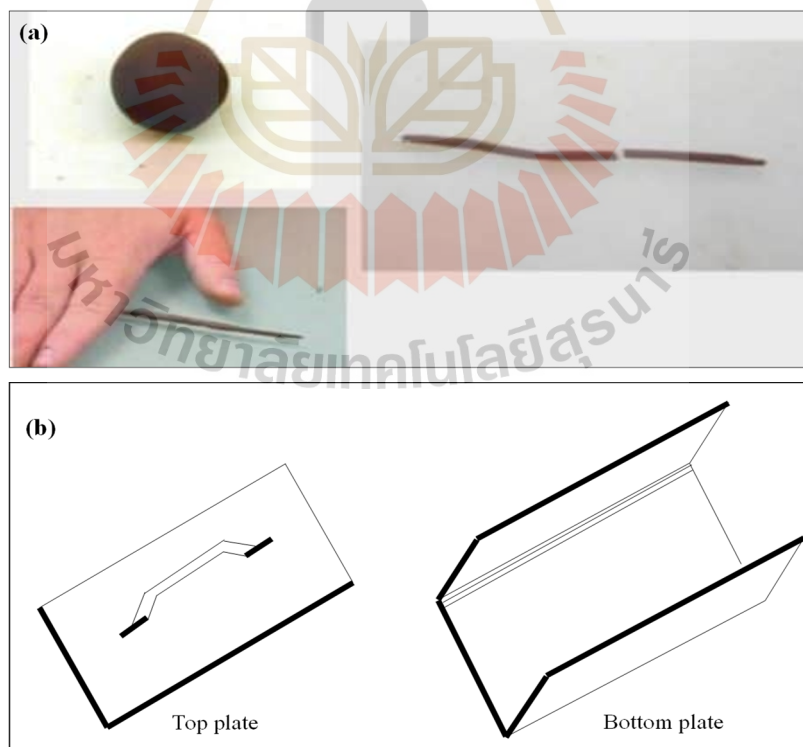


Figure 3.3 Rolling method by (a) hand rolling and (b) rolling device

In device rolling, estimation of fracturing for the rolled clay is dependent on the sense of the operator who runs the plastic limit test. Also, the same amount of pressure is needed be applied by the top plate during each test by consistent rolling speed. A small amount of clay is shaped by hand into an ellipsoid, which is then placed on the center of the bottom plate of the rolling device. This step is repeated on a piece from the same sample with no change in initial moisture content. The clay sample is then rolled to a diameter of 1/8 inch. After the clay sample successfully reaches the criterion of 1/8 inch diameter, it means that sample has a moisture content above the plastic limit. The testing continues until the sample has crumbles, fractures, or barrels, which means that the sample fails the test. It is the moment when the clay is entering the solid-state. To reach the plastic limit, the sample needs to slowly decrease the moisture content with the process of shaping and rolling. Upon repetitive shaping and rolling, sufficient moisture is eventually removed to determine the plastic limit. The rolling method is non-mechanical and so brings with it the most notable drawback; the large variation of final results as the operation of this method is subjective to judgment of the operators.

3.3.3.2 Pfefferkorn method

Plasticity measurement by Pfefferkorn method is based on the moisture content at which the material has some arbitrarily defined consistency (Andrade et al., 2011). It requires incessantly increasing and decreasing moisture content of the sample in order to reach a 30% contraction in relation to the initial height of the test body. To finalize the test, the sample needs to be dried (de Oliveira Modesto and Bernardin, 2008). The results are normally represented as graphs showing height reduction as a function of moisture content. Pfefferkorn method uses a sample with a

diameter of 33 mm and an initial height of 40 mm. It can be produced either manually or by extrusion. The sample is deformed by a free-falling plate with a weight of 1.192 kg using an apparatus as shown in Figure 3.4. The Pfefferkorn method is widely used due to its low equipment cost. However, the main problem of plasticity determination using this method is the determination of the moisture and to the relation between residual and sedimentary clays (de Oliveira Modesto and Bernardin, 2008). In addition, this method is less suitable for stiff bodies, which are usually processed in the advanced ceramics industry, as the low resolution at a small impact deformation height impedes the reproducibility (Händle, 2007).



Figure 3.4 Pfefferkorn apparatus (Andrade et al., 2011)

3.3.3.3 Torque rheometer

The Brabender measuring kneader or torque rheometer is widely used to determine the plasticity of ceramic bodies. The torque rheometer, shown in Figure 3.5, consists of a mixer with eccentric blades. Principle of the measurement is that change in the torque measured reflects change in consistency of dry powder during its transformation to a plastic solid.



Figure 3.5 Torque rheometer (Andrade et al., 2011)

The mixture is placed inside the rheometer, and measuring of plasticity is performed by moving the blades inside the sample by a motor at rotating speed. The torque is recorded and plotted as a function of time as illustrated in Figure 3.6. The clay powder is mixed with a rising amount of water by a proportioning system that allows keeping a steady liquid flow. When water is added to a powder mass, the torque rises from its corresponding initial point, point A, to a maximum torque achievable at that powder-water proportion (τ_x). When more water is added, consistency of the solid

mass decreases and then the torque starts to fall until it attains a new stable point. At point E, the solid is no longer plastic. In general, plasticity can be defined by the maximum relative consistency (τ_x) or the range of plastic behavior (H_e-H_x) (Sanchez et al., 1998). An advantage of this method is to perform an extrusion test with an extrusion screw and can use several types of die in the rheometer, monitoring the force by a pressure transducer. However, this method is suitable for small quantities of material, which has to be considered when passing into the industrial scale (Alfani and Guerrini, 2005).

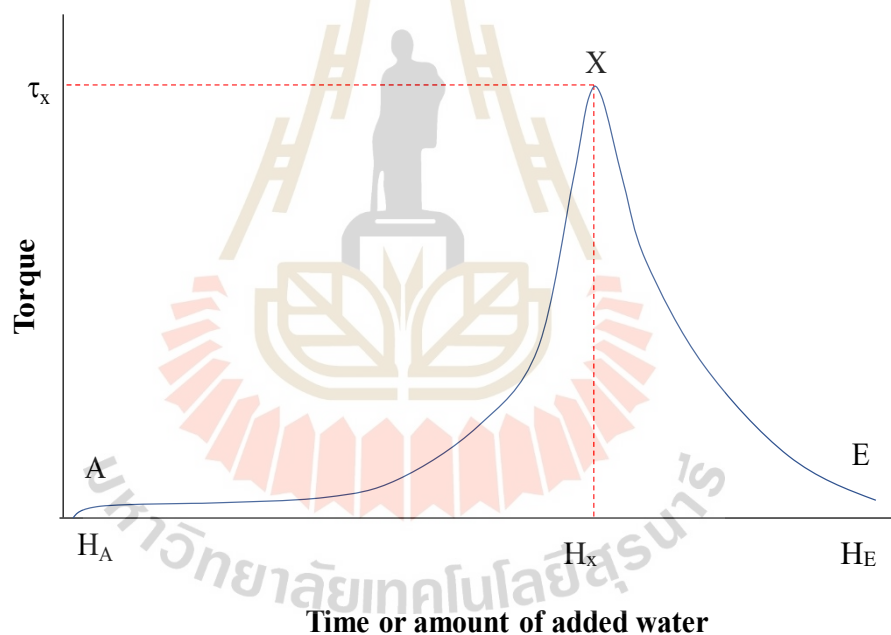


Figure 3.6 Torque rheometer test (Sanchez et al., 1998)

3.3.3.4 Stress-strain curves

Another method to measure plasticity is by stress–deformation compression curves. This method gives information about elastic-type behavior, yield strength, maximum deformation and rupture strength. In this method, the clay is

compressed until the failure of structure or cracks appear as shown in Figure 3.7 and the measurement data is presented in Figure 3.8.

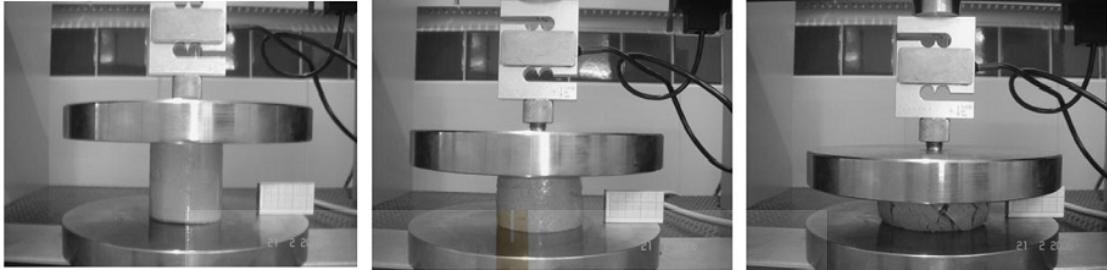


Figure 3.7 Compression test of clay (Flores et al., 2010)

At point A, the material presents elastic behavior. After Point A, a continuous increase of the stress induces plastic deformation. Finally, the maximum deformation occurs at point B, at which the failure of structure starts to appear. Above this limit, clay-based material tends to show abnormal stress increasing instead of a decline, generally related to the enlargement of the area of contact with the support plates caused by compression forces (Ribeiro et al., 2005). However, this method seems to be more precise and independent of the operator's ability (Andrade et al., 2011).

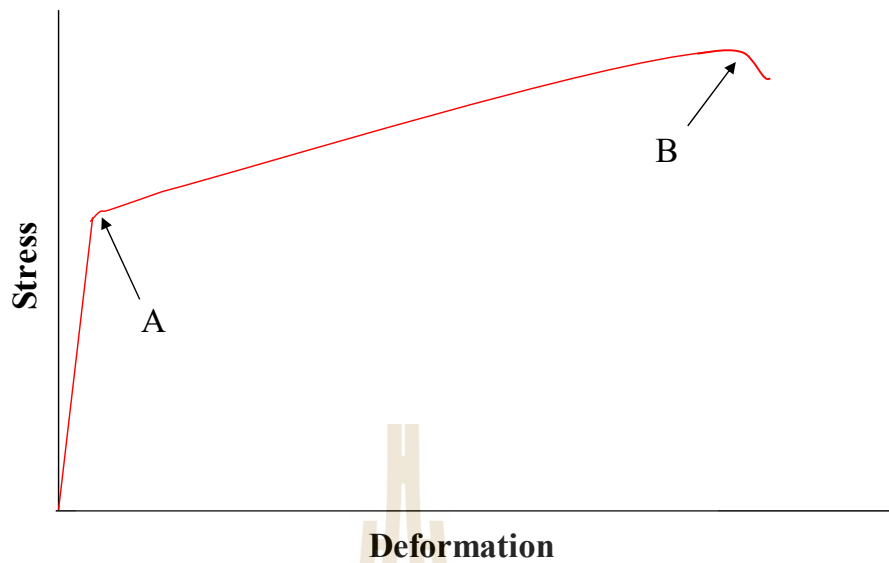


Figure 3.8 Stress-deformation compression curve (Ribeiro et al., 2005)

3.3.3.5 Penetration Method

The principle of penetration method is based on using a tool with varying geometry, which is pushed evenly into the compact body up to a measuring mark. The measured value represents the force needed for penetration. This method is widely used in ceramics fields, because it is easy to manage and can be measured directly on the extrudate. The measuring instruments of this method may be also related to those used for hardness measurement (Händle, 2007). The penetrometer designs endeavor to eliminate the inaccuracies in measuring and reading. The measured value is displayed digitally as a force in a measuring field and, depending on the geometry of penetration tool, can be evaluated as pressure. The example of the penetration apparatus is shown in Figure 3.9. In the falling cone test, a cone with an angle of 30° and a total mass of 240 g is suspended above for just in contact with the clay sample. The cone is permitted to fall freely within 5 second. Water content corresponding to a cone

penetration of 2 mm is defined as the plastic limit of the material (Yu and Mitchell, 1998).



Figure 3.9 Cone penetration apparatus

In the past years, there are several researchers developed and proposed several equipment based on the penetration method. Doménech et al. (1994) proposed the use of a sample-holding mold of circular cross section by neglecting in edge effects. They used a specimen ring with a diameter of 50 mm a height of facilitates the sample preparation and increases the quality of the sample. The clay sample is relatively stiff for lower cone penetration and the traditional specimen cup reduces the measuring resolution of the plastic limit. It is advantageous to use the cone penetration method for also determining the plastic limit. Feng (2004) designed a small specimen ring for fall-cone tests to determine the plastic limit by using a small specimen ring of 20 mm in diameter and 20 mm in height, which is designed for cone penetrations depth between 3 and 10 mm. Measurements of plasticity are considered to be more consistent. It is

suggested the results obtained from the cone penetration test are more closely related to the clay behavior. The measurements have better reproducibility are easier to determine as well as use fewer operators. It is preferable that it is often used for determining the plastic limit. However, Benbow and Bridgwater (1993) found some factors that affect the accuracy of penetration. They reported that the accuracy is limited when the depth of penetration is too small. The penetration was found to depend on the time if the sample is predominantly viscous rather than plastic.

The preparation of paste at the plastic limit point requires sufficient liquid binder and intensive mixing and appropriate mixing time. In addition, the liquid can be evaporated during paste preparation due to the energy supplied by a mixer, resulting in the change of paste state from plastic to the semi-solid state. Thus, there is a need to apply the simple and reliable experimental method to characterize the paste state and to develop the corresponding mathematical correlation that considers the paste mixing conditions.

This chapter, therefore, aims to utilize the modified cone penetration method with the small cup geometry as a simple tool to determine plasticity after extrusion of the paste prepared under different mixing conditions. The response surface methodology is applied to explore the effect of paste composition and preparation parameters on paste plasticity. Ram extrusion technique is used to study the extrudability of the prepared pastes.

3.4 Experimental

3.4.1 Paste and extrudate characterization

The moisture content of both paste and extrudate samples were determined by solvent evaporation technique in a drying oven. Around 3 g of each sample was weighted and then oven dried overnight. The dried sample was re-weighted to calculate the moisture lost as indicated as moisture content in a sample.

3.4.2 Experimental design and statistical analysis for paste preparation

A Box-Behnken design was employed to set up an experimental plan with three independent variables: mass ratio of liquid binder to powder (MR), powder loading (PL) and mixing time (MT), The cone penetration depth was a response variable. The design was generated using an open-source R software (Team, 2008). Levels of each variable established according to the preliminary trials are summarized in Table 3.1. The experimental design consisting of 15 different combinations, which include three replicates of the center point, are shown in Table 3.2. A regression metamodel was constructed by fitting a quadratic polynomial equation, Equation. (3.1), to the experimental data.

$$y = b_0 + \sum_{i=1}^4 b_i x_i + \sum_{i=1}^4 \sum_{j=1}^4 b_{ij} x_i x_j + \sum_{i=1}^4 b_{ii} x_i^2 \quad (3.1)$$

where y is the response, b_0 is the intercept, b_i , b_{ij} and b_{ii} are the linear, interaction and quadratic coefficients, respectively. The levels of the i th and j th coded variables are denoted as x_i and x_j , respectively. The multiple regression analysis was performed using a Microsoft Excel data analysis tool. The analysis of variance (ANOVA) was

then conducted to verify and validate the metamodel. The significance of each term of metamodel was evaluated by using the P-value. If the P-value for the independent variable is less than 0.05, then we assumed that this variable has a significant influence on the responses. The terms with large P-value were eliminated from the metamodel. The F-test was also carried out to confirm the utility of the proposed regression metamodel.

Table 3.1 Levels for independent variables.

Variables	Levels		
MR, [-]	0.95	1	1.05
PL, [g]	20	25	30
MT, [min]	10	15	20

Table 3.2 Experimental conditions of paste preparation generated by R software with cone penetration depth as the response variable.

Run.no	MR, [-]	PL, [g]	MT, [min]
1	1	30	20
2	0.95	30	15
3	0.95	25	10
4	0.95	25	20
5	1	25	15
6	1.05	20	15
7	1.05	30	15
8	1	25	15
9	1	30	10
10	1	20	20
11	0.95	20	15
12	1.05	25	10
13	1	20	10
14	1.05	25	20
15	1	25	15

3.4.3 Paste preparation

The paste for extrusion was prepared by mixing the milled powder with water as a liquid binder using a mixer (Bosch, Mixer MUM48CR1). The powder was firstly heated in the oven overnight at 110°C, then cooled down to room temperature and stored in a desiccator before use. The dried powder was stirred for 2 minutes to deagglomerate the powder. The required amount of water was added dropwise to the powder using a dropper during the first 2 minutes of the paste preparation process. The rotational speed of the mixer was set at the highest for all experiments. The freshly prepared paste was kept in a zipped plastic bag and stored in an ice bucket before testing. Moisture content of the fresh paste sample was measured by an oven drying method.

3.4.4 Cone penetration test

The cone penetration test was performed following Feng's work (Feng, 2004). A standard fall-cone penetrometer (Wykeham Farrance, Cone Penetrometer WF 21600) with a scale reading precision of 0.1 mm was used in all experiments. A test setup for cone penetration into a paste is shown in Figure 3.10. A small specimen ring was filled with freshly prepared paste, and the excess paste above the top of the ring was removed using a spatula. The specimen was placed on the stand under a fall-cone. The fall-cone vertical position was adjusted in such a way that a tip of the cone just touched the specimen surface. To measure the cone penetration depth, the fall-cone was released, and the cone was allowed to penetrate into a paste for 5 seconds. Then, the penetrometer shaft was restrained, and the cone depth was recorded (British Standard (1990)). The measurements were repeated three times.

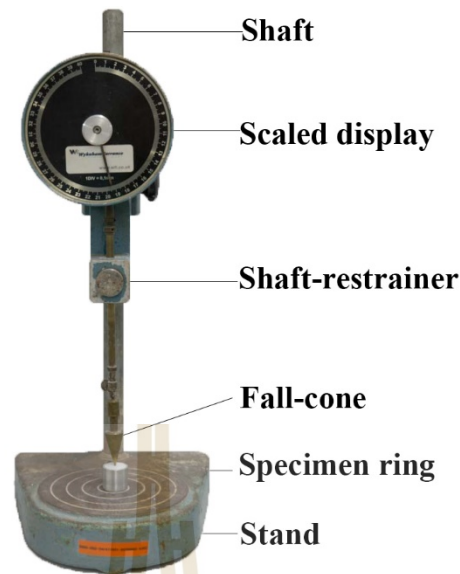


Figure 3.10 Experimental setup for a cone penetration test.

3.4.5 Ram extrusion and paste rheology

Extrusion of the prepared paste was studied by ram extrusion technique using a high-pressure capillary rheometer (GÖTTFERT, RG20) as illustrated in Figure 3.11. The rheometer barrel diameter was 15 mm. The maximum testing force of rheometer was 20 kN and a dynamic speed range from 0.0001 to 40 mm/s. The die diameter was 1.5 mm in diameter with the length-to-diameter (L/D) ratio of 4. The ram extrusion velocity was kept constant at 1 mm/s for all experiments. The preparation paste was put into the barrel and tamped it down with a tamper. The resistance force during extrusion with each extrusion velocity was measured and recorded by the machine software. The paste liquid migration was studied by measuring the moisture content of samples collected at various times during the extrusion process.



Figure 3.11 Capillary rheometer (GÖTTFERT, RG20)

3.4.6 Paste kneading

The kneading process was adopted to control paste characteristics of the prepared paste using the food kneading machine as shown in Figure 3.12. The mixing time was controlled at 15 minutes for every batch of paste preparation. After mixing, the paste was put into the kneader and kneaded one-pass.



Figure 3.12 Paste kneading equipment

3.5 Result and discussions

3.5.1 Cone penetration depth

The response of the cone penetration depth experiment according to the Box-Behnken design was shown in Table 3.3.

มหาวิทยาลัยเทคโนโลยีสุรนารี

Table 3.3. Response on cone penetration depth.

Run.no	MR, [-]	PL, [g]	MT, [min]	Cone depth, [mm]
1	1	30	20	2.100±0.087
2	0.95	30	15	0.183±0.076
3	0.95	25	10	0.117±0.029
4	0.95	25	20	0.133±0.058
5	1	25	15	0.833±0.289
6	1.05	20	15	1.867±0.104
7	1.05	30	15	2.017±0.076
8	1	25	15	0.533±0.058
9	1	30	10	0.350±0.132
10	1	20	20	0.300±0.100
11	0.95	20	15	0.183±0.058
12	1.05	25	10	1.817±0.301
13	1	20	10	0.433±0.208
14	1.05	25	20	2.067±0.208
15	1	25	15	0.283±0.104

3.5.2 Statistical analysis

Effect of input factors was considered in the response equation when their P-values were less than 0.05. Thus, the terms of the square of main effects and interaction parameters with large P-value were excluded from the regression metamodel. The results of regression and ANOVA analyses are summarized in Table 3.4 and Table 3.5, respectively. The F-test was also carried out to confirm the significance of the proposed regression model.

Table 3.4 Correlation coefficients from the quadratic regression analysis.

Source	Coefficients	Standard Error	P-value
Intercept	130.9813	62.2000	0.0645
MR	-268.0774	124.4234	0.0596
PL	-0.2358	0.0926	0.0314
MT	-0.4238	0.1517	0.0210
PLxMT	0.0188	0.0060	0.0120
MR ²	142.9762	62.2026	0.0471

Table 3.5 ANOVA analysis of quadratic regression.

<i>df</i>	<i>SS</i>	<i>MS</i>	<i>F</i>
5	8.6330	1.7266	19.1247
9	0.8125	0.0903	
14	9.4455		

$F_{crit.(5,9,0.05)}=3.482$

The regression model equation for cone penetration depth was derived in terms of response parameters as follows:

$$\begin{aligned} \text{Cone depth} = & 130.9813 - 268.077MR - 0.2358PL - 0.4238MT \\ & + 0.0188PL \times MT + 142.9767MR^2 \end{aligned} \quad (3.2)$$

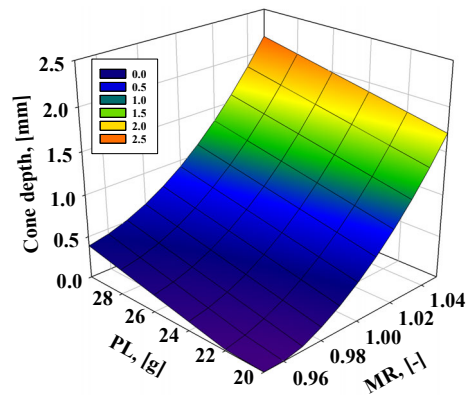
Coefficient of determination (R^2) of >0.914 was obtained, which indicated that the experimental responses in Table 3.3 are well explained by the metamodel in Equation (3.2). The F-test was used to verify whether the metamodel explained any variation in response. The critical F-value (F_{crit}), calculated using an Excel function for F-probability distribution, is shown in Table 3.5. The F-value of regression was larger than the critical F-value. Therefore, most variations were explained by the metamodel in Equation. (3.2).

3.5.2 Effect of process variables on cone penetration depth

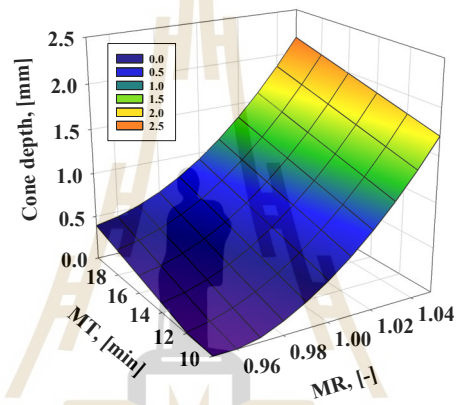
The 3-dimensional response surface plots shown in Figure 3.13 were generated using Equation (3.2). The data for response plots were calculated by fixing one parameter at the middle level, i.e., MT=15 min (Figure 3.13(a)), PL=25 g (Figure 3.13(b)), and MR=1 (Figure 3.13(c)), and by varying two other parameters.

The strong effect of the amount of liquid binder added to the powder (MR) during paste preparation was observed on the cone penetration depth. The increase in cone penetration depth indicated the extent of paste plastic behavior. At the fixed mixing time and constant powder load, increasing the liquid binder to powder ratio resulted in an increase in the amount of liquid available during paste preparation leading to significant enhancement of paste plasticity. The cone penetrated nine times deeper into the paste of ratio MR = 1.05 and solid amount PL = 25 g than into the paste of MR = 0.95 and PL = 25 g, as shown in Figure 3.13 (a). The cone penetrated slightly deeper into the paste prepared using the larger amount of solid. The large total amount of liquid was added to the powder during paste preparation for the batch with high powder load as the ratio of liquid to powder was kept constant. However, the low energy per unit powder weight was available for powder deagglomeration and liquid distribution, because the impeller rotational speed and mixing time were kept constant throughout all experiments. Thus, the presence of large agglomerates with low external specific surface area could have resulted in the formation of a thick binder layer on the outer agglomerate surface, which acts as a lubricant in cone penetration experiments. The larger the amount of liquid available, the thicker the lubricant layer and the deeper the core penetration depth.

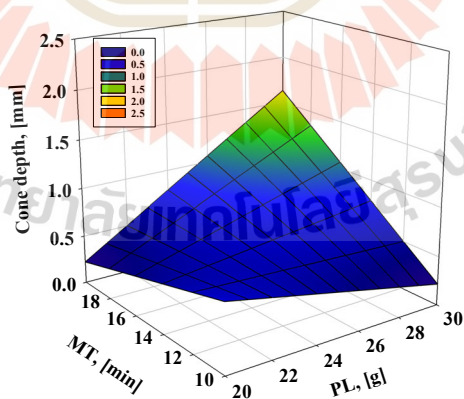
The cone penetration depth appeared to slightly increase with mixing time, as shown in Figure 3.13 (b). Longer mixing time resulted in the preparation of more homogeneous paste. High energy supply to the mixture of powder and liquid binder led to powder deagglomeration and uniform distribution of liquid binder. Thus, the paste of higher plasticity was obtained. The two-sided effects of powder load and mixing time on penetration depth are observed in Figure 3.13 (c). Paste plasticity was found to decrease with increasing mixing time at small powder load and with increasing powder load at short mixing time. The opposite trends were observed at high powder load and for long mixing time. At short mixing times and constant energy supply by the mixer, dispersion of liquid binder in the powder was hindered at high powder load resulting in the paste that lacks the plasticity. However, it was found that paste behavior differs at small powder load and for long mixing time. Increasing mixing time resulted in a decrease in the paste plasticity. This trend is probably due to the effect of moisture lost during paste preparation process because of evaporation of liquid binder, as shown in Figure 3.14.



(a)



(b)



(c)

Figure 3.13 Response surface plots of cone penetration depth; (a) effects of powder load and liquid to powder ratio, (b) effects of mixing time and liquid to powder ratio, (c) effects of mixing time and powder load.

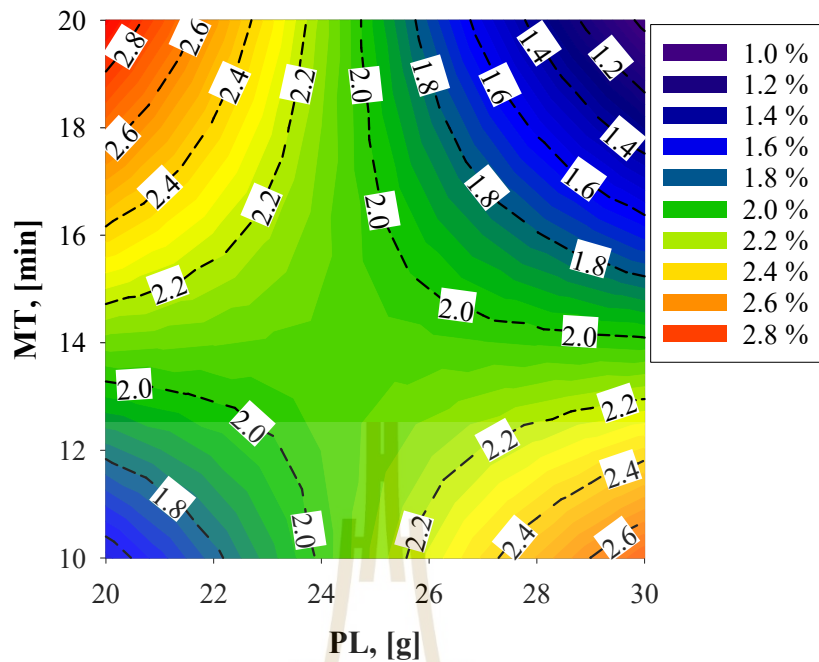


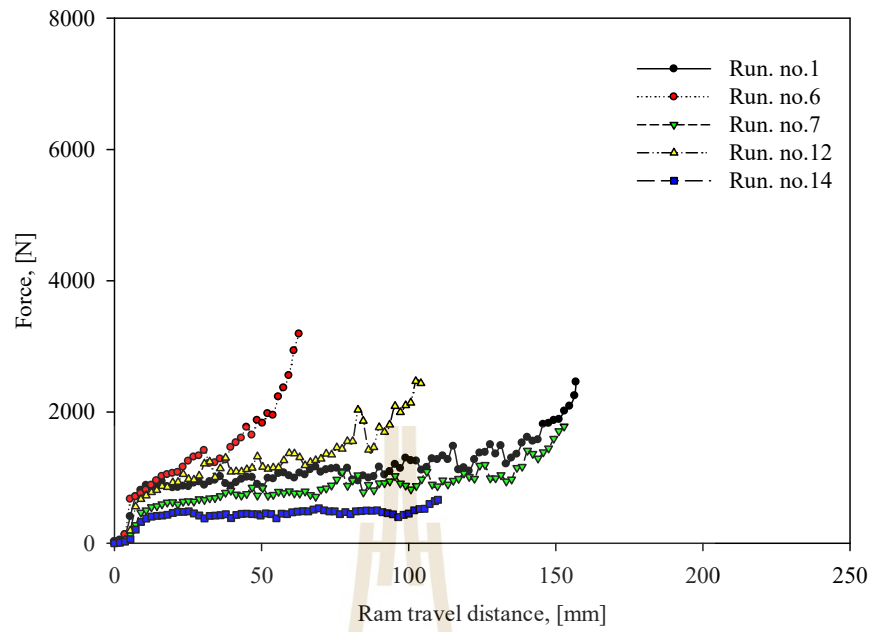
Figure 3.14 Percentage of moisture loss during fresh paste preparation.

Powder mixing at low powder load and longtime led to formation of the well-dispersed powder-binder mixture and, at the same time, to significant moisture loss owing to high energy supply per unit powder weight over a long time, as illustrated by the red painted area in the upper left corner of Figure 3.14. The liquid dispersion had less influence on paste rheology than the loss of liquid binder resulting in the formation of the paste with poor plasticity. The high moisture loss at high powder loading and for short mixing time, as shown in lower right corner, was probably due to inhomogeneity of the paste and existence of agglomerated particles. The smallest amount of moisture lost was observed in mixing of high powder loading for a long time, as demonstrated by the dark blue area in the upper right corner of Figure 3.14.

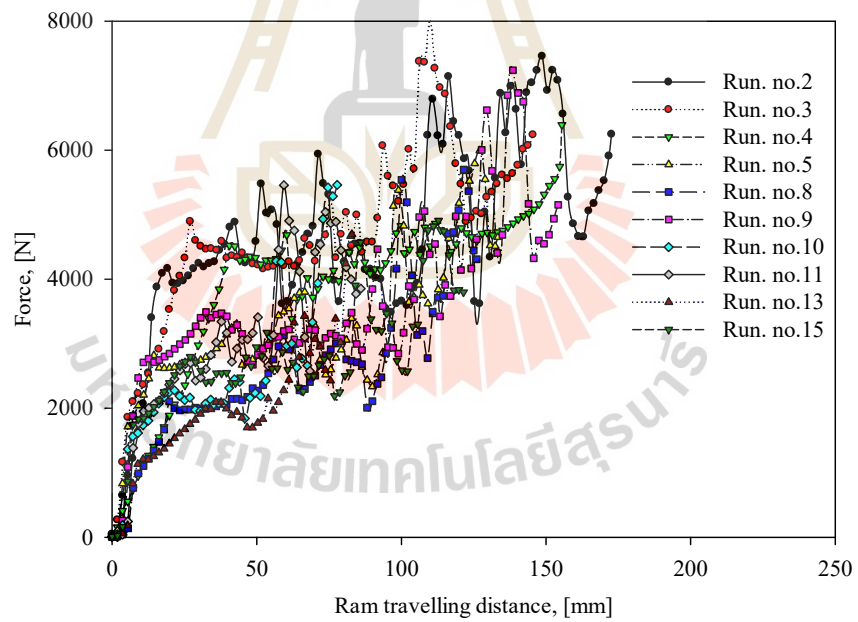
3.5.3 Ram extrusion and paste rheology

The variations of paste resistance force during ram extrusion experiments are shown in Figure 3.15 (a) and Figure 3.15 (b). The pastes of high plasticity with a cone penetration depth of more than 2 mm, Experiment 1, 7 and 14, appeared to have the lowest values of resistance force and significantly lower force deviations during extrusion. Similar behavior was observed for pastes prepared in Experiment 6 and 12 as they had the cone penetration depths close to the value corresponding to the plastic limit. The resistance force was almost constant during extrusion after an initial startup period in Experiment 1, 7 and 14. However, the resistance force tended to increase with ram travel distance in Experiment 6 and 12.

The resistance force of paste with semi-solid behavior was high and fluctuated significantly during extrusion. It also raised with increasing ram travel distance, as shown in Figure 3.15 (b). The fluctuation of force during extrusion could have been attributed to air accumulation in the paste. As observed in Figure 3.16 (a), the paste with semi-solid behavior consisted of small wet agglomerates. When the semi-solid paste was packed into the ram barrel, the air was collected in the void space between agglomerates. This was observed even with the paste that was well-packed with the tamper and had to high paste resistance and high resistance force fluctuation during extrusion. The increase of resistance force with ram travel distance was observed in all experiments except in Experiment 1, 7 and 14. This phenomenon was likely due to the liquid phase migration during extrusion, as illustrated in Figure 3.15.



(a)



(b)

Figure 3.15 Paste resistance force during ram extrusion experiment; (a) Experiment 1,

6, 7, 12 and 14, and (b) Experiment 2-5, 8-11, 13 and 15.

The pastes with plasticity did not show the significant deviation of extrudate moisture content during extrusion because of the low liquid migration effect as illustrated in Figure 3.17. However, considerable liquid migration was observed in extrusion of semi-solid paste. The moisture content of extrudates, which collected at the beginning of the extrusion was higher than the paste moisture content at paste preparation step. When the paste was pressed by the ram piston at the beginning of extrusion, as a result of high pressure and low paste plasticity, the liquid in the paste was moved forward toward the low-pressure area near the die. Hence, the paste near the die had higher water content than the feed paste. In contrast, the paste located near the ram piston had lower moisture content than the feed paste resulting in increasing of resistance force during extrusion and decreasing a decrease of extrudate moisture content.

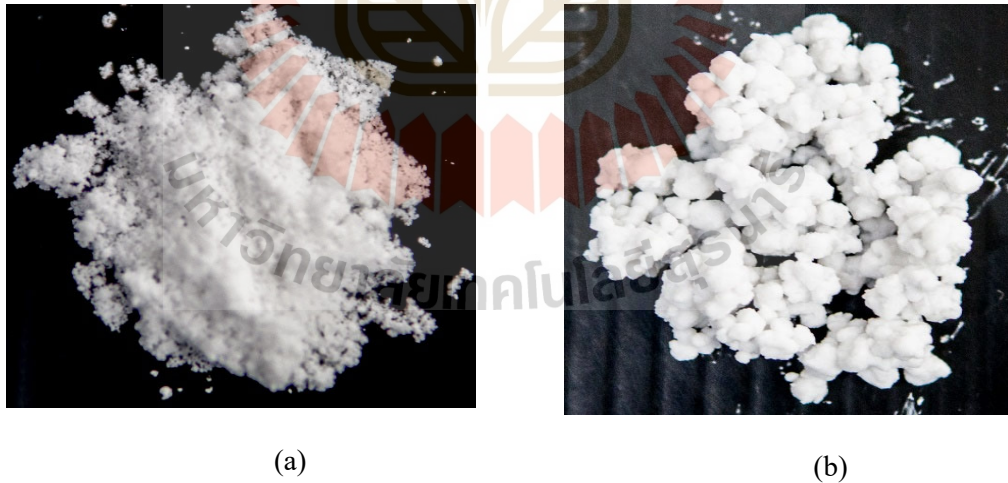


Figure 3.16 Fresh paste after preparation; (a) semi-solid paste, (b) paste with plasticity.

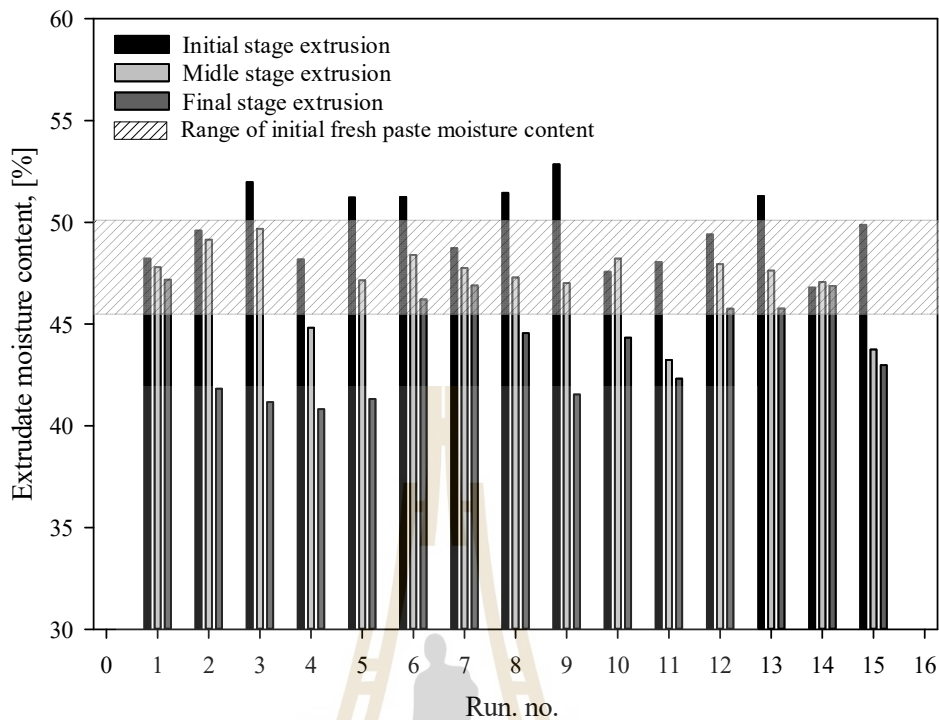


Figure 3.17. Extrudate moisture content during ram extrusion.

3.5.4 Paste kneading

Uncontrolled ambient humidity was found to lead to varying water evaporation rate during past preparation. This situation led to varying characteristics of the final pastes: semi-solid or plastic, even when they were prepared with the same composition and under the same operating conditions. Semi-solid paste was produced in ram extrusion with condition as discussed previously. Therefore, addition of paste kneading process to control the paste characteristics before extrusion was proposed in this study. The paste characteristics after kneading is shown in Figure 3.18. To confirm that the kneading process did not increase liquid migration during ram extrusion, liquid migration, moisture analysis was performed, and the result is as shown in Table 3.6. The percentage of paste moisture content after paste kneading was found to change no

more than 1% of its starting value before kneading. The extrusion profile of paste after kneading process also confirmed that kneading did not interrupt with the paste properties during extrusion process as shown in Figure 3.19. As a result, kneading process could be used to control paste in this study.



Figure 3.18 Paste appearance after kneading

Table 3.6 Percentage of paste moisture before and after kneading process

Experiments	Percentage of paste moisture		
	Before	After	%Change
Experiment No.1	51.25	51.95	0.70
Experiment No.2	51.33	51.83	0.50
Experiment No.3	51.18	51.51	0.34
Experiment No.4	51.27	51.86	0.59
Experiment No.5	51.51	52.02	0.51
Experiment No.6	51.23	51.67	0.44

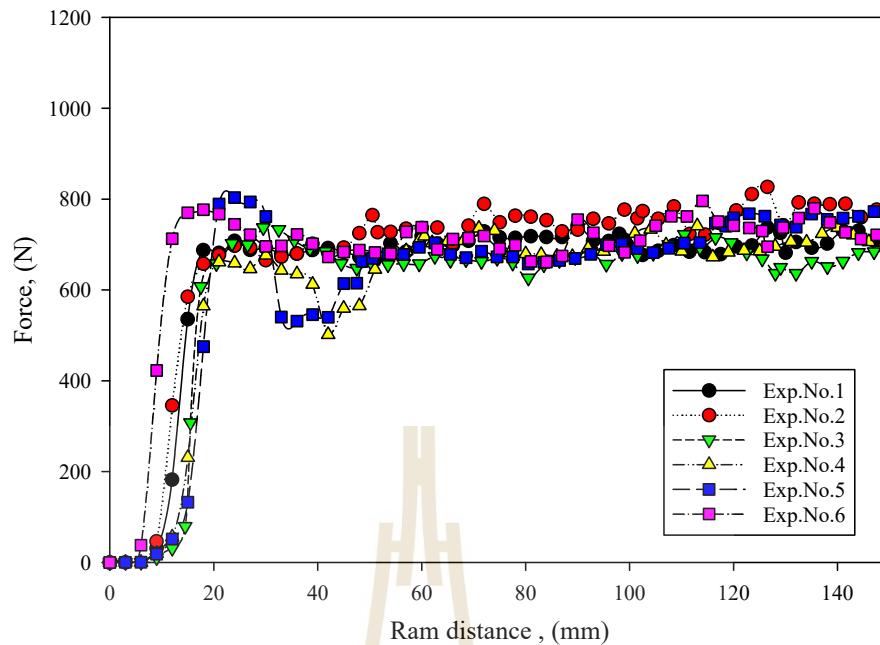


Figure 3.19 Extrusion profile of paste after kneading

3.6 Conclusion

The simple cone penetration method was successfully utilized to classify paste behavior in the extrusion process. This technique had provided a quick characterization method to analyze whether the paste composition was suitable for extrusion. The paste with plasticity lower resistance force and liquid migration during extrusion resulting in more uniform moisture distribution in extrudates than the semi-solid paste. Thus, the extrudates having uniform structural and mechanical properties, which is desirable for their utilization in industrial scale, could be obtained.

3.7 References

- Akhtar, F., Andersson, L., Ogunwumi, S., Hedin, N., and Bergström, L. 2014. Structuring adsorbents and catalysts by processing of porous powders. **Journal of the European Ceramic Society** 34 (7):1643-1666.
- Alfani, R., and Guerrini, G. L. 2005. Rheological test methods for the characterization of extrudable cement-based materials—A review. **Materials and Structures** 38 (2):239-247.
- Andrade, F. A., Al-Qureshi, H. A., and Hotza, D. 2011. Measuring the plasticity of clays: A review. **Applied Clay Science** 51 (1):1-7.
- Azzolini, A., Sglavo, V. M., and Downs, J. A. 2014. Novel method for the identification of the maximum solid loading suitable for optimal extrusion of ceramic pastes. **Journal of Advanced Ceramics** 3 (1):7-16.
- Benbow, J., and Bridgwater, J. 1993. **Paste Flow and Extrusion**. Clarendon Press ; New York : Oxford University Press.
- De Oliveira Modesto, C., and Bernardin, A. M. 2008. Determination of clay plasticity: Indentation method versus Pfefferkorn method. **Applied Clay Science** 40 (1-4):15-19.
- Devyatkov, S. Y., Zinnurova, A. A., Aho, A., Kronlund, D., Peltonen, J., Kuzichkin, N. V., Lisitsyn, N. V., and Murzin, D. Y. 2016. Shaping of sulfated zirconia catalysts by extrusion: understanding the role of binders. **Industrial & Engineering Chemistry Research** 55 (23):6595-6606.
- Doménech, V., Sánchez, E., Sanz, V., García, J., and Ginés, F. 1994. Assessing the Plasticity of Ceramic Masses by Determining Indentation Force. In **III World**

- Congress on Ceramic Tile Quality, AICE/ITC, Castellón, Spain.** Castellón, Spain.
- Feilden, E., Ferraro, C., Zhang, Q., Garcia-Tunon, E., D'Elia, E., Giuliani, F., Vandeperre, L., and Saiz, E. 2017. 3D printing bioinspired ceramic Composites. **Scientific Reports** 7 (1):13759.
- Feng, T.-W. 2004. Using a small ring and a fall-cone to determine the plastic limit. **Journal of Geotechnical and Geoenvironmental Engineering** 130(6):630-635.
- Flores, O., Andrade, F., Hotza, D., and Al-Qureshi, H. 2010. Modeling of plasticity of clays submitted to compression test. **World Academy of Science, Engineering and Technology** 61:191-196.
- Händle, F. 2009. **Extrusion in Ceramics**: Springer Berlin Heidelberg, New York.
- Ma, G., Li, Z., and Wang, L. 2018. Printable properties of cementitious material containing copper tailings for extrusion based 3D printing. **Construction and Building Materials** 162:613-627.
- Parikh, D. M. 2016. **Handbook of Pharmaceutical Granulation Technology, Third Edition**: CRC Press.
- Patil, S. S., and Kaur, C. 2018. Current trends in extrusion: development of functional foods and novel ingredients. **Food Science and Technology Research** 24 (1):23-34.
- Reed, J. S. 1995. **Principles of ceramics processing**, Wiley.
- Ribeiro, M. J., Ferreira, J. M., and Labrincha, J. A. 2005. Plastic behaviour of different ceramic pastes processed by extrusion. **Ceramics International** 31 (4):515-519.

- Salehi, M., and Salem, A. 2008. Effect of moisture content on extrusion process of kaolinitic–illitic clay in manufacturing of ceramic raschig ring. **Journal of Materials Processing Technology** 200 (1-3):232-237.
- Sanchez, E., Ines, F. G., Sanz, V., and Gozalbo, A. 1998. Study of clay plastic behaviour by a torque rheometer. paper read at **V World Congress on Ceramic Tile Quality, AICE/ITC**, at Castellón, Spain.
- Standard, B. 1990. Methods of test for soils for civil engineering purposes: Part 2: Classification tests. **British Standard**:1377-1372.
- R: A Language and Environment for Statistical Computing. R Foundation for Statistical Computing.
- Thiry, J., Krier, F., and Evrard, B. 2015. A review of pharmaceutical extrusion: critical process parameters and scaling-up. **International Journal of Pharmacy and Pharmaceutical Sciences** 479 (1):227-240.
- Yan, X., Hao, L., Xiong, W., and Tang, D. 2017. Research on influencing factors and its optimization of metal powder injection molding without mold via an innovative 3D printing method. **RSC Advances** 7 (87):55232-55239.
- Yu, H. S., and Mitchell, J. K. 1998. Analysis of cone resistance: Review of methods. **Journal of Geotechnical and Geoenvironmental Engineering** 124:140-149.

CHAPTER IV

PELLETS PREPARATION BY EXTRUSION AND SPHERONIZATION

4.1 Abstract

Highly spherical pellet shape with a smooth surface consisting of synthetic clay, adhesive and cohesive materials was successfully prepared by extrusion and spheronization technique. The key success of this process is hot wall spheronization system. However, application of hot wall surface led to variation of process parameters can be varied in narrow ranges. Sphericity of the prepared pellets was increased with increasing spheronization speed (SS) and spheronization time (ST), but, it decreased with increasing extrudate loading (EL). However, using very high SS and ST but low EL led to quick drying of the pellets in the spheronizer and thus resulted in the pellets with low circularity and low crushing strength. Extrusion and spheronization was proven that it did not destructively affect the pellets specific surface area after calcination. However, this technique did not significantly increase the pellet's crushing strength, which could be because the clay primarily consisted of nanoporous starting material.

4.2 Introduction

Extrusion and spheronization is a multiple-step process capable of making uniform-sized spherical particles. In this process, the paste is extruded through a single die, a multi-hole die, or a screen featuring many holes. Then the extrudate is broken up

and rounded on a rotating friction plate to form spherical pellets. This process is also known as extrusion-marumerisation, where a Marumeriser is referred to the spheronizer that was patented by Nakahara in 1964 and commercialized by Fuji Denki Kogyo Co. under the trade name Marumerizer.

The extrusion and spheronization methods were widely used to prepare round shape pellet in pharmaceutical field, especially for micro cellulose bead (Muley et al., 2016; Bryan et al., 2015b; Bryan et al., 2015a; Lau et al., 2014; Sarkar et al., 2014; Zhang et al., 2013; Krueger et al., 2013; Zolkefpele and Wong, 2013; Mascia et al., 2010; Sriamornsak et al., 2008). As far as we know in literature reviews, preparation of clay or synthetic clay granule by extrusion-spheronization has not been proposed. Process for preparation of granules by extrusion and spheronization has similar steps, but, the rheological and physical and chemical properties of granule strongly depend on the powder properties.

Zhang et al. (2013) adopted a ram extrusion technique together with a spheronization technique to prepare microcrystalline-based granule. Effect of single- and multi-holed die on paste rheological such as extrusion parameter and pellet morphology was studied. The paste was prepared at 55% moisture content without using any additive. The liquid migration was found during ram pressing at low speed for a single-holed die, which then disappeared when the ram speed was increased. Liquid migration was not observed in ram extrusion using multi-hold die with the studied range of parameters studied. The pellet prepared without liquid migration was found to have good surface and narrow size distribution with the pellet circularity around 0.8. Ram extrusion with either single- or multi-hole die gave the similar result in this aspect. The pellet prepared with liquid migration was found to have broad size

distribution and poor shape characteristic. However, the spheronization parameters were not studied in this work.

Effect of paste mixing on extrusion-spheronization of microcrystalline cellulose was studied by Bryan et al. (2015b). Difference shear strain rate of pastes mixing studied using the paste with 55% moisture content and no additive. Ram extrusion with single- and multi-hole die was used in this study. It was found that the steady-state pressure of ram extrusion process increased with increasing of shear strain rate due to the reduced size of micro cellulose crystal resulting in unbound water reduction. Increasing of shear strain rate mixing resulted in decreasing of pellet size distribution. In addition, high shear strain rate mixing was found that it is given the bimodal pellet size distribution. These results also were the effect of the reduced size of micro cellulose at high shear strain rate. Effect of spheronization time on the circularity of the pellet was studied, and it was found that pellets with high circularity could be received from the process with long spheronization time.

More effect of spheronization parameters on the evolution of pellets during the spheronization process was studied by Krueger et al. (2013). The authors studied spheronization mechanism of micro cellulose pellet by exploring an effect of spheronization time, extrudate loading, and speed on the evolution of pellets during the spheronization process. The full 3^3 -factorial design was adopted to study the effect of those parameters. Pellets with good circularity were obtained at the long spheronization time, highest speed and highest extrudate loading. The pellet's equivalent diameter was found to increase with increasing of spheronization speed and time, whereas long spheronization time at low speed showed the opposite effect. Effect of extrudate loading on size pellet size appeared to be insignificant. The authors emphasized the large pellet

diameter achieved at high spheronization speed could possibly occur from the fines particle layered onto the pellet again during spheronizer. However, this result was contrasted with other works (Newton et al., 1995; Woodruff and Nuessle, 1972; Yoo and Kleinebudde, 2009; Wan et al., 1993).

Until now, only a few papers utilized the extrusion spheronization technique to prepare an adsorbent were found. Niu et al. (2014) used ram extrusion technique with single- and multi-hole die to prepare canola meal adsorbent used for ethanol dehydration in a packed bed column. With the properties of canola meal, the liquid migration in the extrusion step did not occur in neither processes with single-hole nor multi-hole die. The surface fracture was also not found. The pellets received after spheronization step was well in round shape. The authors confirmed that water uptake of the canola meal pellets was superior to the raw canola meal particles. However, the pellet tensile strength was low. Additives for improvement of the pellet mechanical strength were considerably needed.

Sun et al. (2016) were prepared carbide slag pellets by extrusion and spheronization for the application of CO₂ capture at high temperature. Three additives: cement as a binder, and microcrystalline cellulose as well as rice husk as pore-forming material, were utilized. The extrusion was done by a mini-extruder equipped the die with adjustable-diameters. Effect of extrusion and spheronization as well as effect of liquid migration not studied. Effect of calcination temperature on the adsorption properties was investigated. In this work, CO₂ adsorption decreased gradually with increasing calcination temperature. The specific surface area and average pore volume of pellets were decreased by 37% and 55% from those of the powder. However, the CO₂ sorption performance of the pellets after 25 adsorptions cyclic was lowered around

10% in comparison with the powder. Addition of biomass-based pore-forming materials (microcrystalline cellulose and rice husk) was found to enhance the CO₂ sorption performance of carbide slag pellets, and the addition of cement, appeared to improve the mechanical strength and maintain the relatively good CO₂ sorption performance of the pellets.

As the synthetic clay nano material have superior properties, but its properties have limited utilization in nano material or powdered form. Therefore, the knowledgeable of studies forming synthetic clay to the technical body become the important chance to fulfill the gap between the advanced synthesis powder and industrial utilization. This chapter was aimed to study of forming synthetic clay to the technical body with considerable on intermediate properties and flexibilities to adjust parameters of the forming technique, extrusion and spheronization.

4.3 Theory

The general process of extrusion and spheronization requires at least five units of operation with an optional seven screening step: (i) dry mixed; (ii) wet granulated or paste preparation; (iii) extrusion, (iv) spheronization and (v) drying and finishing and optionally (vi) screened and (vii) extrudate pellet cutting.

Influence of extrusion on the final granules is currently difficult to quantify. With many formulations, one cannot form spheres from the wet powder mass directly. It is firstly needed to be compacted and formed. The correct formulation will give spheres that are stable on the spheronizer plate for up to 30 second, and quality-quantified by granule shape and size distribution will be relatively insensitive to variations in operating parameters. It is also difficult to predict spheronisation

performance simply from monitoring the extrudate pellet quality, as not all smooth and well-compacted extrudates pellet give good spheres (Pinto et al., 1992).

4.3.1. Equipment

4.3.1.1 Dry mixing

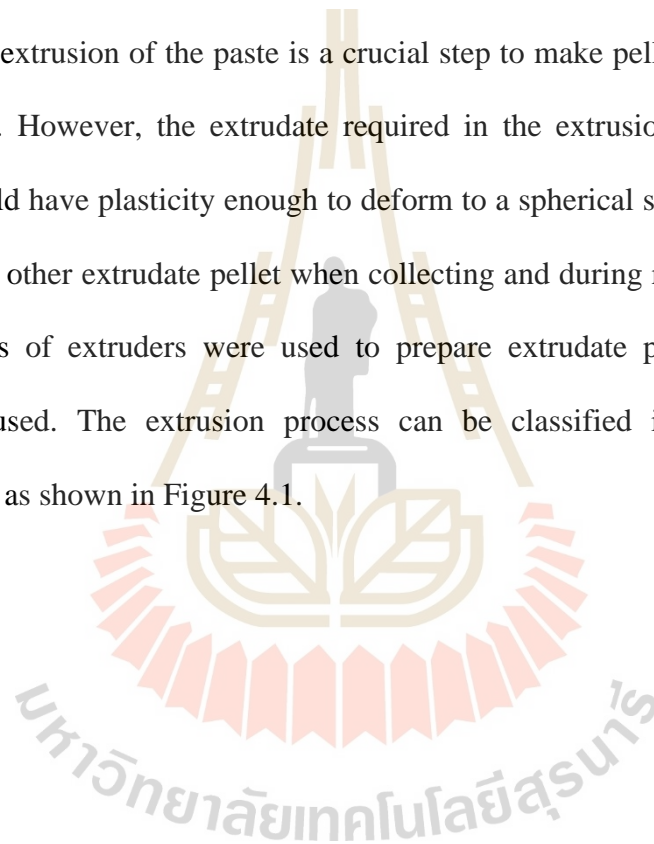
The dry mixing process is used to produce homogeneous powder dispersion before the process of paste preparation. Usually, it is carried out in the same mixing equipment used for the granulation; nevertheless, if a continuous granulator is used, a dry mixed process is normally prepared separately. The uniformity of dry powder mixed, however, probably significant effect on the quality of the granulation as well as the spherical pellet produced. Inhomogeneous of powder mixing may introduce of wide difference powder properties such as difference agglomerate size cause localized overwetting during the initial step of granulation. The fine powder or un-agglomerate power can also be dispersed and become part of the slurry. In addition, the final spherical pellet uniformity (size and shape) is very much dependent on the uniform distribution and composition of the granulating fluid, which includes not only the solvent but also any dispersed of fine powder as slurry form.

4.3.1.2 Granulation (paste preparation)

Generally, batch and continue are used in paste preparation processes. For the batch process, most types of powder mixers have been reported for preparing wet masse such as planetary mixers, vertical or horizontal high shear mixers, and sigma blade mixers while the continuous process is typically used screw extruders and particularly twin-screw extruders. The extruder which operated in the continuous process can be configured in separate zones, such as powder mixing, liquid addition, kneading then forming. The detailed paste preparation was already discussed in Chapter III.

4.3.1.3 Extrusion

The extrusion step is a process utilized to form the paste into the rod-shaped pellet. The paste is forced through the die by extruder formed the cylindrical extrudate pellet, which diameter of extrudate pellet equal to the die diameter. In typical, the extrudate pellet will be broken into cylindrical at different lengths due to its weight. However, to control the length of the extrudate pellet, the cutting head is usually applied. The extrusion of the paste is a crucial step to make pellets densifying (Juppo et al., 1997). However, the extrudate required in the extrusion and spheronization process should have plasticity enough to deform to a spherical shape and not so much adhere to the other extrudate pellet when collecting and during rolling in spheronizer. Several types of extruders were used to prepare extrudate pellet depends on the application used. The extrusion process can be classified into two mains feed mechanisms, as shown in Figure 4.1.



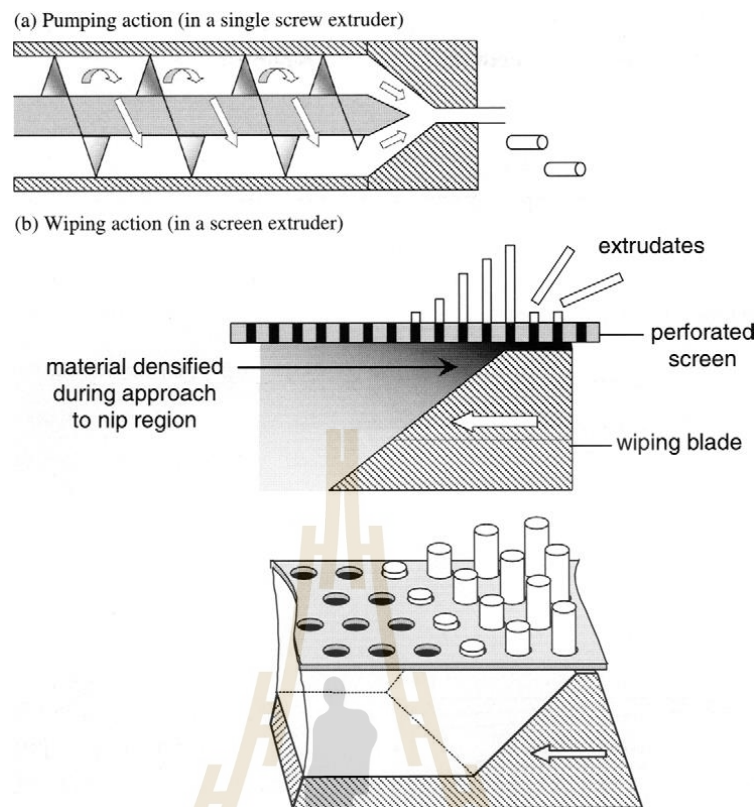


Figure 4.1 The feed mechanism of the extrusion process (Wilson and Rough, 2007)

1) Pumping action: ram, axial single, and twin-screw. The paste is compacted and removed the entrapped air within the pumping area, then paste deforming to the die resulting in a high density of extrudate pellet. The extrudate pellet density is also affected by the distance of the pumping area as well as the space between the beginning of the die and the end of the screw. For screw extruders, the closer screws will generate more compaction yield denser extrudate pellet. The spacing of paste volume before entering the die, increasing this volume space, given more compaction before extrusion.

2) Wiping action: roll, radial screen. The roll extruder is included the cylindrical and gear extruder. Both types are used the two rollers to

generate force deforming paste pass a screen or basket to form extrudate pellet while radial screen extrudate pellet has used the rotating blade to wipe the paste against the screen to form an extrudate pellet. The wiping action is no compaction before the extrusion zone; therefore, the density of extrudate pellet is lower than the pumping action type.

The type of extruder will mainly influence the density of the granules formed. The extrudate pellet with high dense granular can be prepared by the frontal extruder, such as axial and ram extruder. The medium density granular can be produced by the radial extruders, and the low density granular can be provided by dome or screen extruder. Figure 4.2 illustrates the action of different devices.

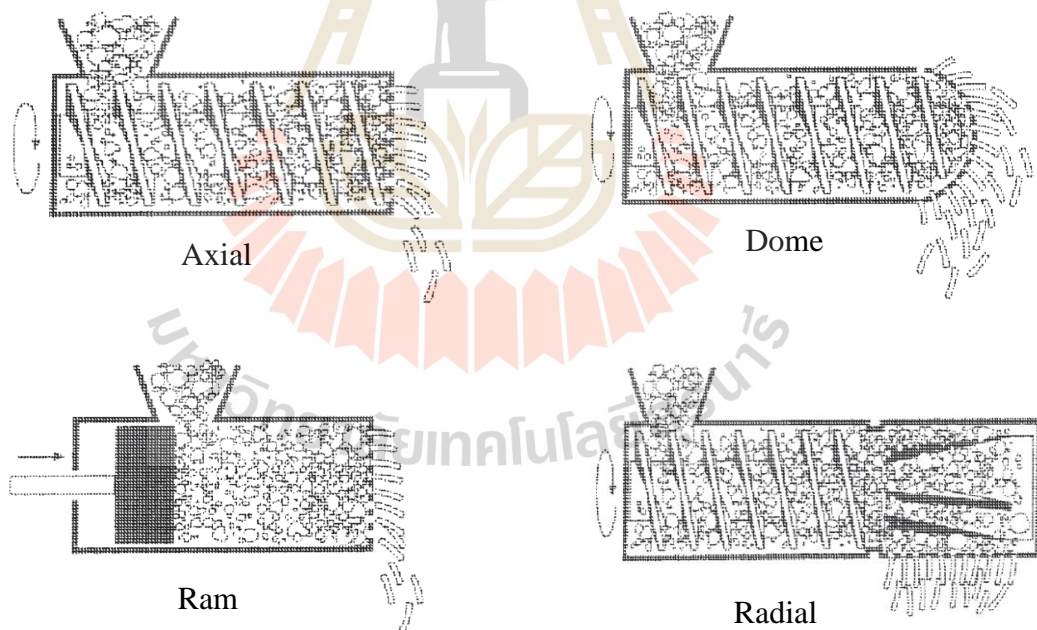


Figure 4.2 Several extruder types used in extrusion spheronization process

(Parikh, 2016)

4.3.1.4 Spheronization

A spheronizer consists of two main parts; a bowl is having a stationary cylindrical wall and a rapidly rotating bottom plate or disk with a grooved surface called friction disk, which connected with rotating drive shaft used to move disk and controlling disk speed. The configurations of the spheronizer illustrated in Figure 4.3.

In general, the extrudates with diameter larger than 5 mm is not recommended to be used in the spheronization process as it is hard to be chopped and rounded. The smallest diameter of the extrudates is limited by the manufacture of the extrusion hole. Drilling the die hole for extruders can be difficult for the hole with diameter smaller than 0.5 mm.

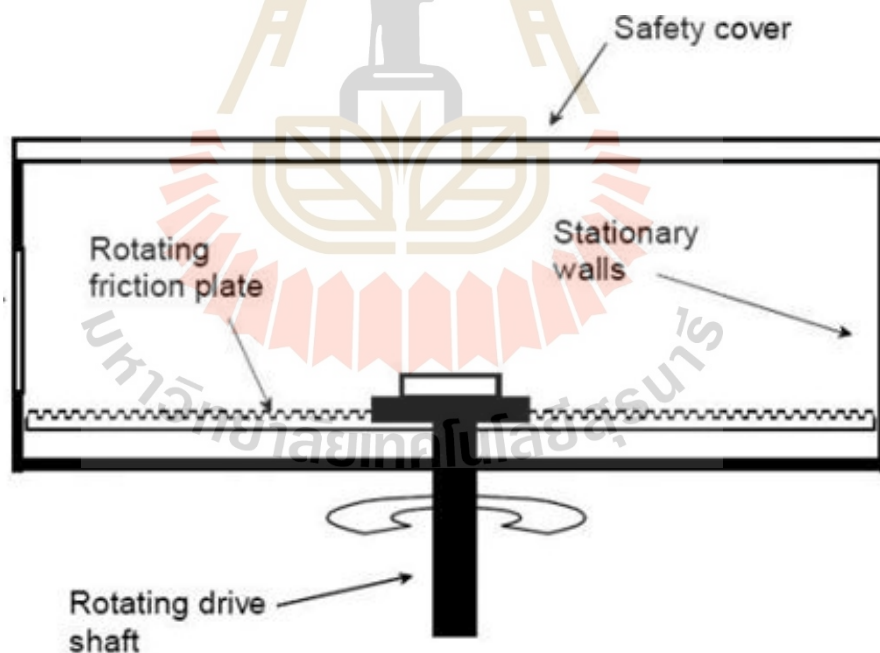


Figure 4.3 Schematic of spheronizer (www.arcon-foodpharma.cz).

Design of friction disk inside the spheronizer is also an important parameter that can influence the process performance. The friction disk is normally designed with the grooves surface to increase the forces generated as particles move across its surface and wall. Friction disk is typically designed and crafted into two patterns: a cross-hatched and the radial pattern, as illustrated in Figure 4.4.

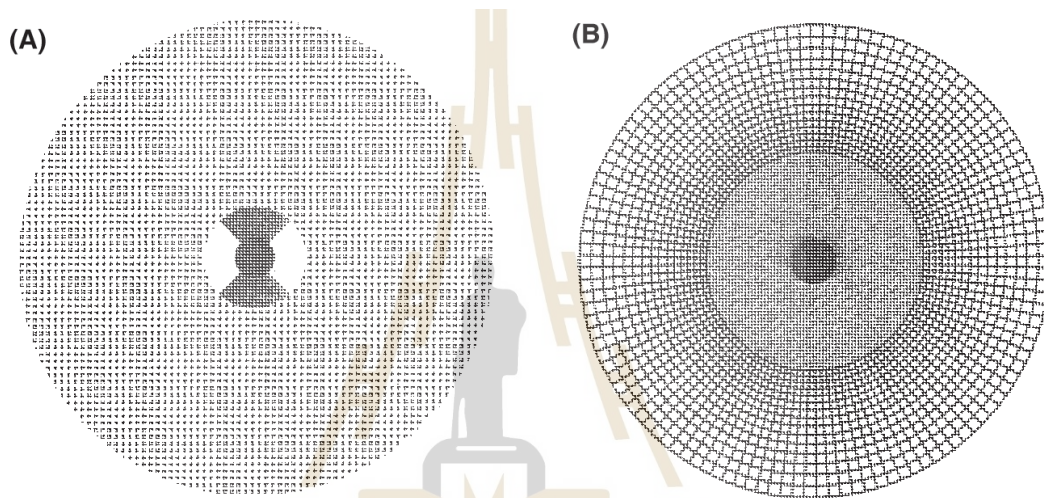


Figure 4.4 Friction patterns: (a) a cross-hatched pattern and (b) a radial pattern

(Parikh, 2016)

Three process parameters are normally used to optimize performance of spheronization process: load, speed, and time. Too low extrudate pellet load in spheronizer normally leads to decreasing contact between the pellets, contact with each other and too high load can increase space-time between friction disk and extrudate pellet. Similarly, low speed changes rod shape slowly, while high speed can result in particle size reduction via unwanted breakage. The spheronization time typically operates at 2 – 10 min; longer spheronization time can produce more

agglomerated pellets and probably pellet dry and resulting breakage while short spheronization time led to pellet not complete deforming to spherical shape as shown in Figure 4.5(b).

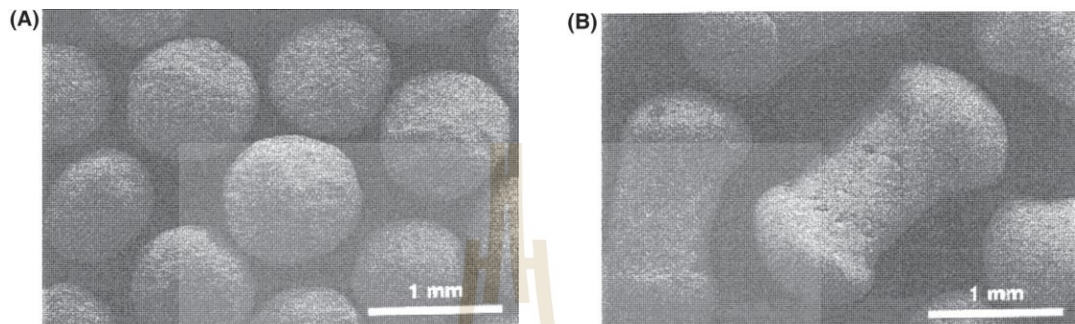


Figure 4.5 An example of (a) good spheres produced (b) dumbbells shape

(Parikh, 2016).

4.3.1.5. Drying and finishing

The final step of the forming process is the drying process. Typical dryers used for drying the pellet form extrusion and spheronization process are tray dryer, column type fluidized beds, and deck type vibratory fluid beds (Parikh, 2016; Wilson and Rough, 2007). Choices of drying equipment's depends on the desired of the rate of water removal. Tray dryer, for example, normally gives, the slowest rate while the fluidized bed provided a high evaporation rate.

4.3.2. Mechanics and mechanisms

4.3.2.1 Paste flow analysis

Rheology of the paste is very dependent on the amount of liquid present. As the liquid content is raised, the pores between the particles are filled first. Small amount on the extra liquid can then have a considerable effect on the thickness

of the films between particles and, consequently, a large effect on the paste properties. It is possible to vary the properties of paste by altering the size, size distribution, and shape of the particles used to form it. All extruder depends on a pressure difference being generated to press the paste through a die. The methods of generating pressure may differ considerably from one to another, but flow through dies is common to all extruder types. Thus, the important practical aspect of paste extrusion is the relation between the pressure and extruding velocity.

Benbow and Bridgwater (1993b) proposed a simple characteristic method for analysis of paste motion from the barrel through the die. Extrusion diagram and terminologies for the analysis are shown in Figure 4.6, and the characteristic model is illustrated in Equation (4.1).

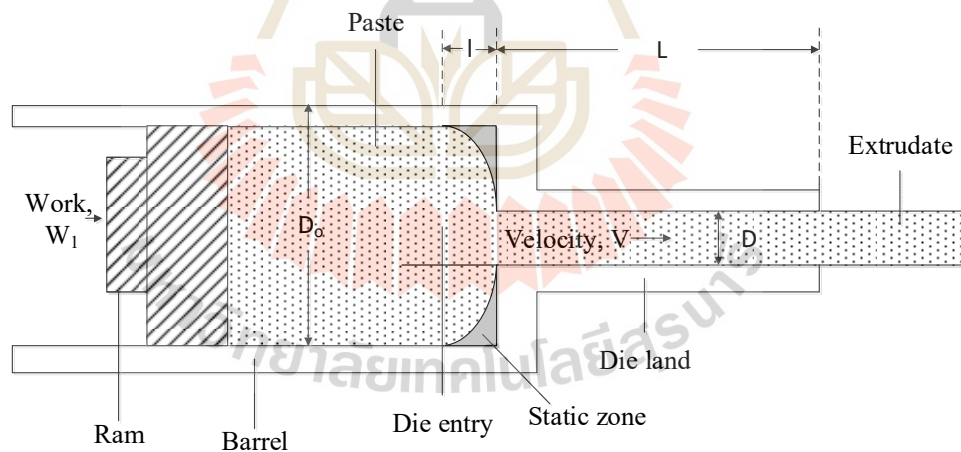


Figure 4.6 Terminologies in Benbow-Bridgwater analysis of ram extrusion

$$P = 2(\sigma_0 + \alpha V) \ln\left(\frac{D_0}{D}\right) + \frac{4L(\tau_0 + \beta V)}{D} \quad (4.1)$$

P is extrusion pressure, V is the paste velocity, σ_0 is the yield stress extrapolated to zero velocity, α is a factor characterizing the effect of velocity, τ_0 is the wall shear stress extrapolated to zero velocity, and β is the factor which accounts for velocity depending on the wall shear stress. The extrusion Equation (4.1) can be obtained by varying the extrusion velocity to different extrusion pressure. This equation has been widely used to study the paste rheology by many works (Bryan et al., 2015b; Azzolini et al., 2014; Vitorino et al., 2014; Niu et al., 2014; Powell et al., 2013; Liu et al., 2012). The extrusion parameters are used to design extruder's die as well as the operation parameter in screw extruder (Zhang et al., 2011; Ribeiro et al., 2009; Engländer et al., 2000). Ram extrusion technique is widely used to determine paste rheology, according to Benbow and Bridgwater model. Components of ram extruder are shown in Figure 4.7

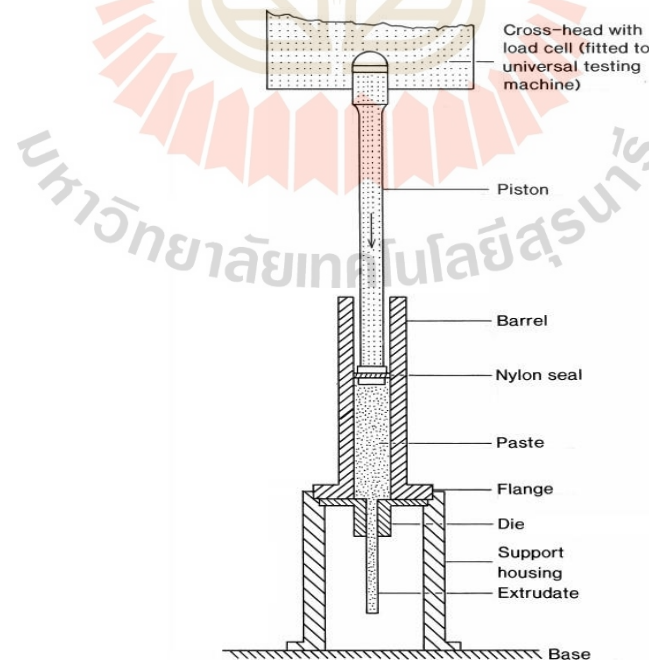


Figure 4.7 Ram extruder configurations

4.3.2.2 Extrudate surface fracture

Surface fracture of extrudates is one of the phenomena that can occur during extrusion step and may significantly affect the spheronization step (Harrison et al., 1985; Mesiha and Valltés, 1993). This phenomenon is called in different names such as feathering, dogs-teeth, and shark-skin. The extrudate with surface fracture is illustrated in Figure 4.8. Factors induce this phenomenon, in addition to the paste formulation, are die shape and extruding conditions (Benbow and Bridgwater, 1993a). Extruding conditions seem to be the most influential parameters. Improper conditions could lead to surface fracture even when the paste is well prepared and the die geometry is appropriate.



Figure 4.8 Surface fracture of extrudates (Rough and Wilson, 2005)

4.3.2.3 Liquid phase migration

Liquid migration is the phenomenon that liquid seep out from the paste due to a different moving rate of the paste components under the force of

pressure acting on the paste during extrusion. This phenomenon depends on the particle size distribution and the rheology of the liquid phase. High rate of liquid phase migration occurs when the permeability through the packing of the particles is high, and liquid viscosity is low. Liquid phase migration occurs during extrusion can lead to inhomogeneity in liquid content and compaction force of the paste resulting in non-uniform moisture content and paste density. Effect of this phenomenon will be more pronounced in the spheronization stage.

According to Benbow and Bridgwater (1993a), the liquid migration effect can be detected in three ways:

1. Liquid droplets appear at the die exit. The liquid normally migrates to and accumulates at the die exit, which is the region with lower pressure or force. Droplets are formed and easily observed there.
2. High extrusion pressure is observed even when the operation is at low velocity, which allows the liquid more time to penetrate through pores between the particles.
3. For the case of ram extrusion, the extrusion force increases with increasing the ram traveling distance, as illustrated in Figure.4.9. The liquid seeps out from the paste during extrusion can led to paste lack in plasticity resulting in high force resistance during an extrusion.

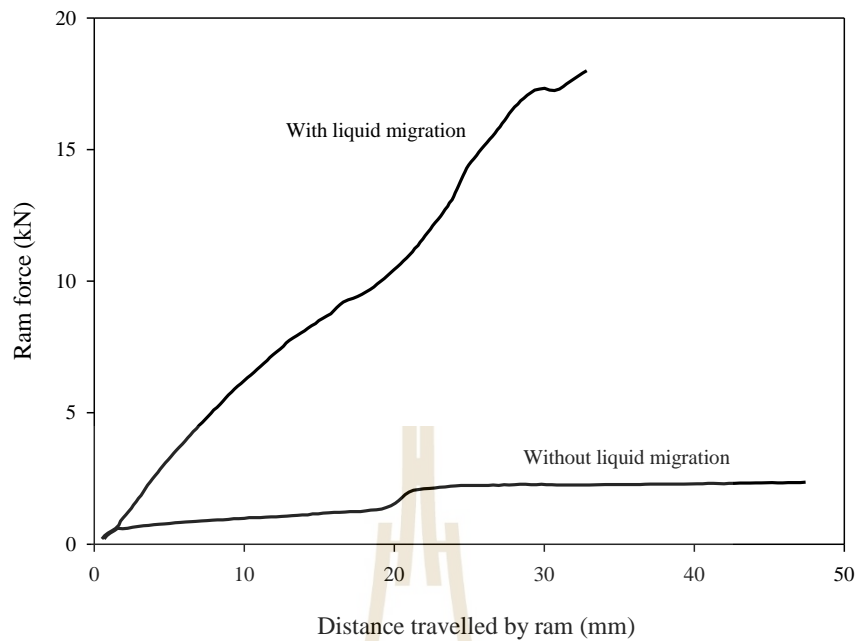


Figure 4.9 Ram extrusion profile with and without liquid migration (Benbow and Bridgwater, 1993a)

4.3.2.4 Wall slip

Wall slip is a common feature of paste extrusion, and can happen when the paste moves in plug flow mode, where deformation of the paste in contact with the die wall is possible, as illustrated in Figure 4.10. Liquid migration at the interface between the paste and the die wall can create a liquid-rich layer, which may act as a lubricant and allow the paste to slip against the wall. Increasing pressure by increased ram speed, can increasingly generate slip layer and, thus, decrease the wall friction resulting in decreasing extrusion pressure (Panaseti et al., 2013).

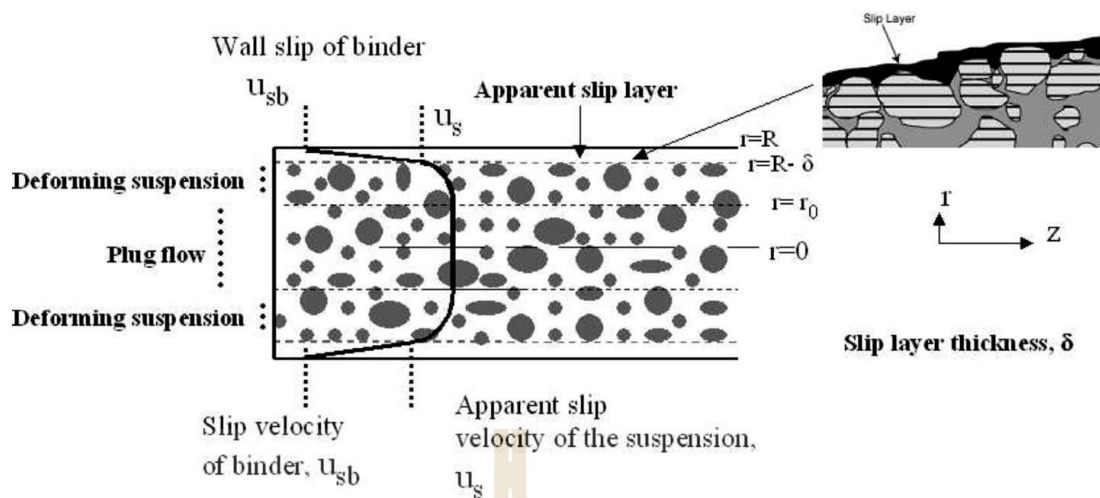


Figure 4.10 Effect of wall slip on extrusion profile (Zhang et al., 2017)

4.3.2.5 Spheronization

Evolution of cylinder shaped extrudate into a sphere typically occurs in three models during spheronization as shown in Figure 4.11. In the first pathway, the extrudates are broken up into short rods due to collision with the friction disk, spheronizer blow, and other extrudates. The edges of the rod starts to deform and drumbell-shaped bodies are gradually formed. Further spheronization induces deformation of the drumbells into ellipsoid or egg-shaped body and finally a sphere due to its plasticity (Rowe, 1985). The second pathway is where the extrudate is first formed into a rope shape due to its more viscous than the first pathway. Then, the collision with the wall, friction disk, and other pellets cause the rope-shaped pellet to twist and break into sub-pellets. Continue action in the spheronizer causes the pellet to round off into the sphere. The twisting action was claimed to explain why some pellets contain a cavity (Baert et al., 1993). In the third pathway, fine particles from extrudate breakage

refill to the mid-plane of dumbbell-shaped pellet and form it into a sphere. subsequently re-attach to larger pellets (Liew et al., 2007; Koester et al., 2012).

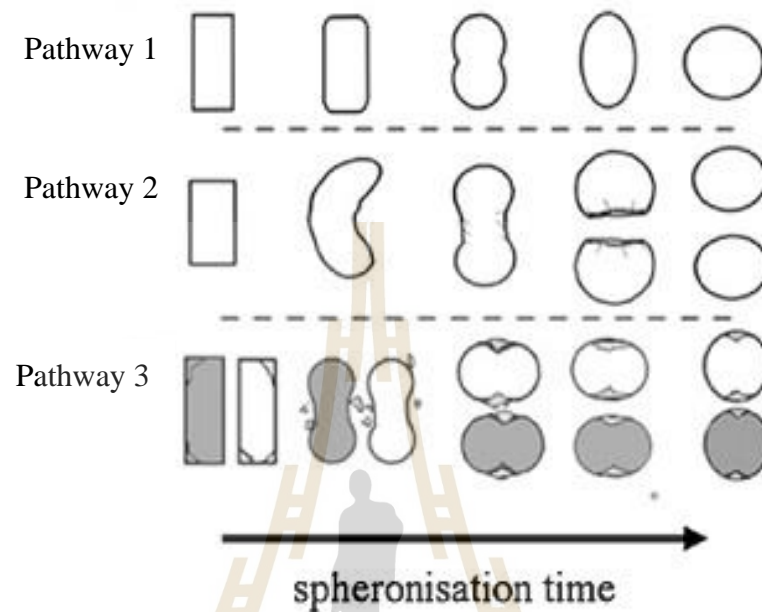


Figure 4.11 Models for evolution of extrudate pellets in spheronization (Bryan et al., 2015a)

4.4 Experimental

4.4.1 Extrudability and extrudate preparation

Extrudability of synthetic clay paste with selected composition was analyzed by ram extrusion technique using a high-pressure capillary rheometer (GÖTTFERT, RG20) at various extrusion velocity and different die length to diameter (L/D) ratio, as shown in Table 4.1. The suitable extrude conditions were chosen to prepare extrudate for spheronization step.

Table 4.1 Die geometry used in the extrudability analysis

L/D	Die diameter (mm)	Die length(mm)
2	3.18	6.35
4	3.18	12.70
8	3.18	25.40

4.4.2 Extrudate cutting

Green extrudates received from extrusion were kept in a plastic zip bag and stored in the ice bucket to prevent moisture loss before and during cutting. The extrudate was then manually cut by a knife into pellets with L/D ratio close to 1.

4.4.3 Spheronization

The spheronizer used in this study was designed and constructed as shown in Figure 4.12. The bowl diameter was 120 mm and the spheronization disk was 120 mm. Speed of spheronization was controlled by the speed controller. The first step of the spheronization experiment was to set-up the spheronizer and to adjust the speed of the friction disk at design value. The cut-extrudate pellets were then put into the spheronizer. After the designed operation time, the spheronization was stopped and then granules were removed from the bowl and stored for further analysis. Effect of spheronization time (ST), friction dish speed (SS), and extrudate loading (EL) on shape and strength of the received granules were studied.

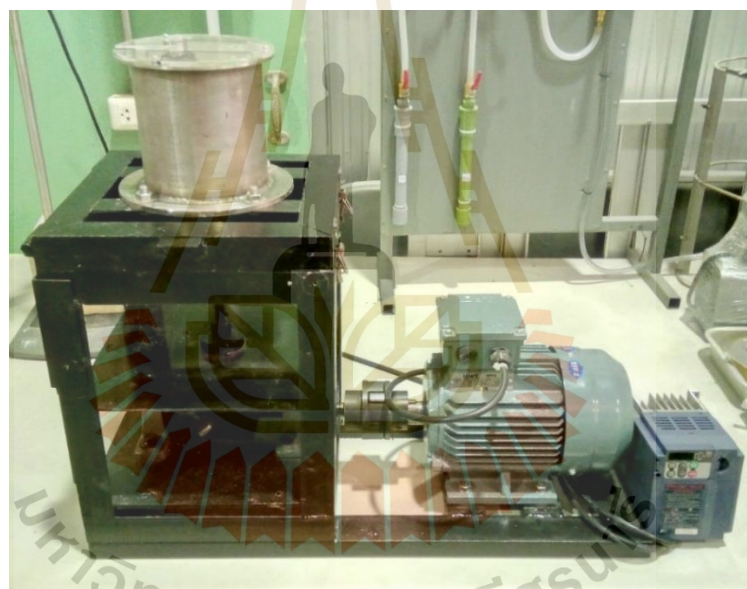
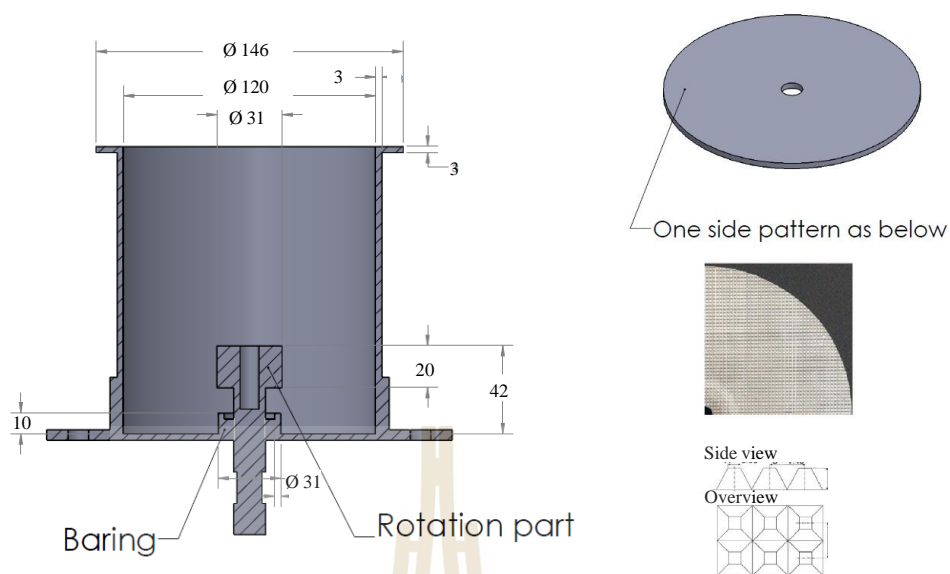


Figure 4.12 Design and construction of the spheronizer used in this thesis.

4.4.4 Material characterizations

The specific surface area of the spheronized granules was determined by Brunauer-Emmett-Teller (BET) method. The nitrogen adsorption-desorption isotherms were measured at 77K (BelSorp mini II , Bel Japan). Before each analysis, the samples were degassed overnight at 110°C for the sample without calcination and 300°C for the

calcined sample. Morphology and shape of the pellets were characterized by an image analysis method. The pellet shape was indicated by pellet circularity (Cps). The spherical pellet shape was given the circularity equal to 1. True density of the extrudate was analyzed by a helium stereopycnometer (Quantachrome multi pycnometer, Florida, USA), where the extrudate was ground into powder in order to remove most of the internal pores (Krokida et al., 1998). Three repetitions were done for each analysis. Crushing strength of the pellet was measured by the universal testing machine, as illustrated in Figure 4.13. Fifty pellets of calcinated pellets were used for each test. The piston speed was fixed at 1 mm/s. The first strength crack was recorded by UTM software, as illustrated in Figure 4.14.



Figure 4.13 Crushing strength experimental setup

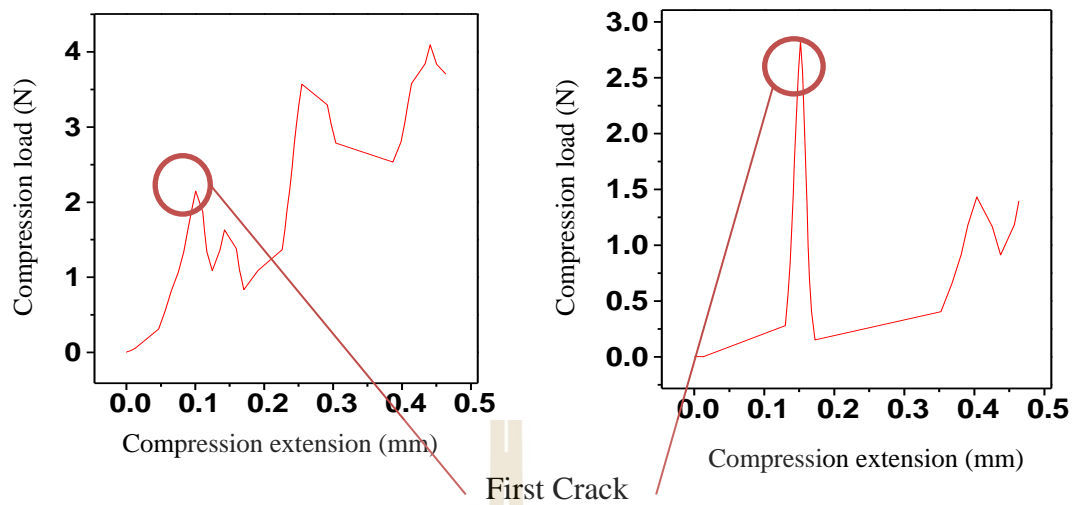


Figure 4.14 Illustration of pellet's first crack during crushing strength test.

The strength recorded at pellet's first crack was used to calculate the pellet's crushing strength (Li et al., 2000; Badoga et al., 2017) as

$$\sigma_{fc} = \frac{2.8F_{fc}}{\pi d^2} \quad (4.2)$$

where σ_{fc} is crushing strength at the first crack, F_{fc} is the first fracture force, d is diameter of the spherical pellet.

4.4.5 Pellet drying and calcination

The green pellets from the spheronization were dried in ambient temperature for 3 days to prevent pellet cracking due to fast evaporating of water inside pellets. The calcination temperature was selected to be at 550°C to induce Lewis-acid properties of the material as shown in Figure 4.15. Water content in the clay was removed by heating it to the temperature around 100°C, where the clay with strongly Bronsted acidity was received. Continuing heating to around 200-300°C led to complete

removal of the water and resulted in the collapse of the clay interlayer. Bronsted acidity was decreased, while the Lewis acidity was increased upon this heating. Heating the clay to the temperature around 450°C caused elimination of hydroxyl group and resulted in entirely amorphous solid with Lewis acidity (Kaur and Kishore 2012).

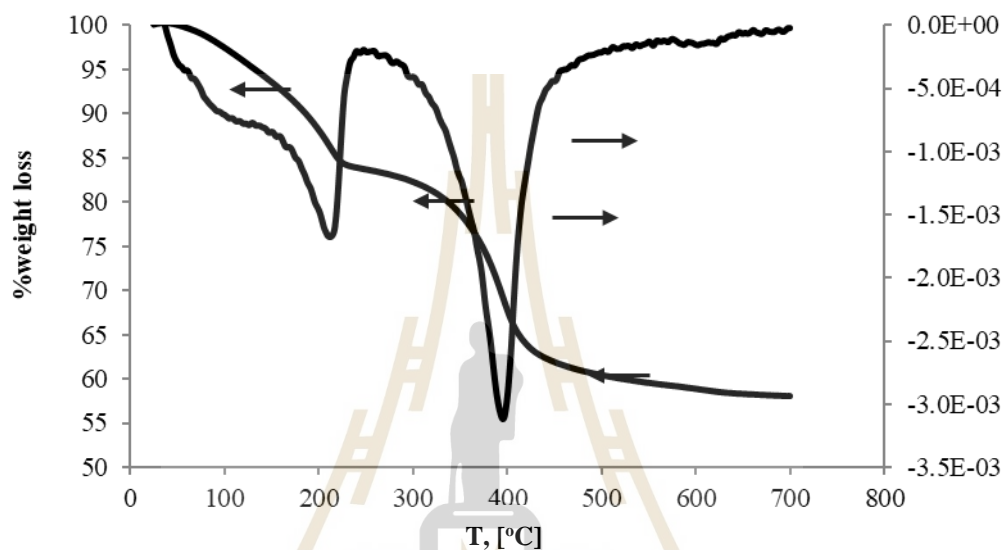


Figure 4.15 TGA-DSC analysis of synthetic clay powder

4.4.6 Experimental design and statistical analysis for spheronization

Experimental design for spheronization experiment was carried out using Box-Benhken method, which is the same one used in the paste preparation part. Three independent variables: including extrudate loading (EL), spheronization time (ST), and spheronization speed (SS), were utilized to investigate effect of process variables on pellet shape and pellet strength using 15 different combinations including three replicates at the center point. The level of parameters for the experimental design in spheronization are shown in Table 4.2.

Table 4.2 Middle value of spheronization parameter for Box-Benhken method.

Variables	Levels		
ST, [min]	1	2	3
EL, [g]	10	20	30
SS, [rpm]	600	900	1200

4.4.7 Pellets strength improvement study

To improve the pellet strength, the extrusion spheronization experiments were carried out by utilizing additives, adjusting the calcination temperature, and using the intermediate powder of different morphologies.

4.4.7.1 Additives utilization

Two additives were utilized in this study, polyvinyl alcohol (PVA) as a viscous liquid and boehmite or aluminium oxide hydroxide (γ -AlO(OH)) as a binder (Mitchell et al., 2013). The viscous liquid was used to decrease an effect of liquid migration during extrusion. This, in turn, appeared to as well decrease wall slip effect resulting in high compaction force in extrudate pellet during extrusion. The alumina binder had been reported to enhance mechanical strength during calcination of the pellet (Mitchell et al., 2013). The PVA solution was prepared by dissolving PVA (Loba Chemie) in DI water at 85°C until clear liquid was obtained. To prepare alumina nano solution, the alumina boehmite (Salson) was peptized in nitric acid at pH lower than 3 (Fauchadour et al., 2000; Zheng et al., 2014). The peptized boehmite was dried at 110°C overnight and dispersed again in DI water before use. Extrusion and spheronization of the pastes without and with additives was carried out under the same operating conditions as previously described. In this study, concentration of the PVA solution was varied at 1 and 3% wt and that of the boehmite solution was varied at 3 and 5% wt.

4.4.7.2 Calcination temperature

Effect of calcination temperature was studied at 450, 550, and 650°C. According to the result from TGA-DSC, increasing calcination temperature usually results in removing of the hydroxyl group in the interlayer of clay, which will enhance the solid-solid contact between the clay sheets. To study the effect of calcination temperature, the pellets from the same batch of extrusion and spheronization were separated into three parts and calcined at different temperatures.

4.4.7.3 Sources of intermediate powder

The spray-dried powder prepared according to the methodology described in Chapter II was used in this part. Effect of morphology and shape of intermediate powder prepared by different drying techniques was investigated paste extrudability of the paste at its plastic limit. The extrusion, spheronization, drying and calcination steps were carried out at the same conditions as in the selected case from the oven-dried powder.

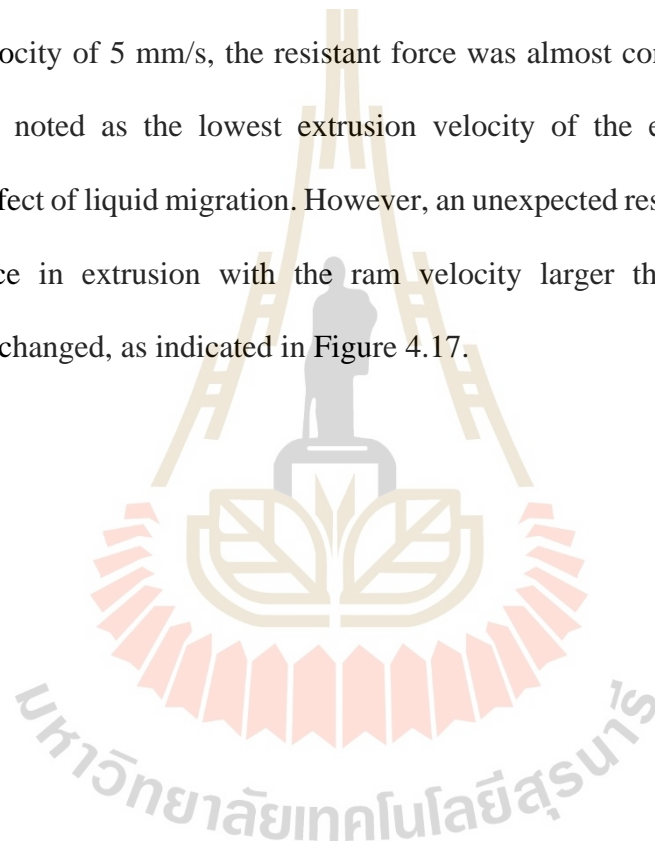
4.5 Result and discussions

4.5.1 Paste flow analysis

Different extrusion pressure, which will be used to estimate extrusion parameters, was obtained by varying the extrusion velocity in the ram extrusion process. Extrudability region is important for material extrusion; high extrusion velocity causes a surface fracture, and low extrusion velocity leads to liquid migration. Therefore, the extrusion parameter were estimated at the highest extrusion velocity without surface fracture and lowest extrusion velocity without liquid migration.

Liquid migration was found to increase with increasing die length (Rough et al., 2000); therefore, the most extended die length ($L/D=8$) was selected for the determination of the lowest extrusion velocity. Results from experiments with different extrusion velocities were shown in Figure 4.16.

At low extrusion velocity, the resistant force was found to increase with increasing ram distance, which was likely due to effect of liquid migration. At the extrusion velocity of 5 mm/s, the resistant force was almost constant. Therefore, this velocity was noted as the lowest extrusion velocity of the extrusion region with acceptable effect of liquid migration. However, an unexpected result was observed. The resistant force in extrusion with the ram velocity larger than 5 mm/s was not significantly changed, as indicated in Figure 4.17.



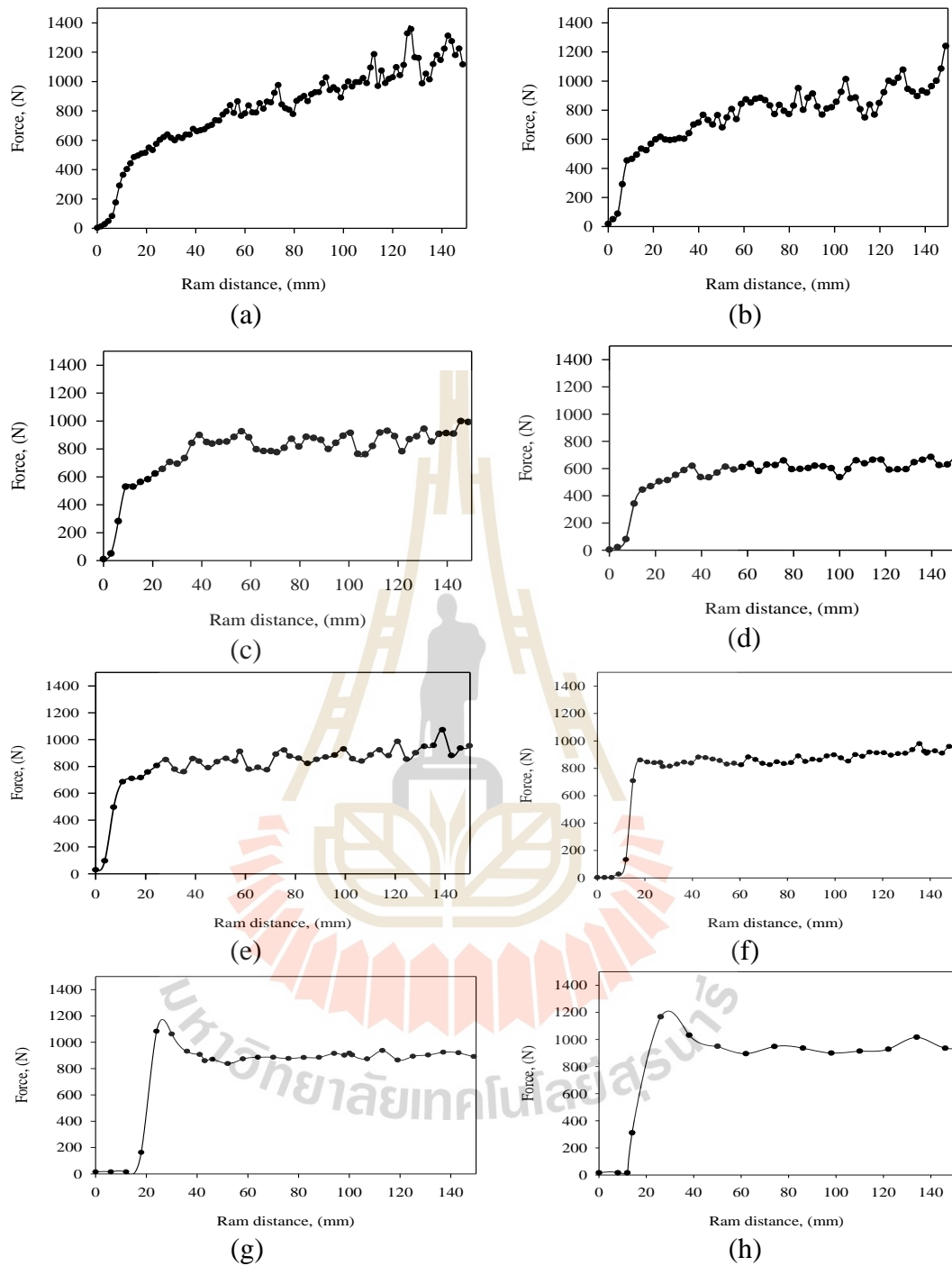


Figure 4.16 Extrusion pressure profile for extrusion with die L/D ratio = 8 and different velocities: (a) $V=0.5$ mm/s, (b) $V=0.7$ mm/s, (c) $V=1.0$ mm/s, (d) $V=1.2$ mm/s, (e) $V=1.5$ mm/s, (f) $V=5.0$ mm/s, (g) $V=10.0$ mm/s, (h) $V=20.0$ mm/s

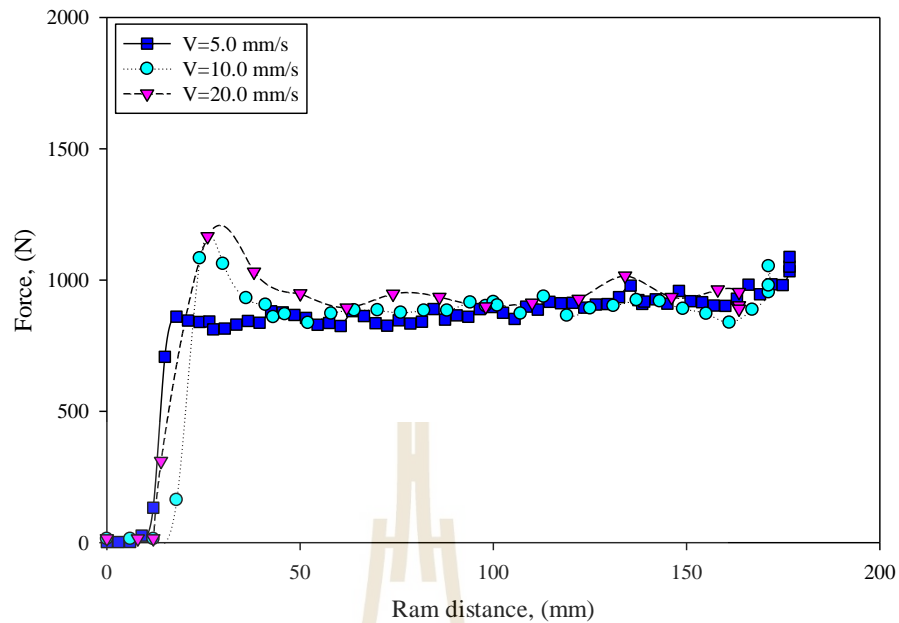
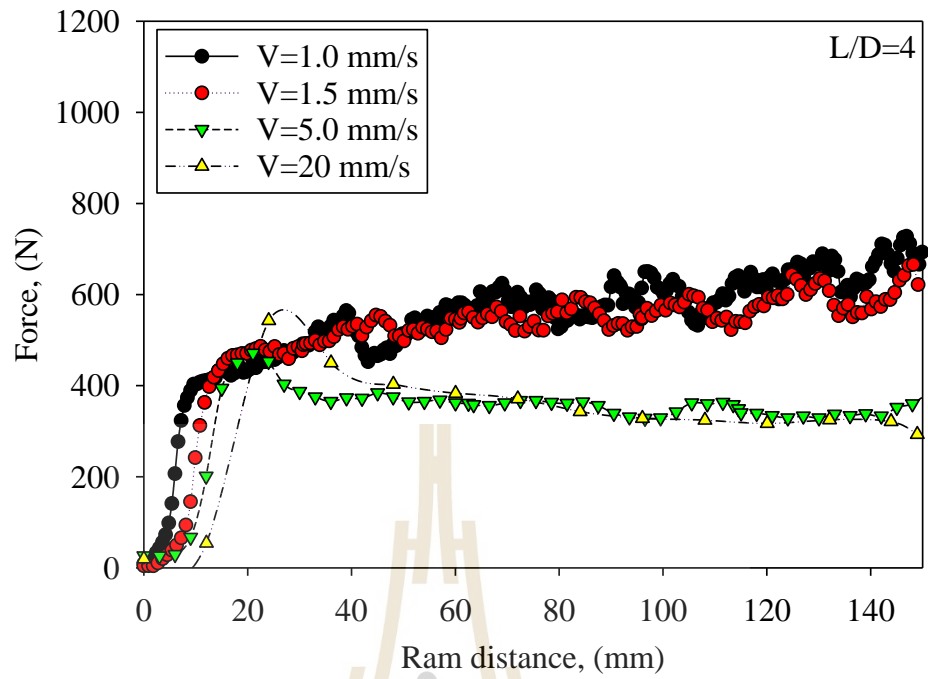
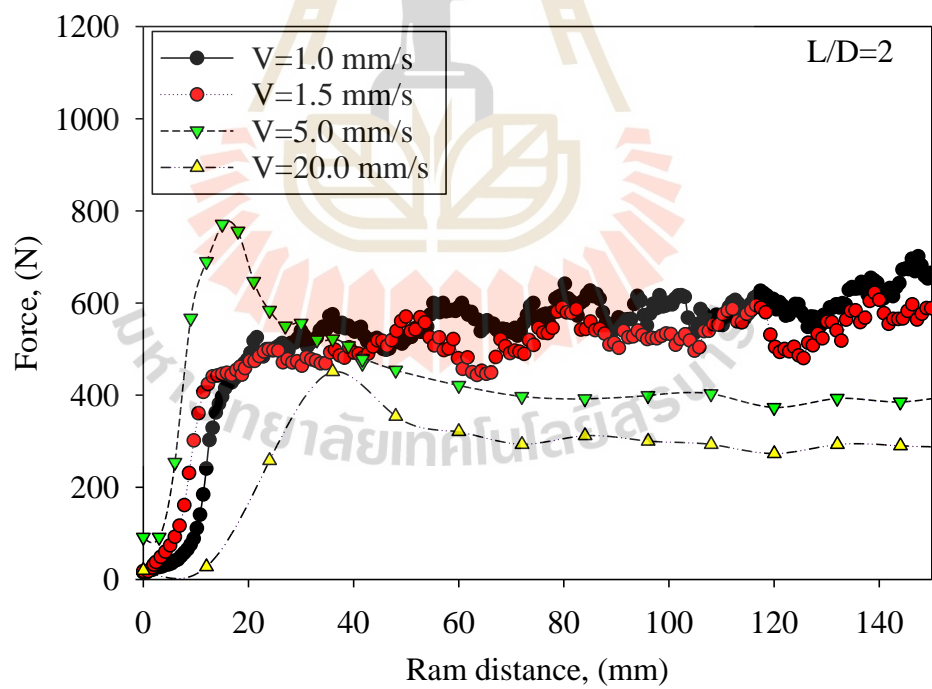


Figure 4.17 Wall slip effect on ram extrusion at high velocity

This extrusion behavior likely occurred due to the effect of wall slip (Kocserha et al., 2017) caused by the liquid with high velocity that migrated from the paste to the die wall and formed the liquid film leading to a decrease in paste resistance at the die wall. Similar behavior was also observed in extrusion with dies of different geometry, as shown in Figure 4.18.



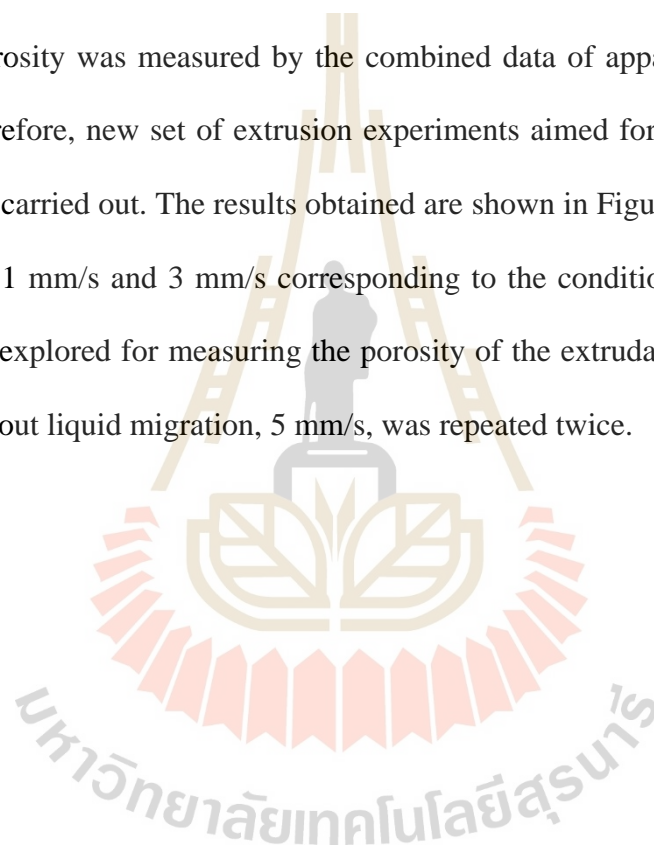
(a)



(b)

Figure 4.18 Wall slip effect at different die geometry (a) at $L/D=4$ and (b) at $L/D=2$

Variation of extrusion pressure was not observed due to the material behavior, and extrudate fracture was not found due to the wall slip effect. The extrudability region, as well as the extrusion parameter, were not determined. Therefore, another criterion for selecting the extrusion conditions was explored. Porosity of dried extrudate was selected for screening suitable extrusion velocity for the ram extrusion process. According to Tsokolar-Tsikopoulos et al. (2015), the extrudate porosity was measured by the combined data of apparent density and true density. Therefore, new set of extrusion experiments aimed for analysis of extrudate porosity was carried out. The results obtained are shown in Figure 4.19. The extrusion velocities of 1 mm/s and 3 mm/s corresponding to the condition of liquid migration were also re-explored for measuring the porosity of the extrudate. The first extrusion velocity without liquid migration, 5 mm/s, was repeated twice.



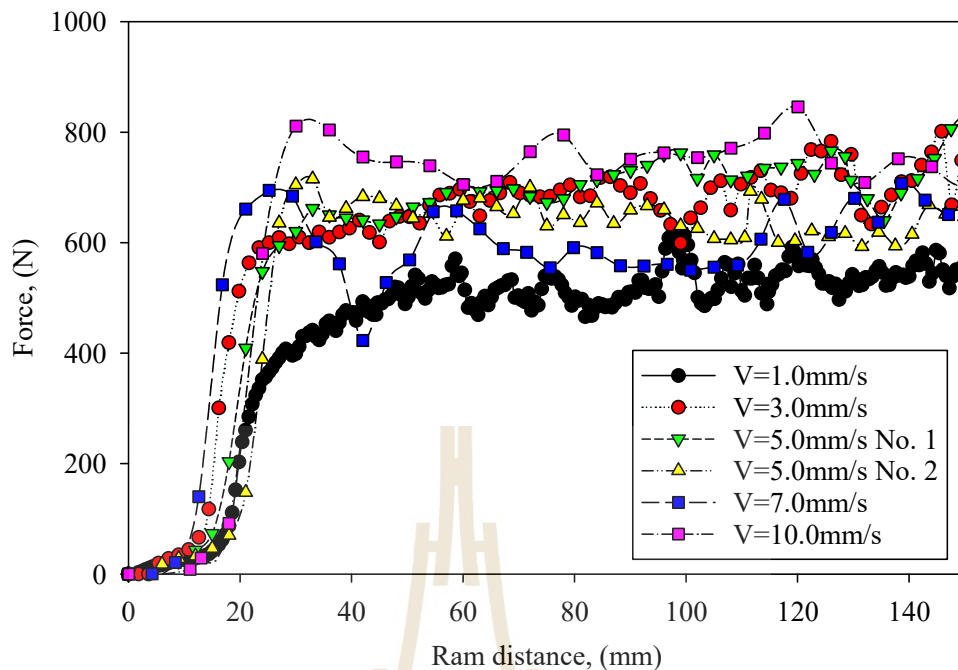


Figure 4.19 Extrusion pressure profiles used for analysis extrudate porosity

Extrusion pressure profile extrusion velocities of 1 mm/s and 3 mm/s again showed the liquid migration behavior, while the profile at extrusion velocities of 5, 7 and 10 mm/s showed slight fluctuations before approaching constant value of force, which indicated that steady-state extrusion was attained. These data also confirmed that, after the wall slip effect appeared, liquid migration was not influenced by other variables. Values of the steady-state resistant force was slightly different for different batches of extrusion due to the sensitivity of paste preparation.

Before determination of the extrudate's apparent density, the green extrudate was cut at length-to-diameter ratio closed to 1 and dried at the ambient temperature. Moisture loss of the extrudate was monitored by measuring the moisture in the extrudate by the oven-dried method. Figure 4.20 illustrates the moisture loss of the extrudate as a function of time upon drying at ambient temperature. The extrudate

pellet moisture content inside the extrudate pellet appeared to be almost constant after drying period of 3 days. The apparent and true densities of the dried extrudate were measured, and the results are shown in Table 4.3.

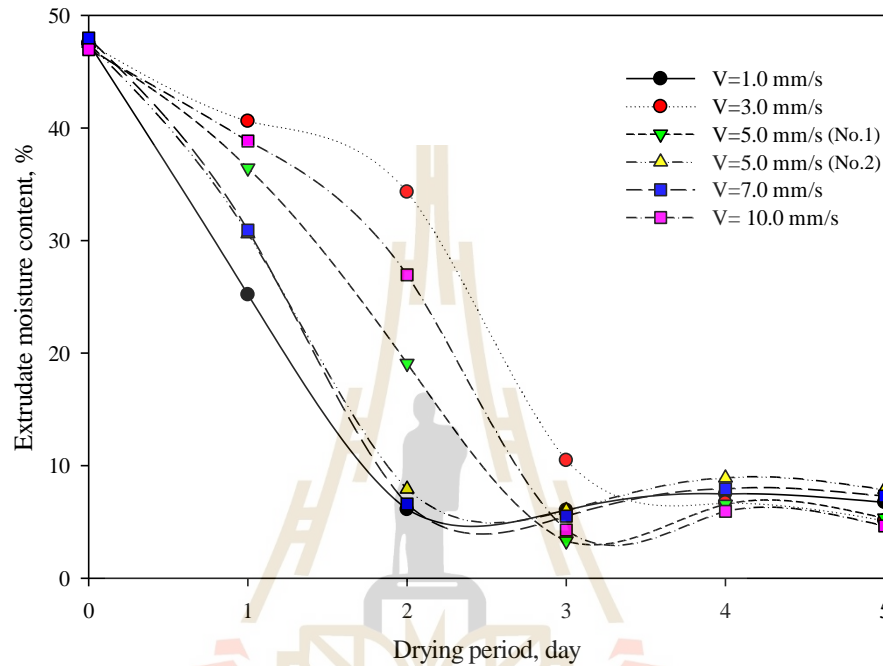


Figure 4.20 Moisture content of green extrudate during drying at ambient temperature

Table 4.3 Apparent density, true density, and porosity of dried extrudate.

Extrudate velocity, (mm/s)	Apparent density, (cc/g)	True density, (cc/g)	Porosity, (-)
1	0.772	1.9923	0.613
3	0.791	2.0322	0.611
5 (No.1)	0.783	2.0297	0.614
5 (No.2)	0.777	2.0181	0.615
7	0.777	1.9863	0.609
10	0.791	1.9964	0.604

The calculated porosity of the extrudates prepared at different extrusion velocities did not differ significantly. The extrudate porosity, though, appeared to slightly decline at very high extrusion velocities of 7 mm/s and 10 mm/s, which could likely be due to the low space-time in the die land and the larger effect of wall slip (Kocserha et al., 2017).

The extrudate compaction was limited by the wall-slip effect, and the highest compaction pressure was obtained from extrusion with the longest die. High extrusion velocity did not improve the compaction force on extrudate pellet. In contrast, it probably caused the decrease in the internal particle arrangement. This hypothesis was supported by Al-Azzawi and Kanaan (2017), and Alazzawi et al. (2017), who mentioned that increasing extrusion velocity decreased the extrudate pellet green body strength and introduced high extrudate pellet porosity. Therefore, with this support of information above, the longest die length ($L/D=8$) and lowest extrusion velocity at 5 mm/s that brought about extrusion without liquid migration were selected for extrusion condition.

4.5.2 Spheronization

Experimental screening for process parameter of the spheronization process was explored by spheronizing of the green extrudate prepared in the extrusion step. Condition for the screening experiment was set at $EL = 10$ g, $ST=2$ min, and $SS = 1000$ rpm. Figure 4.21 shows the spheronized granules received from the screening experiment.



Figure 4.21 Spheronized granules from the spheronization screening experiment.

A large lump of granules was observed in the screening experiment. This probably due to the plasticity and sticky surface of synthetic clay. The plasticity of clay led to extrudate pellet not broken into small parts tend to form a dumbbell-shaped pellet (Koester et al., 2012; Bryan et al., 2015a). The sticky surface of clay pellet was due to liquid migrated from internal extrudate to its surface which liquid migration driven by rotating friction dish when the extrudate impinge it.

The spheronization process was hindered by the two main behaviors of the synthetic clay, as mentioned above: liquid migration and plasticity. During the screening experiment, it is observed that some extrudates stuck to the wall of spheronizing bowl acted as the origin of pellet crumbles. This behavior was due to the

wet surface of spheronizer wall. Therefore, the system of circulating hot water around the outside wall of spheronizer was added to evaporate moisture inside spheronizer wall surface. Moreover, the cutting process was also added for improved pellet sphericity and pellet size distribution.

By applying the both process above, the synthetic clay spherical pellets were successfully prepared by a spheronization process, as shown in Figure 4.22.



Figure 4.22 Spherical synthetic clay pellets obtained by extrusion and heated-wall

4.5.3 Response surface design of spheronization process

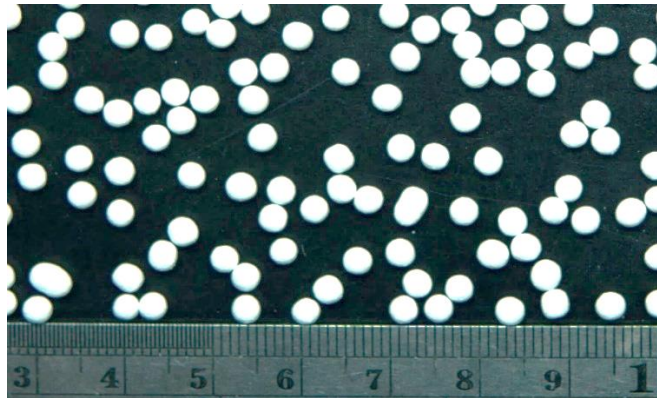
The response surface design for the spheronization process and the response data obtained from experiments are shown in Table 4.4.

Table 4.4 Experimental design for spheronization and the process response data.

Run Order	Load (g)	Time (min)	Speed (rpm)	Equivalent Diameter (mm)	Crush Strength (N/mm ²)	Cps (-)
1	20	2	900	3.15	0.42	0.927
2	20	1	1200	3.21	0.43	0.927
3	20	3	600	3.11	0.40	0.922
4	20	2	900	3.21	0.62	0.933
5	15	3	900	3.17	0.58	0.944
6	25	2	600	3.34	0.35	0.901
7	25	2	1200	3.30	0.33	0.927
8	15	2	1200	3.22	0.32	0.933
9	15	2	600	3.28	0.33	0.911
10	25	1	900	3.25	0.40	0.918
11	20	2	900	3.22	0.36	0.938
12	20	3	1200	3.06	0.38	0.941
13	20	1	600	3.33	0.42	0.920
14	25	3	900	3.25	0.38	0.914
15	15	1	900	3.34	0.31	0.928

4.5.4 Pellet morphology

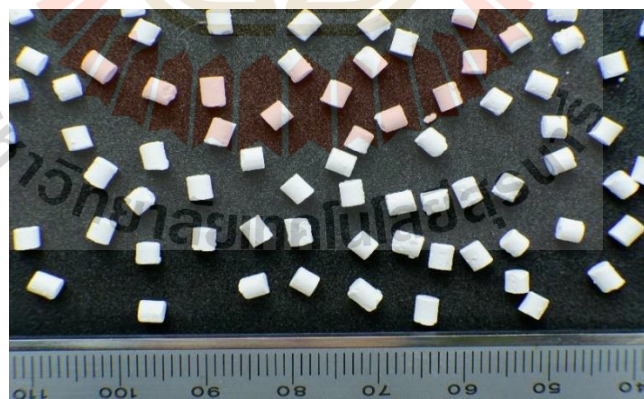
All experiments in the response surface design were successful preparation of spherical pellets with smooth surface. However, formation of elongated granules due to pellet sticking was also found in all tests. Circularity of the spheronized pellets, determined by image analysis, was found to be in a range of 0.901 to 0.944, as shown in Figure 4.23. The elongated granules were not included in the circularity estimation.



(a) $CPS = 0.944$



(b) $CPS = 0.901$



(c) $CPS = 0.812$

Figure 4.23 Shapes of pellets with different circularity (a) spheronized pellets with the highest circularity (b) spheronized pellets with the lowest circularity and (c) cut extrudates before being spheronized

Pellet size distribution is shown in Figure 4.24. As expected, pellets collected after spheronization had narrower size distribution after spheronization due to the control of starting extrudate size. The slight difference in the mean pellet size was likely because the extrudates were cut by hand before being spheronized.

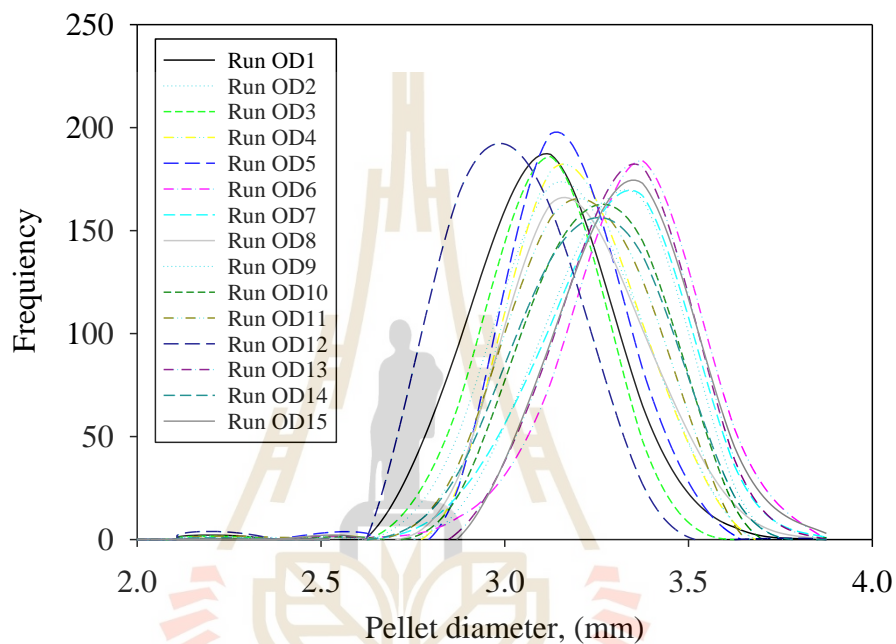


Figure 4.24 Pellet size distribution after extrusion and spheronization

4.5.5 Statistical analysis

Effect of spheronization parameters on pellet shape and strength was considered by constructing the response model equation. The pellet size was not considered as the response variable here because the pellets were cut by hand before being spheronized. The response model for pellet shape and crush strength at 95% confidence ($P < 0.05$) and high coefficient of determination (R^2) could not be realized, so, both models were constructed at a 90% confidence interval ($P < 0.1$) to study the effect of process on the response value. Terms of the square of a main effect and

interaction parameters with large P-value ($P > 0.1$) were excluded from the regression metamodel. The regression analysis was carried out to confirm the applicability of the proposed regression model.

Table 4.5 Statistical analysis of pellet shape

Source	Coefficients	Standard Error	P-value	
Intercept	7.342E-01	5.954E-02	0	
EL	1.189E-02	5.160E-03	0.047	
ST	3.567E-03	2.189E-03	0.138	
SS	1.632E-04	6.468E-05	0.033	
EL ²	-3.319E-04	1.285E-04	0.030	
SS ²	-7.347E-08	3.570E-08	0.070	
ANOVA				
	df	SS	MS	F
Regression	5	0.0016	0.0003	8.1764
Residual	9	0.0003	3.8347E-05	
Total	14	0.0019		

$R^2 = 0.8196$

Table 4.6 Statistical analysis of pellet crushing strength

Source	Coefficients	Standard Error	P-value	
Intercept	0.418	0.190	0.051	
EL	-0.002	0.007	0.762	
ST	0.021	0.035	0.545	
SS	-1.786E-05	0.0001	0.881	
ANOVA				
	df	SS	MS	F
Regression	6	0.057	0.010	1.368
Residual	8	0.056	0.007	
Total	14	0.113		

$R^2 = 0.5060$

The statistical data of the reduction model for the pellet shape confirmed the good fitting with $R^2 = 0.8196$. However, the reduction model for the pellet crushing strength did not yield good agreement with experimental data. The P-value of all the terms were larger than 0.1 and the R^2 was very low at 0.5064. Failure of the response model for the pellet crushing strength could be due to the difference in pellet shape, which could impede the measurement of crushing strength by the two-plane compression technique, illustrated in Figure 4.25, used in this study.

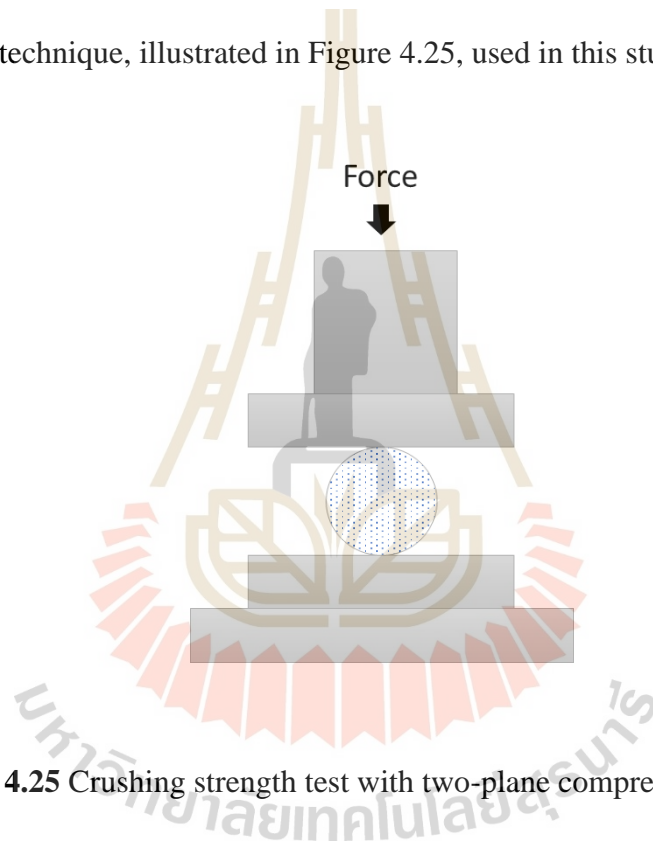


Figure 4.25 Crushing strength test with two-plane compression technique.

Difference in pellet shape resulted in different contact areas between pellets and planes. Therefore, the crushing strength of those pellets could not be directly compared. This led to unsuccessful response model for the pellet crushing strength. In addition, pellets used in those 15 experiments for extrusion and spheronization were prepared in different batches. Even when the pastes were prepared using the same

conditions, they had slightly different rheological characteristics due to heterogeneity of the starting, as illustrated in Figure 4.26.

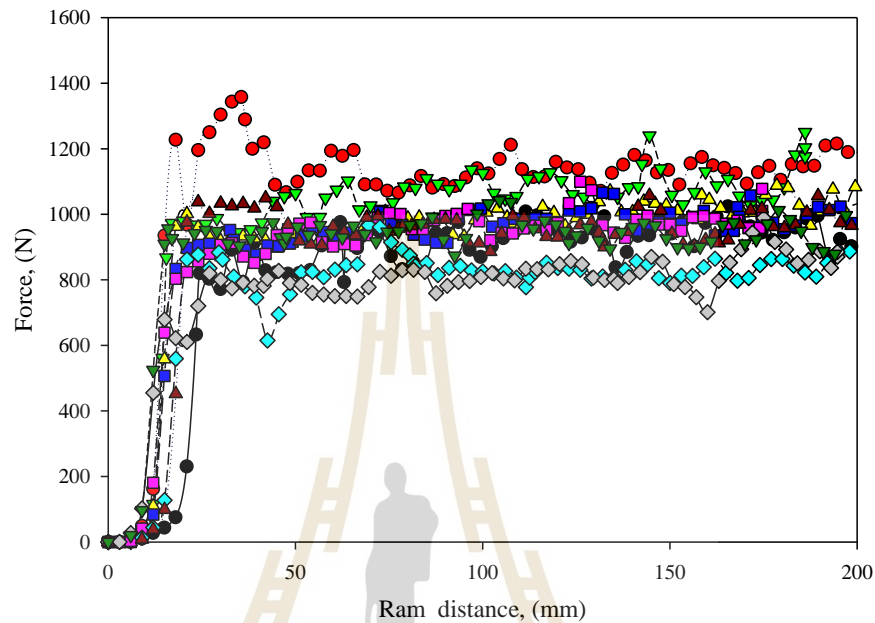


Figure 4.26 Sensitivity of paste extrusion force during extrusion using the pastes with the same composition but prepared in different batches.

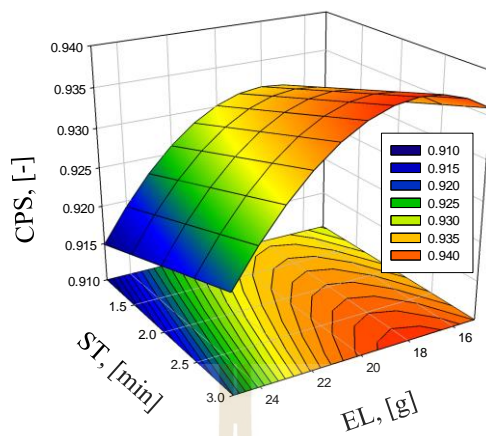
The extrusion resistance profiles of all experiments in Figure 4.26 confirmed the absence of liquid migration during extrusion. The resistance force was varied between 800 – 1200 N, which could have been resulted from the inconsistency of paste preparation leading to the deviation of powder compaction and difference in pellet strength and pellet shape after spheronization. Therefore, the response model of crushing strength was negligible.

The response surface model for the circularity of the pellet is illustrated in Eq.(4.3). The response surface of the effect of spheronization parameters on the pellet circularity plot is shown in Figure 4.27.

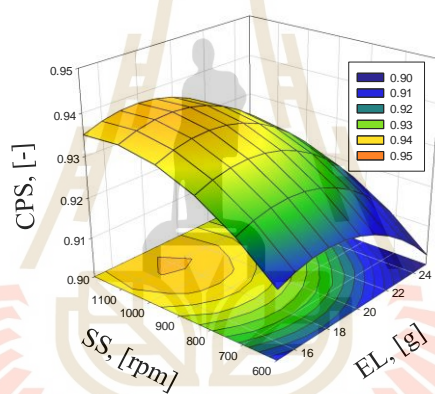
$$CPS = 0.73424 + 1.18874 \times 10^{-2} EL + 3.56705 \times 10^{-3} ST + 1.63174 \times 10^{-4} SS - 3.31940 \times 10^{-4} EL^2 - 7.34749 \times 10^{-8} SS^2 \quad (4.3)$$

Circularity of the pellets tended to increase with increasing spheronization speed and spheronization time, but was found to decrease with increasing extrudate loading, as observed in Figure 4.27. Increasing of spheronization speed and spheronization time might have led to increasing of the energy supplied to the pellets and, in turn, caused deformation of the pellet shape. However, at very high spheronization speed, the pellet circularity slightly decreased (Figure 4.27 (b) and (c), which could be resulted from the liquid migration that was more profound at this condition. As a result, pellets were quickly dried and resistant to shape formation. In addition, at high spheronization speed, the pellet moved faster in the spheronization bowl resulting in an increasing evaporation rate of the pellet.

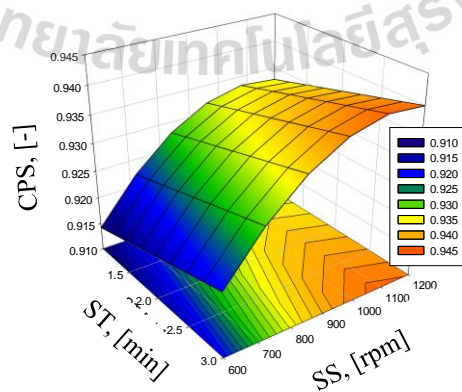
Increasing of extrudate loading, may have decreased energy supply to deform pellets and the frequency of pellets impact with friction disk and spheronization wall. High pellet loading probably increases the chance of pellet stick to each other. However, at small extrudate loading, the circularity of pellets tended to decrease, as observed in Figure 4.27 (a) and (b). This probably due to the high energy supply to pellet resulting in quick pellet drying as described above.



(a)



(b)



(c)

Figure 4.27 Response surface plot of spheronization parameters

Effect of spheronization parameters on the pellet crushing strength was re-investigated by varying one parameter at a time. Due to the sensitivity of the paste process, total amount of paste, which would be sufficient for every concerned experiment, was prepared in one batch. The ranges of spheronization parameter was selected based on the previous experiments which given the same pellet circularity.

At low extrudate loading of 5 g, the low pellet circularity was low as pellet quickly dried. The crushing strength of the pellet was also low. The internal cracks were probably generated in the dried pellet due to continuing force attraction from friction disk and pellet impacts to the spheronization wall. When extrudate loading was increased from 10 to 20 grams, the pellet circularity decreased and, eventually, became constant. The pellet crushing strength showed similar trends. Pellet loading in the range studied here did not seem to affect the pellet crushing strength, which might be due to employment of suitable spheronization parameters. However, as mention above, high extrudate loading did hinder shape formation.

Effect of spheronization speed was clearly illustrated in Figure 4.28 (b) as the circularity of the pellet was almost constant. As spheronization speed increased from 800 rpm to 1000 rpm, the pellet crushing strength improved. But, when the spheronization speed was raised from 1000 to 1400 rpm, pellet crushing strength decreased. This also could be the effect of quick pellet drying during spheronization, as described above.

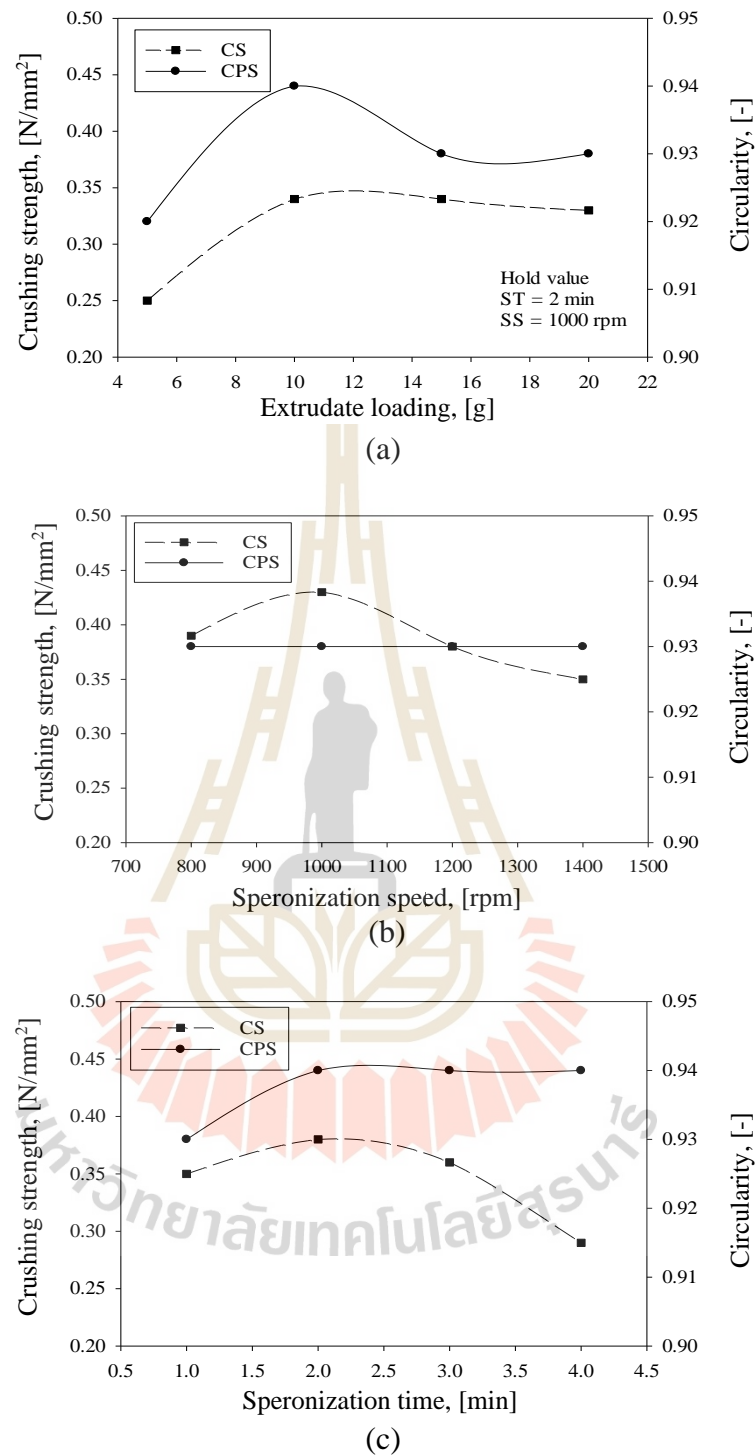


Figure 4.28 Effect of spheronization parameter on pellet crushing strength and circularity.

Figure 4.28 (c) shows effect of spheronization time. For fast spheronization, ST = 1 min, the pellet circularity low likely due to too short processing time to deform the extrudate. Pellet strength was also low due to the low total energy supply for compaction pellets. As spheronization time was increased from 2 to 4 min, the pellet circularity did not seem to change, while the pellet crushing strength decreased significantly. This result was again similar to the previous experiments that obtained from the experiments previously described. Further spheronization, while the pellet is dried, could probably generate internal cracks inside the pellet.

However, the pellet crushing strength was varied in the narrow range, 0.25 - 0.43 N/mm². The spheronization parameter was not much improved on the pellet crushing strength within the ranges of parameter studied above.

4.5.6 Pellet specific surface area

Effect of the spheronization parameters on specific surface area of the calcinated pellet was analyzed. As seen in Figure 4.29, the specific surface area was not significantly changed by varying the spheronization parameters, since it was just varied from 200 to 215 m²/g. The variation of specific surface area upon changing the spheronization parameters was as narrow as that of the pellet crushing strength. The specific surface area of pellets was found to be closed to that of the calcined synthetic clay powder, which was 206.11 m²/g. These data indicated that extrusion-spheronization technique did not destroy surface area properties of the powder. In addition, the pellet specific surface area before calcination, 86.80 m²/g, was slightly increased from 72.87 m²/g of the starting powder. This observation was probably due to the fact that agglomerates powder is break down during paste preparation and extrusion resulting in an increase in the specific surface area.

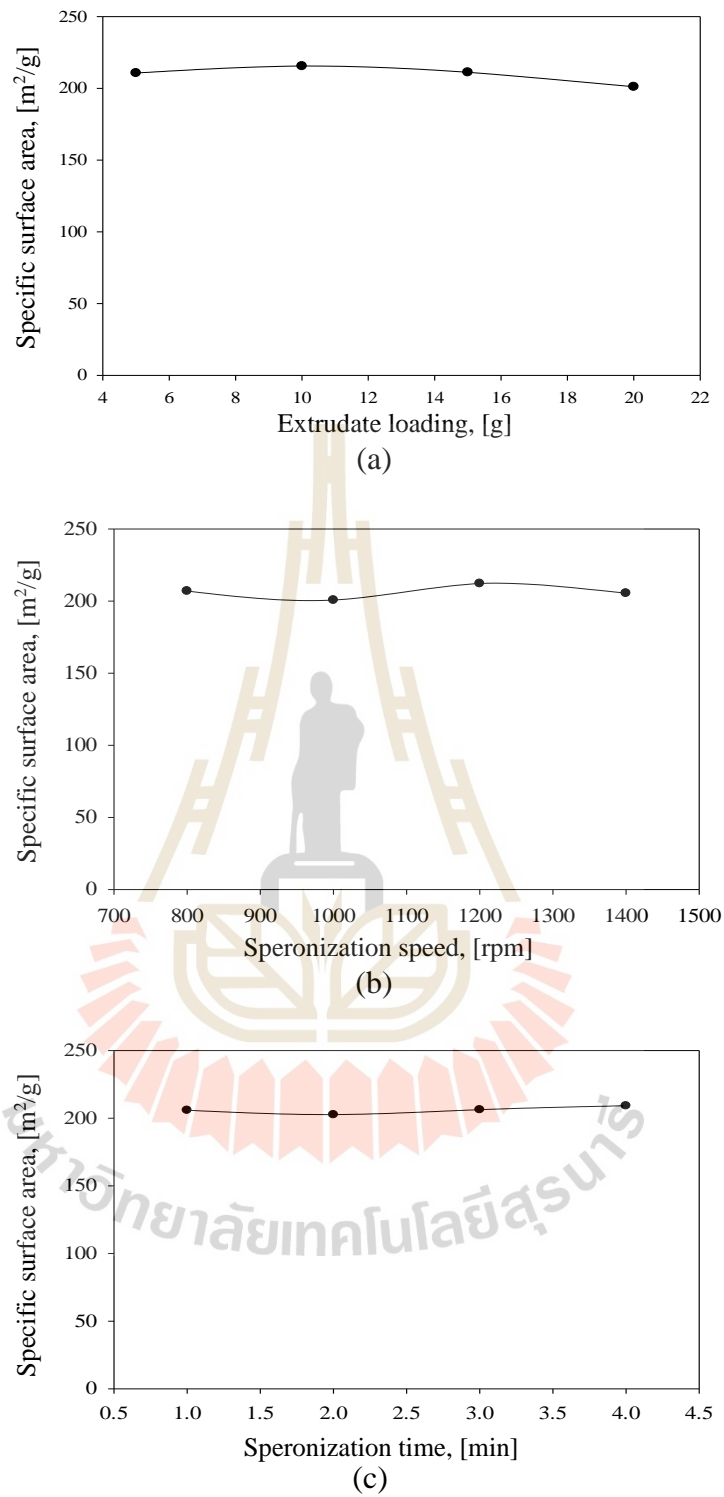


Figure 4.29 Effect of spheronization parameters on the specific surface area of the pellet

4.5.7 Pellet improvement study

4.5.7.1 Extrusion rheology

The steady-state extrusion profile is shown in Figure 4.30. Increasing liquid binder viscosity by increasing PVA content resulted in higher extrusion resistance, which could brought highly compacted extrudate pellet product (Al-Azzawi and Kanaan, 2017; Alazzawi et al., 2017). In contrast, adding more liquid binder, i.e. increasing PVA from 1% to 3%, appeared to decrease the resistance force. Increasing of boehmite content was known to increase the liquid viscosity (Timofeeva et al., 2009), but the extrusion resistance in this case was lower than the extrusion without a binder (base case). This was probably due to effect of pore blocking by boehmite particles of nanoscale, which hindered the liquid filling of pores and led to the availability of free liquid on the outer surface and, therefore, decrease of resistance force.

The extrusion resistance of the paste prepared from spray-dried powder was significantly higher than that of the paste prepared from oven-dried powder. This was likely caused by the rounder shape and the narrower particle size distribution of the spray-dried powder. Round powder or powder with spherical shape usually results in a well-packed structure with low porosity. During the extrusion process, however, the spherical particles may be broken due to the high load. This will hinder liquid penetration through channel of agglomerated powder. Hence, the effect of liquid migration was decreased.

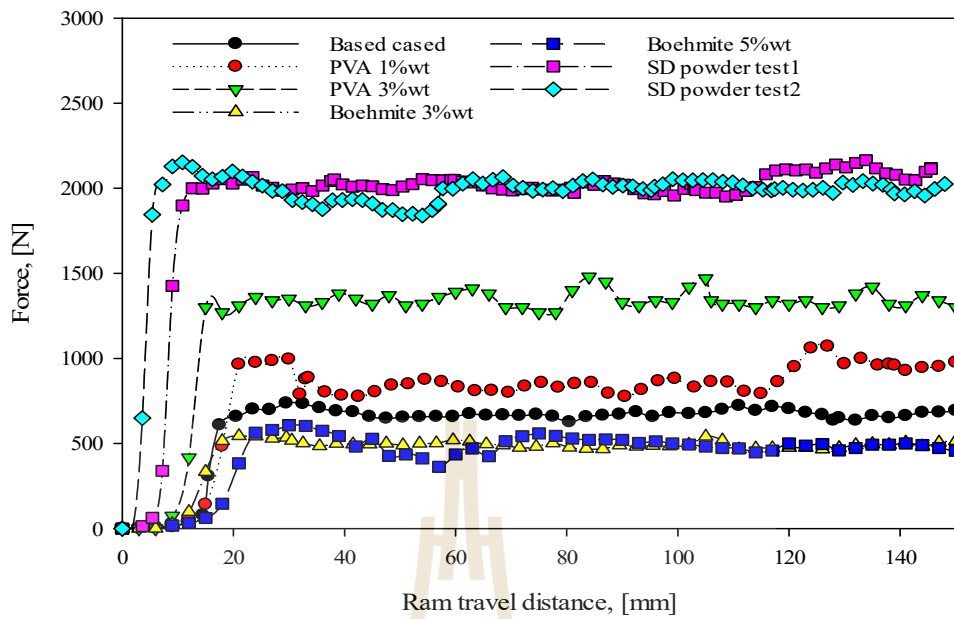


Figure 4.30 Extrusion force resistance of variation of paste composition

4.5.7.2 Pellet crushing strength

The crushing strength of the spheronized pellets obtained in this study is illustrated in Table 4.7.

Table 4.7 Crushing strength of spheronized pellets.

Sample	Crushing strength (N/mm ²)
Base case	3.39
PVA 1%Wt	3.43
PVA 3%Wt	3.91
Boehmite 3%wt	2.82
Boehmite 5%wt	2.89
Spray-dried powder	1.92
Calcination at 450°C	3.89
Calcination at 550°C	3.29
Calcination at 650°C	3.24

Crushing strength of the spheronized pellet was found to increase with increasing of PVA concentration. Owing to the decreasing liquid migration, the extrudate was well compacted under the high extrusion force. The crushing strength of the pellet with addition of boehmite was lower than that of the pellet without it. This could be due to insufficient amount of boehmite, as binder, in this study. Increasing of binder amount means decreasing of pellet functional properties. Therefore, there is a need for optimization between pellet properties and pellet strength.

The increasing calcination temperature tends to decrease the pellet crushing strength. As observed by TGA-DSC, the hydroxyl group starts to decompose at a temperature of around 400°C and is almost gone at around 700°C. Decomposition of hydroxyl group could generate pores between the clay layer, which might have led to a decrease in the pellet strength.

Extrusion force acting on the extrudate prepared the spray-dried powder was higher than that the paste from oven-dried powder. However, the crushing strength paste with spray-dried powder was significantly lower than its oven-dried counterpart due to the high porosity of spray-dried particles, evidenced by their specific pore volume that was about 39 m²/g higher that of the oven-dried ones.

As observed, the crushing strength of the spheronized pellets prepared with oven-dried powder did not differ significantly from other. Similar observation was obtained from all the spheronized pellets except the ones prepared with the spray-dried powder. The pellet crushing strength measured in study ranged from 1.92 to 3.91 N/mm², which was still far lower than that of clay adsorbents. Attapulgate, for example, Kaitelver company has crushing strength higher than 8.91 N/mm². Other examples

include zeolite molecular sieve pellets from Richon and aluminium oxide pellets from Xelvneng, which come with the crushing strength higher than 8.41 N/mm² and 4.95 N/mm², respectively. This was probably due to shape and particle porosity of the primary material, as shown in Figure 4.31. The pellets were highly porous due to the synthesis procedure of primary particles.



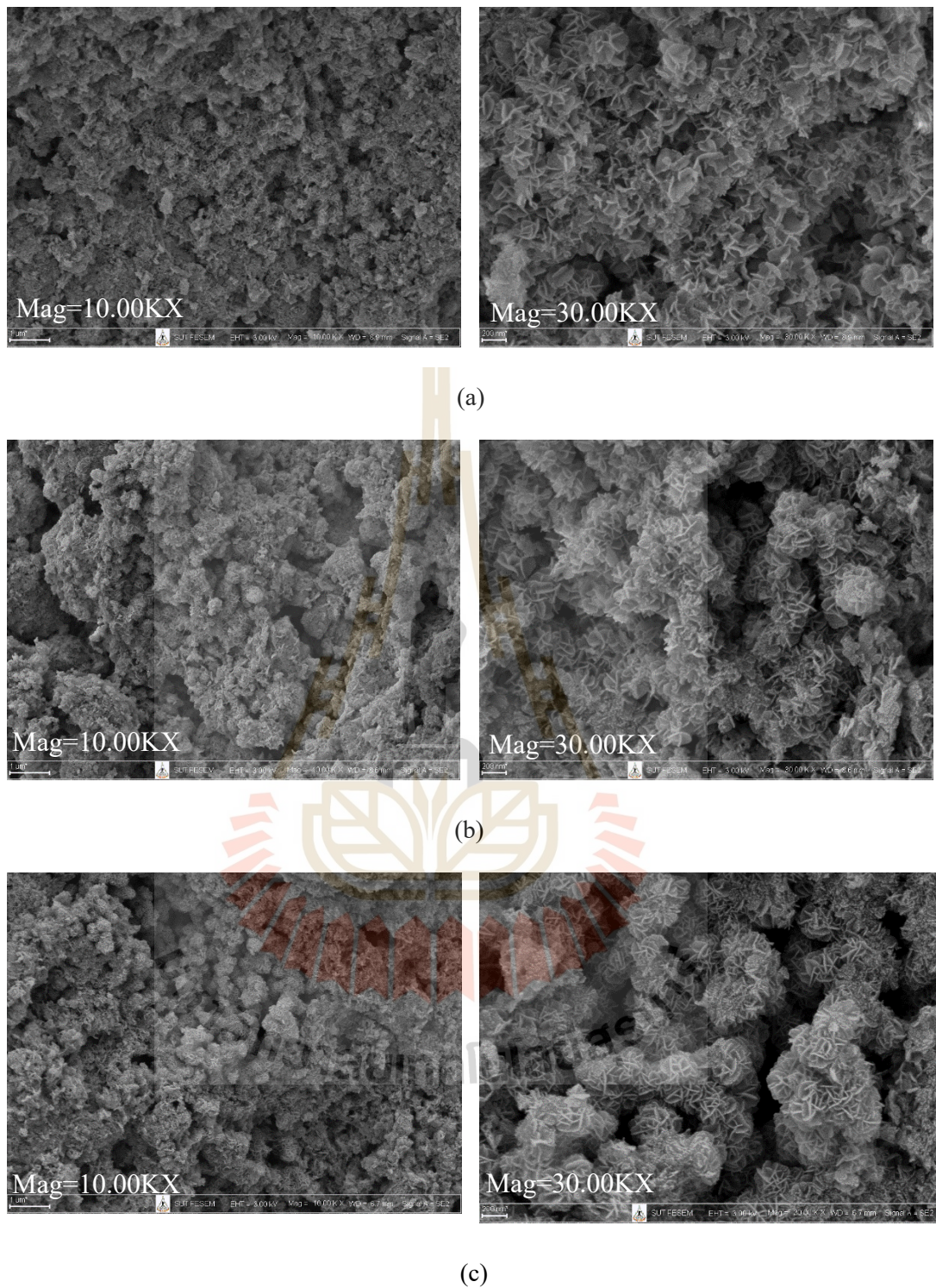


Figure 4.31 SEM image of spheronized pellets: (a) base case, (b) PVA 3%wt, (c) boehmite 5%wt, (d) calcination at 600°C, (e) spray-dried powder.

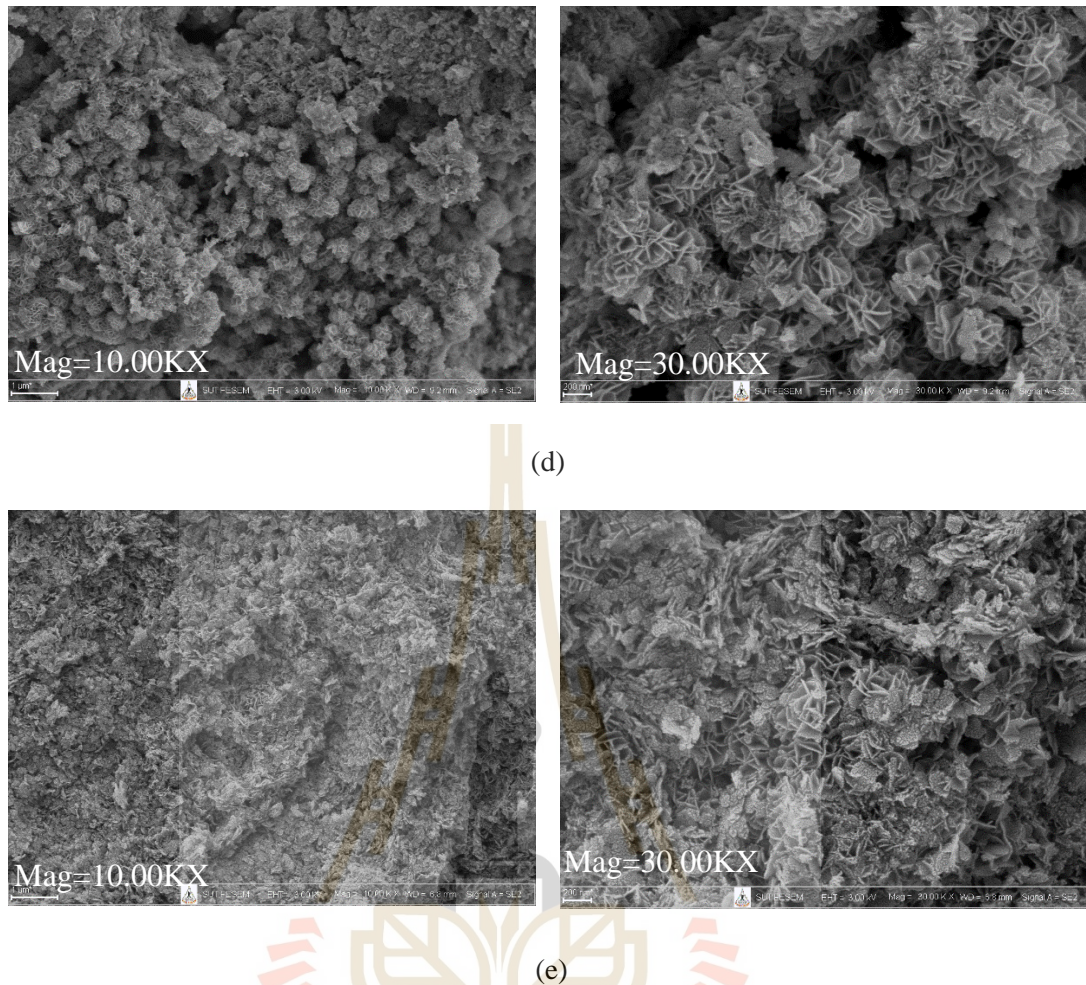


Figure 4.31 (Continue) SEM image of spheronized pellets: (a) base case, (b) PVA 3%wt, (c) boehmite 5%wt, (d) calcination at 600°C, (e) spray-dried powder.

4.6 Conclusion

Spherical pellet of synthetic clay was successfully prepared by the extrusion and spheronization method. Pellet was good in shape and size distribution and possessed strength to retain its shape during packing. The specific surface area of powder was also retained and not diminished by the shaping process. Clay rheology during extrusion illustrated that liquid migration occurred at low extrusion velocity, and the wall slip

effect hindered compaction force at high extrusion velocity. Extrudate fracture was not found in the presence of wall slip. Liquid migration also affected on the spheronization step resulting in formation of large granules. Heating the spheronizer wall led to successful spheronization process. Pellet circularity increased with increasing spheronization speed and spheronization time but decreased with increasing extrudate loading. However, very high spheronization speed and spheronization time and low extrudate loading yielded in quick pellet drying that impeded shape formation resulting in the formation of low circularity pellets with low strength. Furthermore, the received dry spheronized pellet appeared to have internal cracks.

Morphology of synthetic clay powder had the main dominant effect on the pellet strength. The synthesized clay primary particles consist of nanoporous material, thus, it was difficult to prepare high-strength pellets with synthetic clay powder.

4.7 References

- Al-Azzawi, and Kanaan, M. 2017. Evaluation of the effect of extrusion velocity and paste water content on the microstructural variability and green strength of extruded titanium dioxide. (Masters dissertation, Rutgers, The State University of New Jersey).
- Alazzawi, M. K., Murali, S., and Haber, R. A. 2017. Visualizing the effect of extrusion velocity on the spatial variation of porosity in a titanium dioxide/binder system. **Materials Sciences and Applications** 8 (13):15.
- Azzolini, A., Sglavo, V. M., and Downs, J. A. 2014. Novel method for the identification of the maximum solid loading suitable for optimal extrusion of ceramic pastes. **Journal of Advanced Ceramics** 3 (1):7-16.

- Badoga, S., Vosoughi, V., and Dalai, A. K. 2017. Performance of promoted iron/CNT catalyst for fischer–tropsch synthesis: influence of pellet shapes and binder loading. **Energy & Fuels** 31 (11):12633-12644.
- Baert, L., Vermeersch, H., Remon, J. P., Smeyers-Verbeke, J., and Massart, D. L. 1993. Study of parameters important in the spheronisation process. **International Journal of Pharmaceutics** 96 (1–3):225-229.
- Benbow, J., and Bridgwater, J. 1993a. Paste Flow and Extrusion. 1993b. **Paste Flow and Extrusion**: Clarendon Press.
- Bryan, M. P., Atherton, L. N., Duffield, S., Rough, S. L., and Wilson, D. I. 2015a. Stages in spheronisation: Evolution of pellet size and shape during spheronisation of microcrystalline cellulose-based paste extrudates. **Powder Technology** 270:163-175.
- Bryan, M. P., Kent, M. D., Rickenbach, J., Rimmer, G., Wilson, D. I., and Rough, S. L. 2015b. The effect of mixing on the extrusion–spheronisation of a microcrystalline cellulose paste. **International Journal of Pharmaceutics** 479 (1):1-10.
- Engländer, A., Burbidge, A., and Blackburn, S. 2000. A preliminary evaluation of single screw paste extrusion. **Chemical Engineering Research and Design** 78 (5):790-794.
- Fauchadour, D., Kolenda, F., Rouleau, L., Barré, L., and Normand, L. 2000. Peptization mechanisms of boehmite used as precursors for catalysts. **Studies in Surface Science and Catalysis** 143:453-461.
- Harrison, P. J., Newton, J. M., and Rowe, R. C. 1985. Flow defects in wet powder mass extrusion. **Journal of Pharmacy and Pharmacology** 37 (2):81-83.

- Juppo, A., Hellén, L., Pullinen-Strander, V., Kalsta, K., Yliruusi, J., and Kristoffersson, E. 1997. Application of mercury porosimetry in evaluation of extrusion-spheronisation process. **European Journal of Pharmaceutics and Biopharmaceutics** 44:205-214.
- Kocserha, I., Gömze, A. L., Kulkov, S., Kalatur, E., Buyakova, S. P., Géber, R., and Buzimov, A. Y. 2017. Characterisation of the wall-slip during extrusion of heavy-clay products. **Journal of Physics: Conference Series** 790 (1):012013.
- Koester, M., Willemsen, E., Krueger, C., and Thommes, M. 2012. Systematic evaluations regarding interparticular mass transfer in spheronization. **International Journal of Pharmaceutics** 431 (1-2):84-89.
- Krokida, M. K., Karathanos, V. T., and Maroulis, Z. B. 1998. Effect of freeze-dried conditions on shrinkage and porosity of dehydrated agricultural products. **Journal of food engineering**. 35 (4):369-380.
- Krueger, C., Thommes, M., and Kleinebudde, P. 2013. Spheronisation mechanism of MCC II-based pellets. **Powder Technology** 238:176-187.
- Lau, C. L. S., Yu, Q., Lister, V. Y., Rough, S. L., Wilson, D. I., and Zhang, M. 2014. The evolution of pellet size and shape during spheronisation of an extruded microcrystalline cellulose paste. **Chemical Engineering Research and Design** 92 (11):2413-2424.
- Li, Y., Wu, D., Zhang, J., Chang, L., Wu, D., Fang, Z., and Shi, Y. 2000. Measurement and statistics of single pellet mechanical strength of differently shaped catalysts. **Powder Technology** 113 (1-2):176-184.
- Liew, C. V., Chua, S. M., and Heng, P. W. S. 2007. Elucidation of spheroid formation with and without the extrusion step. **AAPS PharmSciTech** 8 (1):E70-E81.

- Liu, H., Liu, J., Leu, M. C., Landers, R., and Huang, T. 2012. Factors influencing paste extrusion pressure and liquid content of extrudate in freeze-form extrusion fabrication. **The International Journal of Advanced Manufacturing Technology** 67 (1-4):899-906.
- Mascia, S., Seiler, C., Fitzpatrick, S., and Wilson, D. I. 2010. Extrusion-spheronisation of microcrystalline cellulose pastes using a non-aqueous liquid binder. **International Journal of Pharmaceutics** 389 (1-2):1-9.
- Mesiha, M. S., and Valltés, J. 1993. A screening study of lubricants in wet powder masses suitable for extrusion-spheronization. **Drug Development and Industrial Pharmacy** 19 (8):943-959.
- Mitchell, S., Michels, N.-L., and Pérez-Ramírez, J. 2013. From powder to technical body: the undervalued science of catalyst scale up. **Chemical Society Reviews** 42 (14):6094.
- Muley, S., Nandgude, T., and Poddar, S. 2016. Extrusion-spheronization a promising pelletization technique: in-depth review. **Asian Journal of Pharmaceutical Sciences** 11(6):684-699.
- Newton, J. M., Chapman, S. R., and Rowe, R. C. 1995. The influence of process variables on the preparation and properties of spherical granules by the process of extrusion and spheronisation. **International Journal of Pharmaceutics** 120 (1):101-109.
- Niu, C. H., Baylak, T., Wilson, D. I., and Zhang, M. 2014. Pelletisation of canola meal by extrusion–spheronisation for ethanol dehydration. **Biomass and Bioenergy** 66:116-125.

- Panaseti, P., Housiadas, K. D., and Georgiou, G. C. 2013. Newtonian Poiseuille flows with pressure-dependent wall slip. **Journal of Rheology** 57 (1):315-332.
- Parikh, D. M. 2016. **Handbook of Pharmaceutical Granulation Technology**, Third Edition: CRC Press.
- Pinto, J. F., Buckton, G., and Newton, J. M. 1992. The influence of four selected processing and formulation factors on the production of spheres by extrusion and spheronisation. **International Journal of Pharmaceutics** 83 (1):187-196.
- Powell, J., Assabumrungrat, S., and Blackburn, S. 2013. Design of ceramic paste formulations for co-extrusion. **Powder Technology** 245:21-27.
- Ribeiro, M. J., Blackburn, S., and Labrincha, J. A. 2009. Single screw extrusion of mullite-based tubes containing Al-rich anodising sludge. **Ceramics International** 35 (3):1095-1101.
- Rough, S. L., Bridgwater, J., and Wilson, D. I. 2000. Effects of liquid phase migration on extrusion of microcrystalline cellulose pastes. **International Journal of Pharmaceutics** 204 (1-2):117-126.
- Rowe, R. C. 1985. Spheronisation: A novel pill-making process **Pharm. Int** 6:119-123.
- Sarkar, S., Ang, B. H., and Liew, C. V. 2014. Influence of starting material particle size on pellet surface roughness. **AAPS Pharm SciTech** 15 (1):131-139.
- Sriamornsak, P., Nunthanid, J., Luangtana-anan, M., Weerapol, Y., and Puttipipatkachorn, S. 2008. Alginate-based pellets prepared by extrusion/spheronization: effect of the amount and type of sodium alginate and calcium salts. **European Journal of Pharmaceutics and Biopharmaceutics** 69 (1):274-284.

- Sun, J., Liu, W., Hu, Y., Wu, J., Li, M., Yang, X., Wang, W., and Xu, M. 2016. Enhanced performance of extruded–spheronized carbide slag pellets for high temperature CO₂ capture. **Chemical Engineering Journal** 285:293-303.
- Timofeeva, E. V., Routbort, J. L., and Singh, D. 2009. Particle shape effects on thermophysical properties of alumina nanofluids. **Journal of Applied Physics** 106 (1).
- Tsokolar-Tsikopoulos, K. C., Katsavou, I. D., and Krokida, M. K. 2015. ‘The effect of inulin addition on structural and textural properties of extruded products under several extrusion conditions’: The effect of inulin addition on structural and textural properties of rice flour extrudates. **Journal of Food Science and Technology** 52 (10):6170-6181.
- Vitorino, N., Ribeiro, M. J., Abrantes, J. C. C., Labrincha, J. A., and Frade, J. R. 2014. Extrusion of ceramic pastes: An alternative approach to obtain the Benbow’s model parameters. **Ceramics International** 40 (9):14543-14547.
- Wan, L. S. C., Heng, P. W. S., and Liew, C. V. 1993. Spheronization conditions on spheroid shape and size. **International Journal of Pharmaceutics** 96 (1):59-65.
- Wilson, D. I., and Rough, S. L. 2007. Chapter 3 Extrusion—spheronisation. In **Handbook of Powder Technology**, edited by A. D. Salman, M. J. Hounslow and J. P. K. Seville: Elsevier Science B.V., 189-217.
- Woodruff, C. W., and Nuessle, N. O. 1972. Effect of processing variables on particles obtained by extrusion–spheronization processing. **Journal of Pharmaceutical Sciences** 61 (5):787-790.

- Yoo, A., and Kleinebudde, P. 2009. Spheronization of small extrudates containing κ -carrageenan. **Journal of Pharmaceutical Sciences** 98 (10):3776-3787.
- Zhang, M., Rough, S. L., Ward, R., Seiler, C., and Wilson, D. I. 2011. A comparison of ram extrusion by single-holed and multi-holed dies for extrusion-spheronisation of microcrystalline-based pastes. **International Journal of Pharmaceutics** 416 (1):210-222.
- Zhang, M., Wilson, D. I., Ward, R., Seiler, C., and Rough, S. L. 2013. A comparison of screen and ram extrusion-spheronisation of simple pharmaceutical pastes based on microcrystalline cellulose. **International Journal of Pharmaceutics** 456 (2):489-498.
- Zhang, X., Liu, M., Bikane, K., and Li, Y. 2017. Evaluation of wall slip effects on the flow characteristics of petroleum coke-water slurry flow along pipelines. **Asia-Pacific Journal of Chemical Engineering** 12 (5):818-826.
- Zheng, Y., Song, J., Xu, X., He, M., Wang, Q., and Yan, L. 2014. Peptization mechanism of boehmite and its effect on the preparation of a fluid catalytic cracking catalyst. **Industrial & Engineering Chemistry Research** 53 (24):10029-10034.
- Zolkefeli, S. N. M., and Wong, T. W. 2013. Design of microcrystalline cellulose-free alginate spheroids by extrusion-spheronization technique. **Chemical Engineering Research and Design** 91 (12):2437-2446.

CHAPTER V

PELLET UTILIZATION IN FIXED-BED LIQUID ADSORPTION

5.1 Abstract

Bulk synthetic-clay pellets prepared by extrusion and spheronization were used as adsorbent for liquid adsorption of methyl orange in a fixed-bed column. Effect of solvent: water and ethanol, as well as effect of initial concentration of the adsorbate on adsorption performance was studied. Three adsorption models, Adams–Bohart, Thomas, and Yoon-Nelson models, were used to evaluate adsorption parameters. Fixed-bed adsorption of methyl orange in water, the inorganic solvent, failed due to severe swelling of the adsorbents. Adsorption in ethanol, the organic solvent, was successfully studied. The Thomas and Yoon-Nelson models appeared to fit well with the experimental data.

5.2 Introduction

Clay mineral has been of great interest in an industrial fixed bed adsorption process in recent years due to its unique properties, lack of toxicity, low cost, and ready availability. The unique properties of clay in adsorption include the potential of ion exchanger, high specific surface area and surface chemistry, and a variety of surface and structural properties (Bergaya and Lagaly, 2013; Adeyemo et al., 2017). Due to the varieties of clay properties, it can be used to adsorb both inorganic and organic

molecules (Borisover and Davis, 2015). In recent years, clay adsorbent has been reported in the literature typically powdered form or small granular shape, micron size (Vahidhabanu et al., 2017; Uddin, 2017; Adeyemo et al., 2017; Lima et al., 2017; Ahmad et al., 2017). Powder or small granule size has not been utilization fixed-bed adsorption in industrial scale due to a high-pressure drop across the column and difficulty in separating it from the product effluent. Pelletization of clay millimeter size, which typically used in industrial applications, is still lack in the literature reported.

Yu et al. (2017) prepared spherical granular adsorbent for fixed-bed adsorption by mixing Hangjin clay, montmorillonite, and corn straw powder. The granular pellet was prepared manually at the size of 2-3 mm and calcined at 600°C to prepare clay surface chemistry. The fixed-bed column used in the study was 22 mm in diameter and 200 mm in height. Process parameters studied were initial concentration, adsorbate feed rate, and bed height. Five mathematical models: the Adams-Bohart, Thomas, Yoon-Nelson, Clark, and BDST models, were used to predict breakthrough curves behavior in the adsorption column. S-shape sorption isotherm was received in all the systems studied. The authors concluded that both breakthrough time and exhaustion time increased with increasing bed depth and decreasing influent phosphorus concentration and flow rate. Both the Adams-Bohart model and Clark model were found to adequately describe adsorption behavior of phosphorus in dynamic system. Yoon-Nelson model and BDST model successfully explained the breakthrough behavior and predicted the breakthrough time of the adsorption process. However, effect of bed depth and feed flow rate on adsorption capacity was quite strange. As the bed depth increased, the total adsorption capacities decreased. Increasing feed flow rate resulted in both increasing

and decreasing the adsorption capacity. The author did not give clear explanation for this point. Also, the pellet characteristic during and after adsorption, such as hydration effect and swelling properties, did not explore. The mechanical strength of the prepared pellets was not studied. In addition, the palletization technique was not practically used on in industrial scale pellet preparation.

Spherical granules of mixed bentonite clay and activated carbon was also prepared manually by Kamińska (2018). The granular used to adsorb organic micropollutants in the wastewater. The granular size was 5 mm and was calcined at 250°C and 400°C before use to improve surface chemistry. The fixed bed column was 15 mm in diameter. The absorbate solution was fed at the top of the column and distributed through the sand, which was packed above the pellet. Efficiency of the clay adsorbent in removing organic micropollutants was high at 99%. However, the authors did not study the effect of dynamic adsorption parameters, such as feed rate, bed height, and initial concentration. Also, pellet physical and chemical properties were not mentioned.

Immobile clay pellet was widely prepared and used in fixed-bed adsorption. Examples include mixture of local clay and chitosan that was as adsorbent for methylene blue adsorption (Auta and Hameed, 2014), pellet of mixed bentonite clay and chitosan for adsorption of Pb(II), Cu(II), and Ni(II) from aqueous solution (Tsai et al., 2016), a clay composite adsorbent pellet prepared from clay, chitosan, powdered activated carbon, and magnetic nanoparticles used to removal of hydrophilic and hydrophobic pharmaceuticals (Vijayanandan et al., 2018), chitosan-montmorillonite beads for anionic dye removal (Pereira et al., 2017), and sepiolite clay with embedded ZnO combined with sodium alginate as adsorbent for removal of congo red from

wastewater (Vahidhabanu et al., 2017). Performance of pellet preparation was analyzed adsorption the breakthrough curve. The obtained data were fitted with a breakthrough curve model, typically Adams-Bohart, Thomas, Yoon-Nelson, and Clark model to obtain fixed-bed operation parameter. The authors showed that the prepared pellet was good adsorbent. However, utilization of immobile pellet was limited for low-temperature adsorption because of melting of polymer and difficulty in control of the pellet shape, which resulted in unpredictable packing structure of the bed.

This chapter aimed to investigate how synthetic clay pellet prepared by extrusion and spheronization performed as adsorbent for adsorption of methyl orange from liquid solution. Effect of solvent types as well as other adsorption variable were investigated. Experimental data were fitted with three adsorption models, Adams-Bohart, Thomas, and Yoon-Nelson models for evaluation of adsorption parameters.

5.3 Theory

5.3.1 Characteristic of fixed-bed adsorption

In fixed-bed adsorbate concentration in fluid phase and solid phase change with time and position in the bed, and the separation occurs under dynamic condition. Concentration profile of the adsorbate in fluid flowing through adsorbent in the fixed-bed column is as shown in Figure 5.1. In Figure 5.1, C_t is referred to the actual concentration during adsorption, C_0 is referred to the initial concentration, L is referred to length of adsorbent and t is referred to adsorption time.

In adsorption using fresh adsorbent, mass transfer of adsorbate begins near the inlet of the bed, and the adsorbate concentration decreases exponentially along the length of the bed and reaches near-zero concentration at the end of the column.

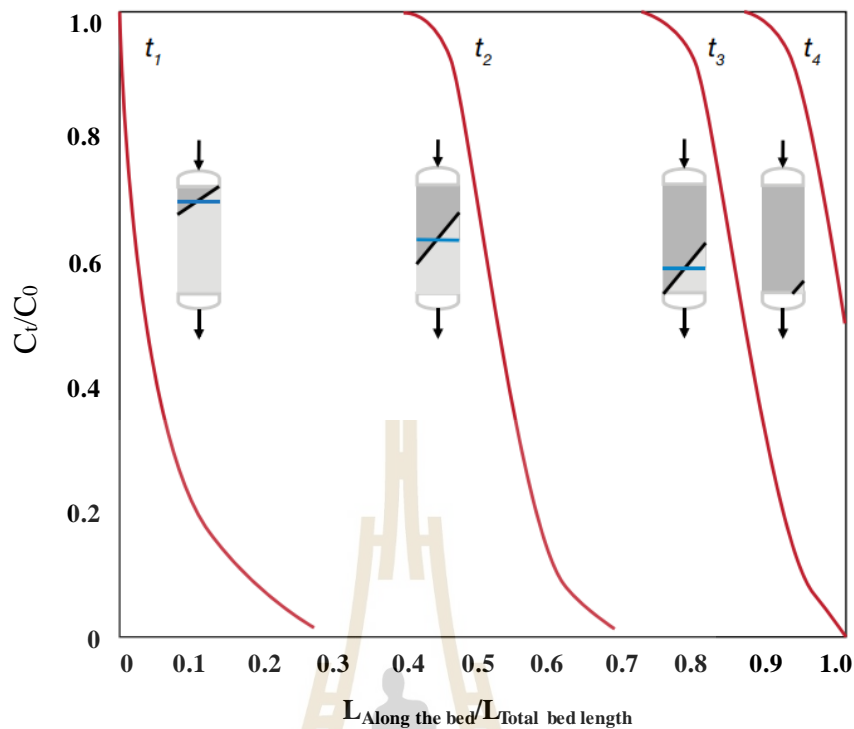


Figure 5.1 Concentration profile of adsorbate in fluid moving along the fixed-bed adsorption column. Mass transfer zone is depicted by the black diagonal line in each column.

During the operation, the fresh feed is continuously enters the column. Portion of the bed is continually exposed to the fluid at the feed concentration until the part of the bed reaches equilibrium with the feed, and no additional net mass transfer occurs. The region where most of the change in concentration occurs is called the mass transfer zone (MTZ). As the continuous process, the adsorbent reaches equilibrium with the feed is indicated by dark color in the depictions of the column, and the mass transfer zone is represented by the black diagonal line, as shown in Figure 5.1. At time t_3 , the mass transfer zone reaches the end of the bed, and after that, some adsorbate leaves the column effluent, which usually is not desirable. This is called breakthrough, and t_3 is

referred to as the breakthrough time. The performance of continuous adsorption in a fixed-bed adsorption column can explain in terms of a breakthrough curve. The time required for breakthrough and the shape of the breakthrough curves are very important characteristics for estimation of the dynamic response in the adsorption system (Malkoc and Nuhoglu, 2006).

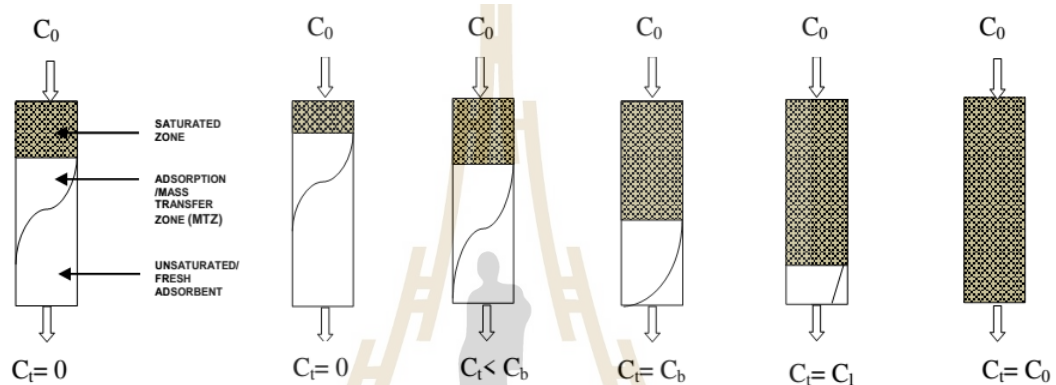


Figure 5.2 Schematic representation of saturated, mass transfer or adsorption, and unsaturated or fresh adsorbent zones in fixed-bed adsorption column (Chowdhury et al., 2014)

Figure 5.2 shows different adsorption steps in fixed-bed adsorption column, whereas Figure 5.3 illustrates the breakthrough curve as a function of time. As the sorption sites are progressively filled, the adsorption zone moves through the bed until its edge reaches the outer end. From then onwards, the effluent concentration increases from C_0 to a value C_b . This is called the breakpoint. The concentration profile between C_0 and C_b dominates a characteristic of sigmoidal shape, and the breakpoint marks bed saturation as well as an exhaustion of the adsorption column.

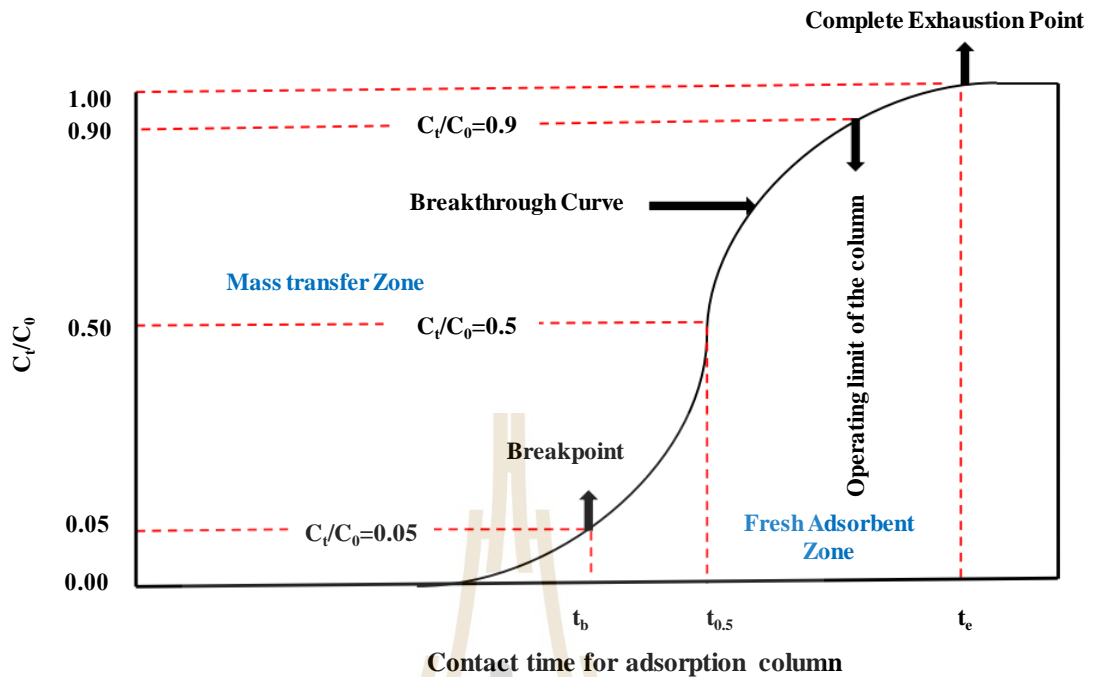


Figure 5.3 Breakthrough curve characteristics in the fixed-bed adsorption column (Chowdhury et al., 2014)

However, the breakthrough point is usually defined as the point of relative concentration (C_t/C_0) becomes 0.05 to 0.90 as represented in Figure 5.3. The adsorbent is usually replaced when the relative concentration becomes 0.50 at time $t_{0.5}$ in the case of industrial scale. The column sorption capacity is calculated at this point (Baral et al., 2009). After the 50% breakthrough point, the column can still operate until the relative concentration becomes 0.90. This point is termed as the operating limit of the column, and at this point, the outlet concentration is denoted as C_l . The column will be completely exhausted when the pre-determined inlet concentration is almost equal to the outlet concentration ($C_0 \approx C_t$ or C_l) at time t_e .

5.3.2 Analysis of the breakthrough curve

The total quantity of adsorbate adsorbed in the column (q , mg) is evaluated by determination of area under the curve of adsorbed concentration versus time multiplied by the flow rate of the solution, as described by equation (5.1).

$$q = \frac{Q}{100} \int_{t=t_0}^{t=t_{total}} (C_t - C_0) dt \quad (5.1)$$

where Q is the solution flow rate (mL min^{-1}), C_0 is the initial concentration (mg L^{-1}), C_t is the effluent adsorbate concentration (mg L^{-1}), and t is adsorption time (min). The equilibrium capacity, (mg/g), is computed by:

$$q_e = \frac{q}{m} \quad (5.2)$$

where m is the mass of adsorbent (g) used in the column.

5.3.2.1 Breakthrough curve modeling

5.3.2.1.1 Thomas model

Thomas model (Thomas, 1948) features non-axial dispersions and a rate driving force that follows pseudo-second-order reversible reaction kinetics for an equilibrium Langmuir isotherm. This model is generally used for adsorption processes where the external and internal diffusion limitations are absent and, as well as can be applied to both favorable and unfavorable adsorption conditions. The linearized equation of the Thomas model is expressed as follows;

$$\ln\left(\frac{C_t}{C_0} - 1\right) = \frac{k_{TH} q_e m}{Q} - k_{TH} C_0 t \quad (5.3)$$

where k_{TH} is the Thomas rate constant ($\text{mL min}^{-1} \cdot \text{mg}^{-1}$);

and m is the amount of adsorbent in the column (g);

5.3.2.1.2 Bohart and Adams model

Fundamental equations describing the relationship between adsorbate concentration and time in a flowing system were established by Bohart and Adams (1920). Bohart and Adams model is frequently selected for the delineation of fixed-bed column breakthrough for the initial state of the operation. The adsorption rate is proportional to both the residual capacity of the sorbent and adsorbate concentration (Aksu and Gönen, 2004). The model explains that the adsorption kinetic is controlled by external mass transfer in the initial part of adsorption. The mathematical equation of the model can be written as:

$$\ln\left(\frac{C_t}{C_0}\right) = k_{AB} C_0 t - \frac{k_{AB} N_0 z}{F} \quad (5.4)$$

where k_{AB} is the kinetic constant ($\text{L mg}^{-1} \text{min}^{-1}$); F is the linear velocity (cm min^{-1}); z is the length of the bed (cm), and N_0 is the saturation concentration (mg L^{-1}).

5.3.2.1.3 Yoon-Nelson model

This model is scientifically equal to the Thomas model. It is based on assumption that the rate of decreasing probability of adsorption

for each adsorbate molecule is proportional to the probability of adsorbate adsorption and the probability of adsorbate breakthrough on the adsorbate. Besides being the least complex model, Yoon-Nelson model also does not require data concerning characteristics of the adsorbate and type of adsorbent or physical properties of the bed. It is frequently used to predict dynamic behavior of single or binary composition systems (Yoon and Nelson, 1984). The linear form of the Yoon and Nelson equation regarding a single-component system is expressed as

$$\ln\left(\frac{C_t}{C_0 - C_t}\right) = k_{YN}(t - \tau) \quad (5.5)$$

where k_{YN} is the rate constant of the model, τ is the time required for 50% adsorbate breakthrough (min).

According to the symmetrical nature of the breakthrough curves of the Yoon-Nelson model, Thus, the fixed bed should be completely saturated at $t = 2\tau$. Consequently, the adsorption capacity of the column can be expressed as:

$$q_{YN} = \frac{C_0 Q \tau}{m} \quad (5.6)$$

5.3.3 Statistical test

Good agreement between the breakthrough model and experimental adsorption data is judged by high value of coefficient of determination (R^2) and low value of sum of squared error (%SSE), which is calculated as shown in equation (5.7):

$$\% SSE = \sqrt{\frac{\left(\frac{(q_{\text{exp}} - q_e)}{q_{\text{exp}}}\right)^2}{N-1}} \times 100 \quad (5.7)$$

where N is the number of data points. The higher the value of R^2 and the lower the value of % SSE; the better data fitting and agreement.

5.4 Experimental

5.4.1 Pellets preparation

Spherical synthetic clay adsorbent pellet was prepared by the extrusion and spheronization using the selected pellet forming conditions and the procedures as described in Chapter IV. The extrusion and spheronization process was prepared with die of $L/D = 8$, and the extrusion speed of 5 mm/s. The extrudate was cut manually before it was subjected into the spheronizer. The spheronization parameters was performed at extrudate loading of 20 g, spheronization time of 2 min and spheronization speed of 1000 rpm. The wall of the spheronizing bowl was heated at constant temperature of 50°C using hot water circulating bath throughout the spheronization process. The fresh spheronized pellet was dried in ambient condition for 3 days being calcined.

5.4.2 Adsorbate solution preparation

Methyl orange (MO) purchased from Honeywell Fluka™ (MW=327.34 g/mol) was used to represent anionic adsorbate (K. Aziz et al., 2019). The MO molecular structure is illustrated in Figure 5.4.

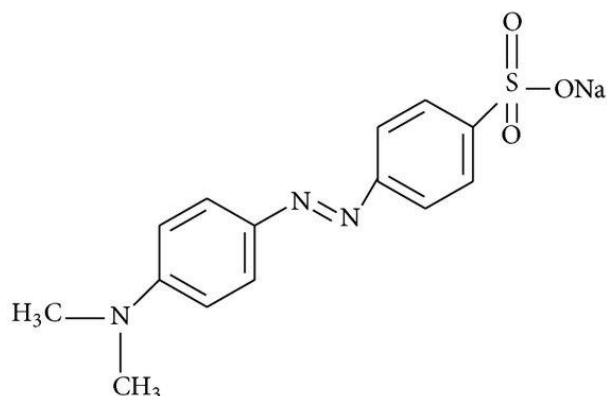


Figure 5.4 Molecular structure of methyl orange

Methyl orange adsorbate was prepared using two types of solvent: water as inorganic solvent (MO-H₂O) and ethanol as organic solvent (MO-EtOH) using procedure as described by Eltaboni et al., 2017. One gram of methyl orange was diluted in 1 liter of the solvent to prepare methyl orange stock solution at a concentration of 1000 mg/L. The methyl orange stock solution was stirred by a magnetic stirrer for 24 h to obtain a clear solution.

5.4.3 Adsorbent preparation

The dried synthetic clay pellet was calcined at 550°C in a muffle furnace (Carbolite) as shown in Figure 5.5. This calcination temperature was used because it could improve the pellet specific surface area as described in previous chapter and the Lewis acidity of the clay surface (Kaur and Kishore, 2012; Bergaya et al., 2006). The heating rate was controlled at 3°C/min and the holding time at 550°C was 3 hr. Pellet was removed from muffle furnace at a temperature lower than 50°C and stored in a desiccator before use.



Figure 5.5 Muffle furnace (Carbolite)

5.4.4 Fixed bed adsorption

Continuous adsorption experiments in a fixed bed column were carried out using a glass column with the diameter of 30 mm and the length of 300 mm. The schematic diagram for the adsorption process is as shown in Figure 5.6. Raschig rings and glass wool were placed at the bottom and the top of the column to control the bed height and prevent the bed from moving. Synthetic clay pellets were packed in the middle of the column. Methyl orange solution of known concentration was pumped to the column at the bottom of the packed bed at the designed flow rate. Samples were collected at regular time intervals from the sampling point, and the concentration of methyl orange in the effluent was determined by UV-VIS spectrometer.

For the pellet adsorption of methyl orange in inorganic or aqueous environment, the MO-H₂O solution, at concentrations of 100, 200, and 300 mg/L was used. The bed height and solution feed flow rate was fixed at 60 mm and 2 mL/min,

respectively. For adsorption in organic or non-aqueous environment, the MO-EtOH solution with methyl orange concentration at 20, 50, and 100 mg/L. The solution feed flow rate in this case was fixed at 1 mL/min, and the bed height was fixed at 60 mm. Adsorption time was fixed at 48 h for both systems. The adsorption data obtained were subjected to fitting by Adams–Bohart, Thomas and Yoon-Nelson adsorption models.

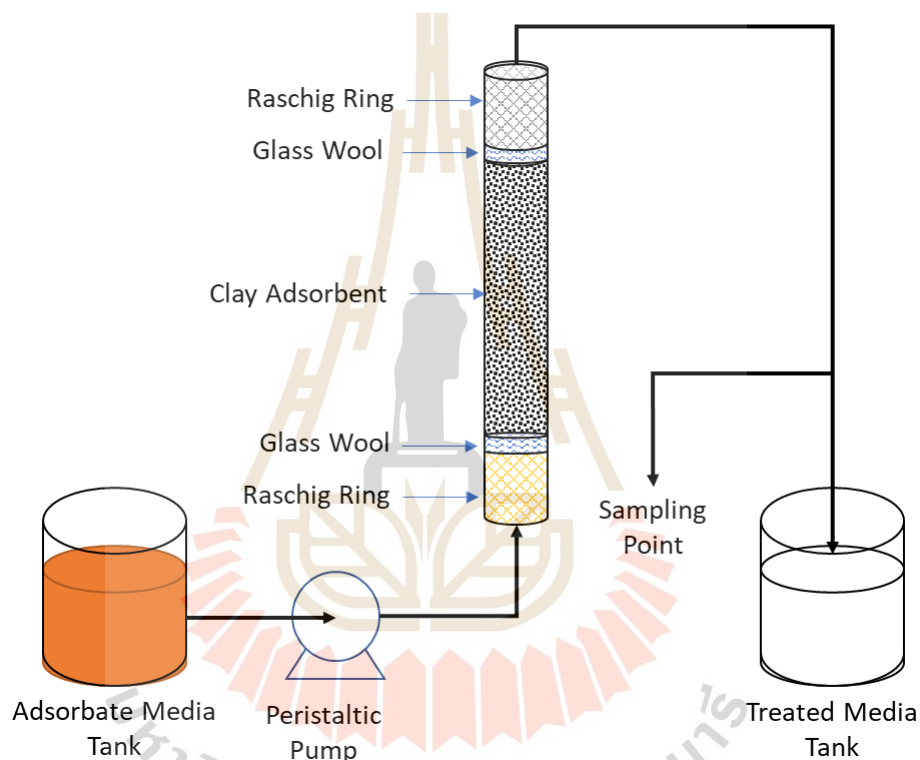


Figure 5.6 Fixed-bed adsorption process diagram adsorption.

5.4.5 Material characterization

The specific surface area and pore size distribution of the synthetic clay adsorbent were analyzed by BET and BJH method using N_2 adsorption isotherm. Methyl orange concentration in the received effluent was analyzed by UV-VIS spectrometer (UV-Vis spectrophotometer, T80), as illustrated in Figure 5.7. The

concentration of methyl orange in an inorganic and organic solvent were analyzed at $\lambda_{\max}=464$ and $\lambda_{\max}=425$ nm, respectively. (Eltaboni et al., 2017).



Figure 5.7 UV-VIS spectrometer (UV-Vis spectrophotometer, T80)

5.5 Result and discussion

5.5.1 Adsorbent characterization

Specific surface area of the adsorbent was 194.75 m²/g, which is the same as that of the pellet received from extrusion and spheronization in Chapter IV. This confirmed that extrusion-spheronization process used in this work was reproducible. The mean pore diameter of the adsorbent was 19.416 nm, which was larger than the molecular size of methyl orange (1.2 nm). Therefore, methyl orange molecules should be able to travel into the adsorbent's pores. Sizes of mesopores in the adsorbent ranged from 2 – 200 nm, as illustrated in Figure 5.8.

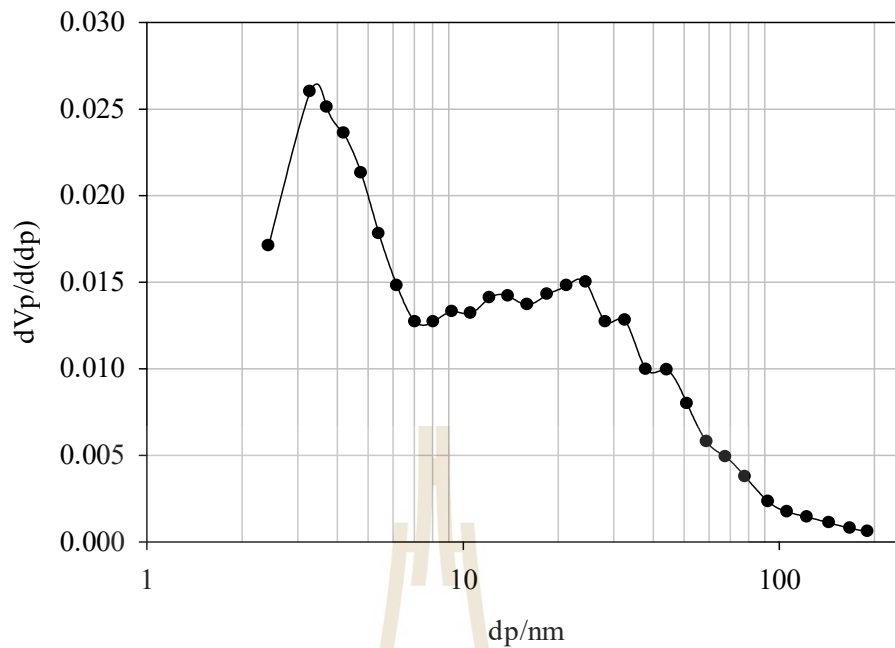


Figure 5.8 Size distribution of adsorbent's mesopores by BJH method

5.5.2 Synthetic clay pellets as adsorbent in fixed-bed adsorption of methyl orange

In order to understand the adsorption behavior of synthetic clay pellet, in a fixed-bed column, which is crucial for industrial process scale up, for industrial applications, three kinetic models, Adams–Bohart, Thomas, and Yoon-Nelson model were used to obtain kinetic model and to estimate breakthrough curves for the adsorption.

5.5.2.1 Adsorption of methyl orange in aqueous environment

Breakthrough curve of methyl orange adsorption from its aqueous solution with synthetic clay adsorbent is shown in Figure 5.9.

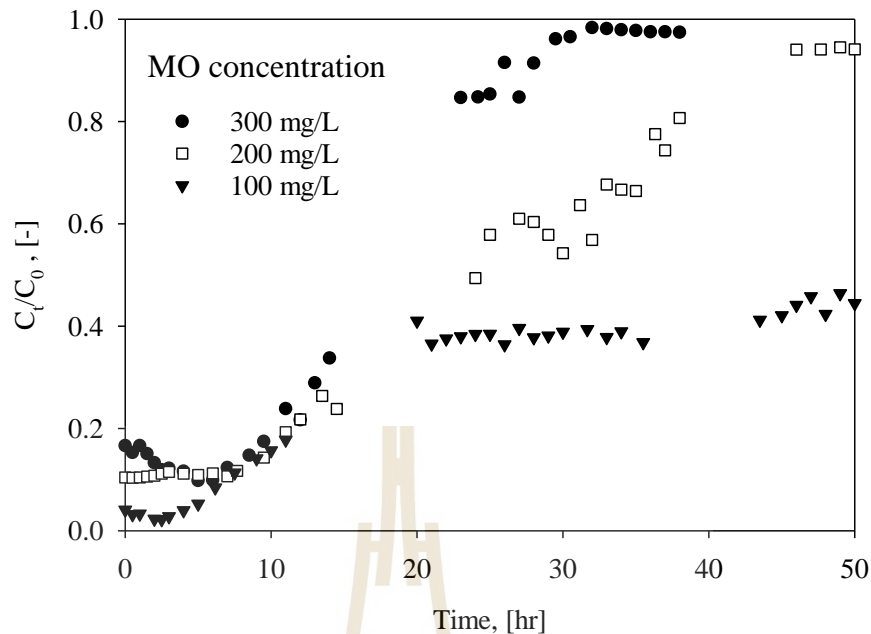


Figure 5.9 Breakthrough curve of methyl orange adsorption in aqueous environment using synthetic clay adsorbent under ambient condition.

It can be seen from the breakthrough curve that the adsorption with initial methyl orange concentration of 200 and 300 mg/L reached to the saturation point ($C_t/C_0 > 0.90$) within the adsorption time. The saturation point for adsorption with initial methyl orange concentration of 100 mg/L, however, was at $C_t/C_0 = 0.5$. The S-shaped breakthrough curve received at methyl orange concentration of 200 and 300 mg/L indicated that the internal and external mass transfer resistances were significant. The steeper breakthrough curve at the higher initial adsorbate concentration was possibly due to higher mass transfer rate resulted from the larger concentration gradient in the system. The adsorbent was, as a consequence, saturated more quickly in such adsorption. Slight decline of the breakthrough curve was observed at the beginning of adsorption, which was probably because of liquid filling the pore of pellets. This effect was decreased upon decreasing initial concentration the adsorbate.

The breakthrough curve of the adsorption with initial adsorbate concentration of 100 mg/L did not seem to follow ideal adsorption behavior so S-shaped breakthrough curve was not attained. The curve was increased slowly after the C/C_0 of 0.4 and was steady at maximum C/C_0 around 0.5. This might be due to failure of the pellet observed during the adsorption caused by clay hydration and pellet swelling, which was found in previous study of adsorption with clay adsorbent (Bergaya et al., 2006). It was hypothesized that clay could re-adsorb water molecule into its interlayer and reform its structure into the one before calcination. The interlayer space of the calcined clay was expanded, resulting in clay swelling. This behavior was commonly found in the smectite clay, such as montmorillonite, saponite, hectorite, beidellite, and nontronite except pyrophyllite and talc. The expansion of clay interlayer led to the increase in pellet adsorption capacity and the adsorbents can be used for longer adsorption time. Therefore, the adsorption capacity was increased. Clay swelling, however, also led to decreasing void space inside the adsorption column. At some point, the liquid was plugged, and flow channeling was observed, as illustrated in Figure 5.10.



Figure 5.10 Flow channeling in adsorption under aqueous environment of methyl orange at its initial concentration of 100 mg/L

Hydration of synthetic clay pellet was also found in adsorption of methyl orange with its initial concentration of 200 and 300 mg/L. As the adsorption time was short due to the high mass transfer rate, this effect in such system was not obvious. The hydration seemed to strongly affect the pellet morphology after complete adsorption. because the spent clay adsorbent could not retain its original shape after being dried. Some pellet were even broken down, as illustrated in Figure 5.11.



Figure 5.11 Spent clay adsorbent from adsorption of methyl orange in aqueous solution.

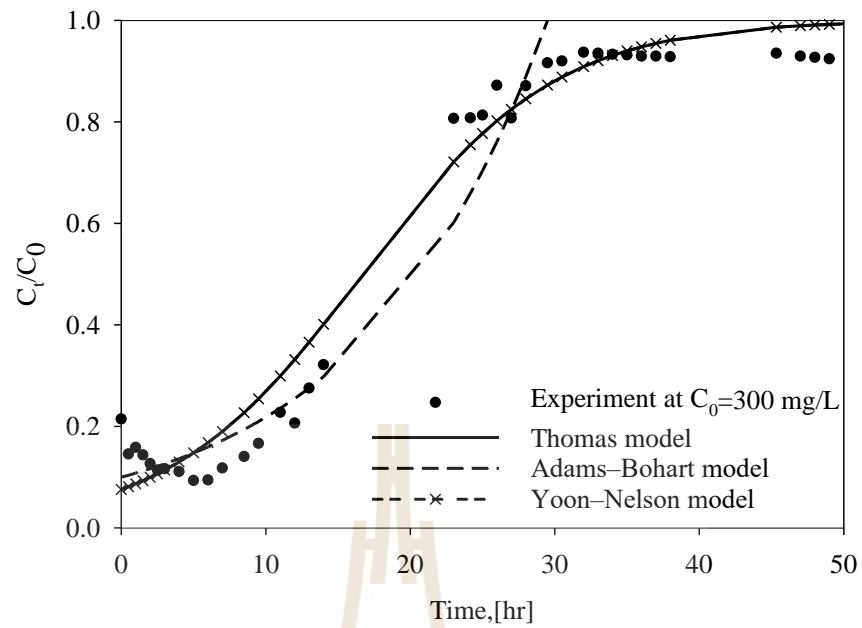
5.5.2.2 Breakthrough model for methyl orange adsorption in aqueous solution

Adams–Bohart, Thomas, and Yoon–Nelson adsorption models were employed to fitting dynamic adsorption parameters, which values are shown in

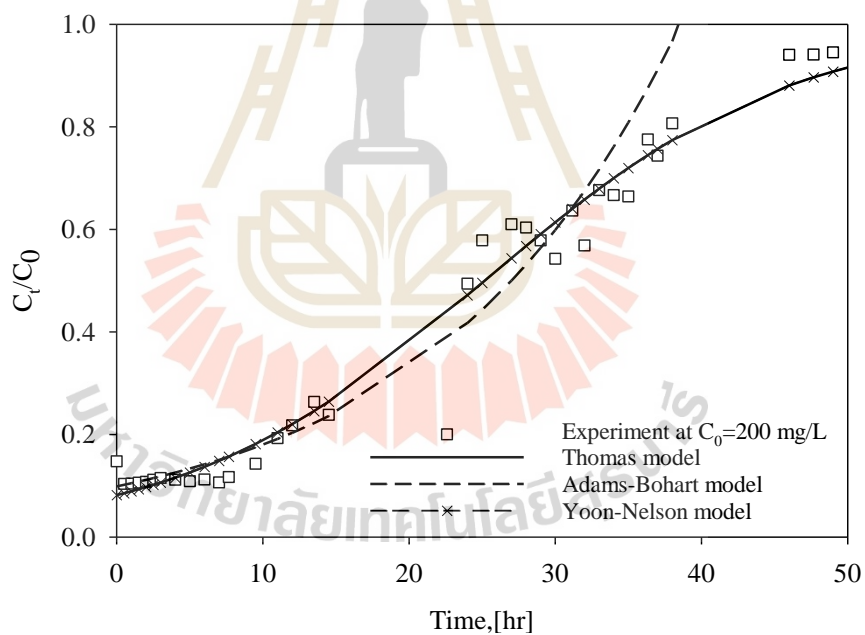
Table 5.1. The simulated breakthrough curve is shown in Figure 5.12. Adsorption with initial concentration of methyl orange of 100 mg/L was excluded from parameter fitting due to the highly swelling effect led abnormality in adsorption behavior.

Table 5.1 Adsorption parameter obtained from Adams–Bohart, Thomas, and Yoon–Nelson models for methyl orange adsorption in aqueous solution.

Thomas model							
F (mg/L)	C ₀ (mg/L)	H (cm)	k _{TH} (mL/min mg)	q _e (mg/g)	R ²	q _{exp} (mg/g)	%SSE
2	300	6	8.333E-03	38.999	0.9013	39.086	0.047
2	200	6	8.000E-03	42.160	0.9649	41.018	0.500
Adams–Bohart model							
F (mg/L)	C ₀ (mg/L)	H (cm)	k _{AM} (mL/min mg)	N ₀ (mg/g)	R ²	q _{exp} (mg/g)	%SSE
2	300	6	4.333E-03	25.050	0.8804	39.086	7.488
2	200	6	5.000E-03	21.817	0.9539	41.018	8.408
Yoon–Nelson model							
F (mg/L)	C ₀ (mg/L)	H (cm)	k _{YN} (mL/min)	τ _{YN} (min)	R ²	q _{exp} (mg/g)	%SSE
2	300	6	2.500E-03	999.840	0.9013	39.086	0.047
2	200	6	1.600E-03	1510.313	0.9649	41.018	0.500



(a)



(b)

Figure 5.12 Experimental and simulated breakthrough curve from Adams–Bohart, Thomas, and Yoon–Nelson models for methyl orange adsorption in aqueous solution with (a) initial adsorbate concentration of 300 mg/L and (b) initial adsorbate concentration of 200 mg/L

The Thomas and Yoon-Nelson appeared to fit well with the experimental data as a high value of R^2 and low value of %SSE were received. Adam-Bohart model did not give good data fitting as seen from high value of %SSE. The mass transfer coefficient obtained from both Thomas and Yoon-Nelson models, indicated that this parameter depended strongly on the initial adsorbate concentration. Opposite relationship, however, was found for the initial adsorbate concentration and equilibrium adsorption capacity, which was decreased significantly with increasing initial adsorbate concentration. This observation was in contrast with the reported general behavior of adsorption (Vahidhabanu et al., 2017; Tsai et al., 2016; Mohammed et al., 2016). As explained above, the effect of calcined clay hydration and swelling in water might have led to increasing adsorption capacities of pellets at low initial adsorbate concentration.

5.5.2.3 Adsorption of methyl orange in non-aqueous environment

Breakthrough curve for methyl orange adsorption using clay adsorbent in non-aqueous solution is shown in Figure 5.13

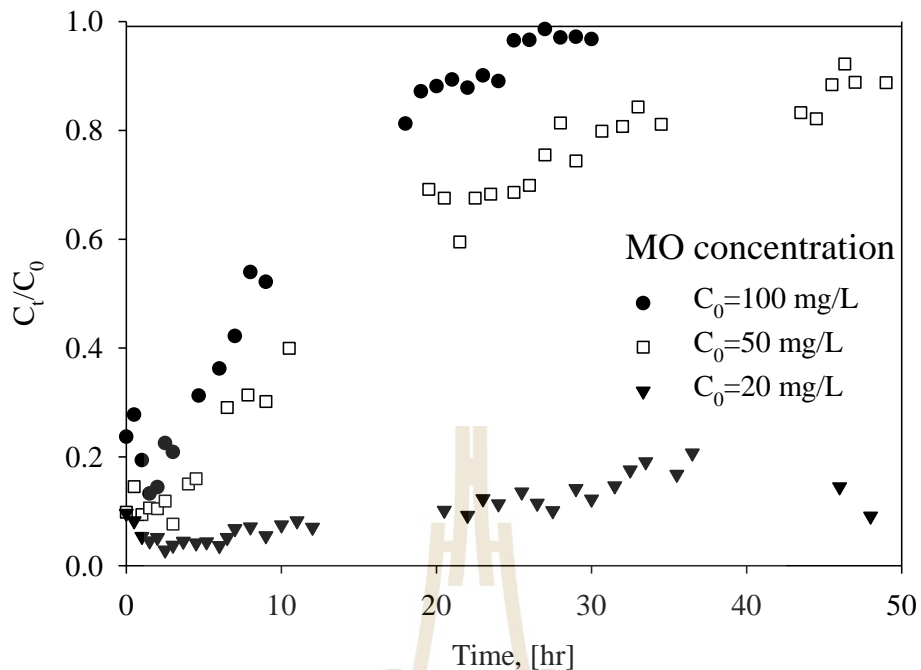


Figure 5.13 Breakthrough curve for methyl orange adsorption using clay adsorbent in non-aqueous solution under ambient condition

The breakthrough curve for methyl orange adsorption in non-aqueous system was in S-shape and appeared to be similar to the process in aqueous solution. Adsorption at high initial adsorbate with higher mass transfer rate than that with lower initial adsorbate concentration. This was likely caused by larger concentration gradient and was evidence by the more steeper mass transfer zone in the breakthrough curve. Due to the low mass transfer caused by low initial adsorbate concentration of 20 mg/L, the breakthrough curve of this adsorption was steady at C/C_0 of 0.2 during the adsorption period used in this study. Effect of pellet hydration and swelling was not observed, so the clay adsorbent in non-aqueous adsorption could retain its original shape after being from the column at the end of the adsorption process, as illustrated in Figure 5.14.



Figure 5.14 Synthetic clay adsorbent in non-aqueous adsorption of methyl orange: (a) in the fixed-bed column, (b) after adsorption.

5.5.2.4 Breakthrough model for methyl orange adsorption in non-aqueous solution

Adsorption parameters for methyl orange adsorption in non-aqueous solution are illustrated in Table 5.2, and the simulated breakthrough curve is shown in Figure 5.15. The initial adsorbate of 20 mg/L was excluded from parameter fitting because the process was not complete.

Table 5.2 Adsorption parameter from Adams–Bohart, Thomas, and Yoon–Nelson models for adsorption of methyl orange in non-aqueous solution.

Thomas model							
F (mg/L)	C ₀ (mg/L)	H (cm)	k _{TH} (mL/min mg)	q _e (mg/g)	R ²	q _{exp} (mg/g)	%SSE
1	50	6	3.000E-02	3.983	0.91	3.820	0.744
1	100	6	2.800E-02	4.154	0.9617	4.030	0.745
Adams–Bohart model							
F (mg/L)	C ₀ (mg/L)	H (cm)	k _{AM} (mL/min mg)	N ₀ (mg/g)	R ²	q _{exp} (mg/g)	%SSE
1	50	6	1.600E-02	2.754	0.7774	3.820	4.858
1	100	6	1.200E-02	3.133	0.8864	4.030	5.399
Yoon–Nelson model							
F (mg/L)	C ₀ (mg/L)	H (cm)	k _{YN} (mL/min)	τ _{YN} (min)	R ²	q _{exp} (mg/g)	%SSE
1	50	6	1.500E-03	1204.333	0.91	3.820	0.744
1	100	6	2.900E-03	547.103	0.9622	4.030	0.201

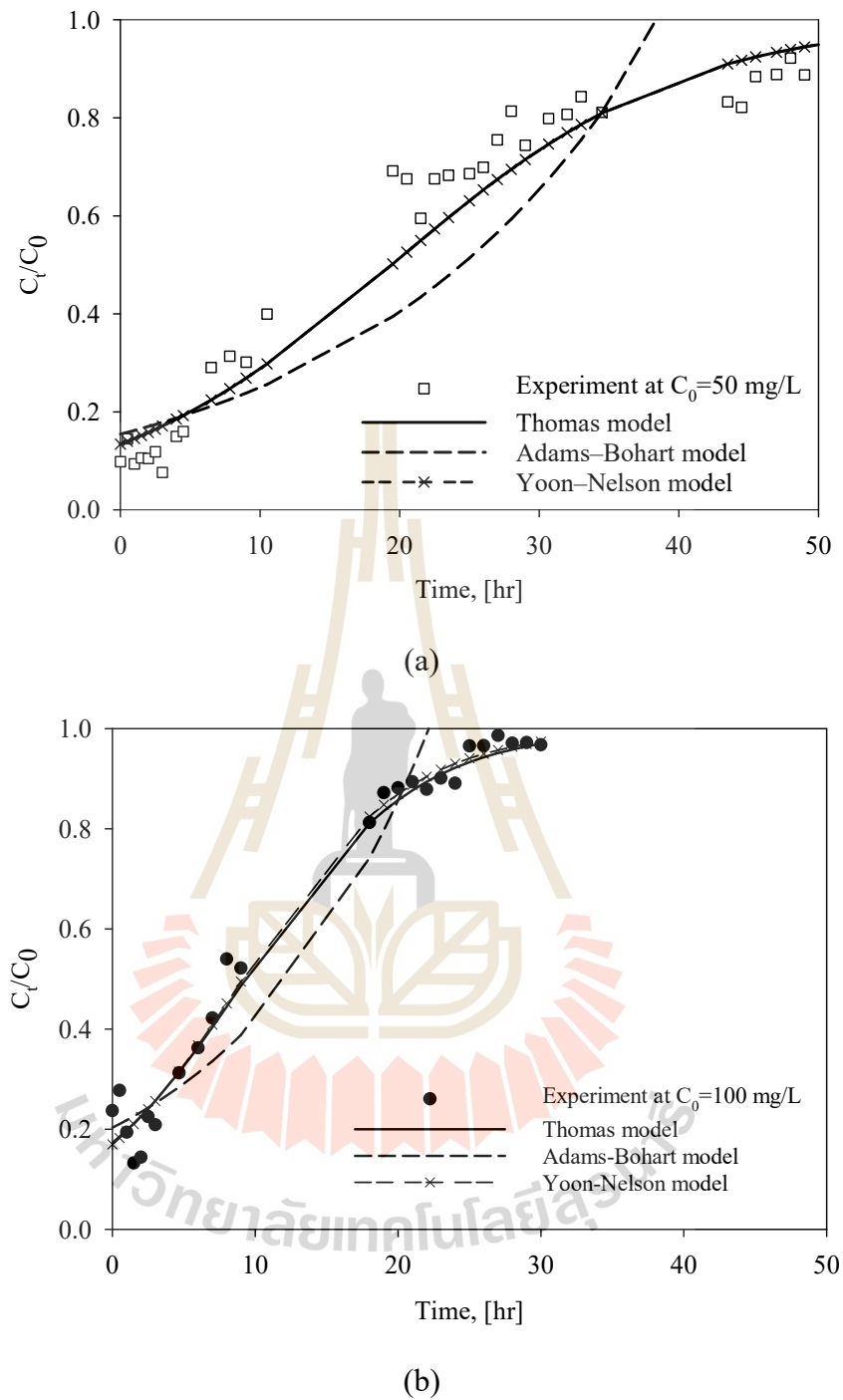


Figure 5.15 Experimental and simulated breakthrough curve from Adams–Bohart, Thomas, and Yoon–Nelson models for methyl orange adsorption in non-aqueous solution (a) initial adsorbate concentration of 100 mg/L and (b) initial adsorbate concentration of 50 mg/L.

Similar to methyl orange adsorption in aqueous solution, Thomas, and Yoon–Nelson showed good fitting with experimental data. The adsorption capacity was increased with the increase in initial adsorbate concentration. This observation confirmed the aforementioned hypothesis that hydration and swelling of clay led to more adsorption capacity of clay adsorbent at low initial adsorbate concentration in non-aqueous solution.

5.6 Conclusion

Consistent properties of spheronized pellets including pellet shape and specific surface area confirmed the reproducibility of pellet preparation by extrusion and spheronization technique. The prepared pellets were used as adsorbent for adsorption of methyl orange in fixed-bed column. Effect of clay hydration and swelling led to caused changes in characteristic of bed packing in the adsorption column, which then led to unpredictable column adsorption characteristics. Also, swelling of pellets led to the decrease in bed porosity, which, in turn, obstructed the liquid flowing through the bed of adsorbent. However, this effect was found to increase the adsorption capacity of anionic approximately 10 times comparing adsorption in organic solvent study. Methyl orange adsorption in non-aqueous solution was successful and without pellet failure. The breakthrough curve obtained from both systems was found to be S-shaped, which indicated ideal adsorption characteristic. Both Thomas and Yoon-Nelson adsorption model was fitted well with the experimental breakthrough curve with R^2 larger than 90% and %SSE lower than 1%.

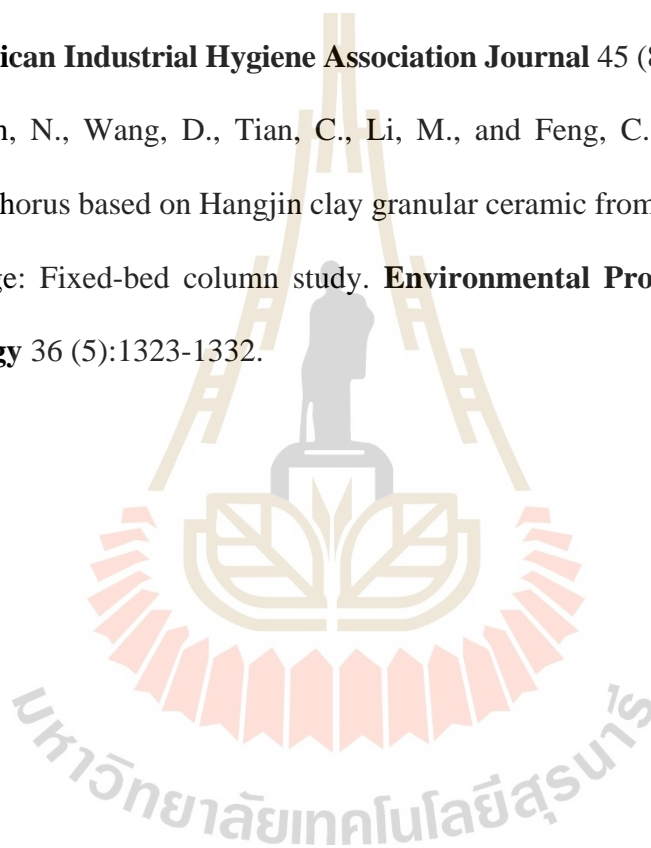
5.7 References

- Adeyemo, A. A., Adeoye, I. O., and Bello, O. S. 2017. Adsorption of dyes using different types of clay: a review. **Applied Water Science** 7 (2):543-568.
- Ahmad, W., Ahmad, I., Ishaq, M., and Ihsan, K. 2017. Adsorptive desulfurization of kerosene and diesel oil by Zn impregnated montmorillonite clay. **Arabian Journal of Chemistry** 10:S3263-S3269.
- Aksu, Z., and Gönen, F. 2004. Biosorption of phenol by immobilized activated sludge in a continuous packed bed: Prediction of breakthrough curves. **Process Biochemistry** 39:599-613.
- Auta, M., and Hameed, B. H. 2014. Chitosan–clay composite as highly effective and low-cost adsorbent for batch and fixed-bed adsorption of methylene blue. **Chemical Engineering Journal** 237:352-361.
- Baral, S. S., Das, N., Ramulu, T. S., Sahoo, S. K., Das, S. N., and Chaudhury, G. R. 2009. Removal of Cr(VI) by thermally activated weed *Salvinia cucullata* in a fixed-bed column. **Journal of Hazardous Materials** 161 (2):1427-1435.
- Bergaya, F., and Lagaly, G. 2013. Chapter 1 - General Introduction: clays, clay minerals, and clay science. **Developments in Clay Science**, edited by Bergaya Faïza and Lagaly Gerhard: Elsevier, 1-19.
- Bergaya, F., Theng, B. K. G., and Lagaly, G. 2006. **Handbook of Clay Science**: Elsevier.
- Bohart, G. S., and Adams, E. Q. 1920. Some aspects of the behavior of charcoal with respect to chlorine. **Journal of the American Chemical Society** 42 (3):523-544.

- Borisover, M., and Davis, J. A. 2015. Adsorption of inorganic and organic solutes by clay minerals. **Natural and Engineered Clay Barriers**, 6:33-70.
- Chowdhury, Z., Abd Hamid, S. B., and Zain, S. 2014. Evaluating design parameters for breakthrough curve analysis and kinetics of fixed bed columns for cu(ii) cations using lignocellulosic wastes. **BioResources** 10(1):732-749.
- Eltaboni, F., Hemdan, S., and Khairallah, F. 2017. Spectral parameters of methyl orange interacted with ethanol-water mixtures. **Global Libyan Journal** 27:1-7 .
- Hensen, E. J. M., and Smit, B. 2002. Why Clays Swell. **The Journal of Physical Chemistry B** 106 (49):12664-12667.
- K. Aziz, B., M. Salh, D., Kaufhold, S., and Bertier, P. 2019. The high efficiency of anionic dye removal using ce-al13/pillared clay from darbandikhan natural clay. **Molecules** 24 (15):2720.
- Kamińska, G. 2018. Removal of organic micropollutants by grainy bentonite-activated carbon adsorbent in a fixed bed column. **Water** 10 (12):1791.
- Kaur, N., and Kishore, D. 2012. Montmorillonite: An efficient, heterogeneous and green catalyst for organic synthesis. **Journal of Chemical and Pharmaceutical Research** 4 (2):991-1015.
- Lima, L. F., de Andrade, J. R., da Silva, M. G. C., and Vieira, M. G. A. 2017. Fixed bed adsorption of benzene, toluene, and xylene (btx) contaminants from monocomponent and multicomponent solutions using a commercial organoclay. **Industrial & Engineering Chemistry Research** 56 (21):6326-6336.

- Malkoc, E., and Nuhoglu, Y. 2006. Removal of Ni(II) ions from aqueous solutions using waste of tea factory: Adsorption on a fixed-bed column. **Journal of Hazardous Materials** 135 (1):328-336.
- Mohammed, N., Grishkewich, N., Waeijen, H. A., Berry, R. M., and Tam, K. C. 2016. Continuous flow adsorption of methylene blue by cellulose nanocrystal-alginate hydrogel beads in fixed bed columns. **Carbohydrate Polymers** 136:1194-1202.
- Pereira, F. A. R., Sousa, K. S., Cavalcanti, G. R. S., França, D. B., Queiroga, L. N. F., Santos, I. M. G., Fonseca, M. G., and Jaber, M. 2017. Green biosorbents based on chitosan-montmorillonite beads for anionic dye removal. **Journal of Environmental Chemical Engineering** 5 (4):3309-3318.
- Thomas, H. C. 1948. Chromatography: a problem in kinetics. **Annals of the New York Academy of Sciences** 49 (2):161-182.
- Tsai, W.-C., de Luna, M. D. G., Bermillo-Arriescado, H. L. P., Futralan, C. M., Colades, J. I., and Wan, M.-W. 2016. Competitive fixed-bed adsorption of pb(ii), cu(ii), and ni(ii) from aqueous solution using chitosan-coated bentonite. **International Journal of Polymer Science** 2016:1-11.
- Uddin, M. K. 2017. A review on the adsorption of heavy metals by clay minerals, with special focus on the past decade. **Chemical Engineering Journal** 308:438-462.
- Vahidhabanu, S., Karuppasamy, D., Adeogun, A. I., and Babu, B. R. 2017. Impregnation of zinc oxide modified clay over alginate beads: a novel material for the effective removal of congo red from wastewater. **RSC Advances** 7(10):5669-5678.

- Vijayanandan, A., Philip, L., and Bhallamudi, S. M. 2018. Analysis of breakthrough behaviors of hydrophilic and hydrophobic pharmaceuticals in a novel clay composite adsorbent column in the presence and absence of biofilm. **Industrial & Engineering Chemistry Research** 57 (27):8978-8988.
- Yoon, Y. H., and Nelson, J. H. 1984. Application of gas adsorption kinetics — ii. A theoretical model for respirator cartridge service life and its practical applications. **American Industrial Hygiene Association Journal** 45 (8):517-524.
- Yu, Y., Chen, N., Wang, D., Tian, C., Li, M., and Feng, C. 2017. Adsorption of phosphorus based on Hangjin clay granular ceramic from aqueous solution and sewage: Fixed-bed column study. **Environmental Progress & Sustainable Energy** 36 (5):1323-1332.



CHAPTER VI

CONCLUSIONS AND RECOMMENDATIONS

6.1 Conclusion

This research intended to investigate and apply powder forming technique in production of millimeter-sized spherical pellets, which might fill the gap in utilization of synthesis powder on an industrial scale. Synthetic clay is an interesting material with unique properties. Nevertheless, it also has some properties such as liquid migration, slip, and sticky surface that can make forming process difficult and result in low quality pellets received. Several pellet shapes have been used on an industrial scale, but the spherical one is generally preferred even though it is quite complicated to prepare. Based on a detailed study on formation of clay pellet by extrusion and spheronization technique, spherical synthetic clay pellet was successfully prepared with knowledges and findings summarized as follows.

- 1) Initial powder shape was a significant factor in liquid migration. Pellet with more uniform size and narrow size distribution prepared by spray drying show low effect of liquid migration in comparison with the pellet prepared with the powder prepared by integrated oven drying and ball milling. This could be due to the effect of pore space between the agglomerated particle happened in each technique. Powder with narrower size distribution appeared to give lower pore space than powder with broader size distribution.

2) Spray drying technique was found to give powder with a higher specific surface area integrated oven drying and ball milling.

3) Paste preparation was the important step to prepare a good quality pellet. Extrusion using the paste at its plastic limit tended to be readily successful and give extrudate with homogeneous moisture content, shape and surface. Simple cone penetration method was successfully used to identify plastic limit of the paste.

4) Paste preparation parameter was found to highly affect to paste preparation at its plastic limit point. Under the range of parameter studied in this research, for the same mixing time, the paste plasticity was found to increase with increasing powder loading and ratio of liquid to dried powder. Increasing of mixing time and ratio of liquid to dried powder loading at constant powder loading also seemed to improve the paste plasticity. In paste preparation with constant ratio of liquid to dried powder, increasing mixing time and powder loading tended to give the paste with plasticity. Using too long mixing time, however, appeared to cause moisture loss from the paste and semi-solid paste was received.

5) Variation in ambient humidity, which was uncontrollable in this study, seemed to affect the phase morphology, even when the paste was prepared under the same condition. The affected morphology noticeably influenced the paste extrusion. To lessen this problem, paste kneading was applied before extrusion. The kneading appeared to facilitate the paste extrusion without significantly change the paste moisture content.

6) In extrusion, the extrusion velocity should be high enough to avoid liquid migration and low enough to allow well particle packing of the extrudate. Based on the ram extrusion type, low extrusion velocity led liquid migration. Steady-state

extrusion profile occurred at the extrusion velocity higher than liquid migration velocity. In the presence of wall slip, however, high extrusion velocity did not seem to improve particle packing of the received extrudate.

7) The key success factors in preparation of spherical synthetic clay pellets using extrusion and spheronization technique was came from by two important steps: extrudate cutting, and hot spheronizing bowl. The clay paste appeared to be quite sticky, so without prior cutting, the extrudate did not break up well when it was spheronized. This situation led to formation to large pellet lump as the pellet adhered to each other and, also, to the wall of spheronizing bowl. To solve this problem, the bowl wall was heated to keep it at high enough temperature to cause liquid evaporation and prevent sticking of the extrudate pellet to the bowl wall and to each other. Too high wall temperature, however, could lead to too pellet drying during spheronization, which, in turn, led to narrow range of operational spherionization parameters.

8) Based on the studies ranges of spheronization parameter, circularity of the pellet was found to increase with increasing spheronization speed (SS) and spheronization time (ST), and, in contrast, decrease with increasing extrudate loading (EL). However, very high spheronization speed and spheronization time and low extrudate loading yielded in quick pellet drying that resisted shape formation resulting in the formation of spheronized pellet with low circularity and crushing strength.

9) Preparation of spherical synthetic clay pellets by extrusion and spheronization techniques did not significantly hinder the pellet specific surface area in comparison with that of the powder calcined at the same temperature. However, extrusion and spheronization technique did not seem to significantly improve the pellet crushing strength as effect of nanoporous of nano material.

10) Performance of the pellets forming by extrusion and spheronization was tested by using them as adsorbent in liquid fixed-bed adsorption column. Hydration of calcinated clay structure and clay swelling was observed. Upon swelling of the pellet, porosity of the bed was changed and, eventually, led to pellet failure in adsorption of methyl orange in aqueous solution. The spheronized pellet was successfully used as adsorbent for adsorption of methyl orange in non-aqueous solution, where the adsorption capacity was about ten times lower than its capacity observed in adsorption in aqueous solution.

6.2 Recommendation for future work

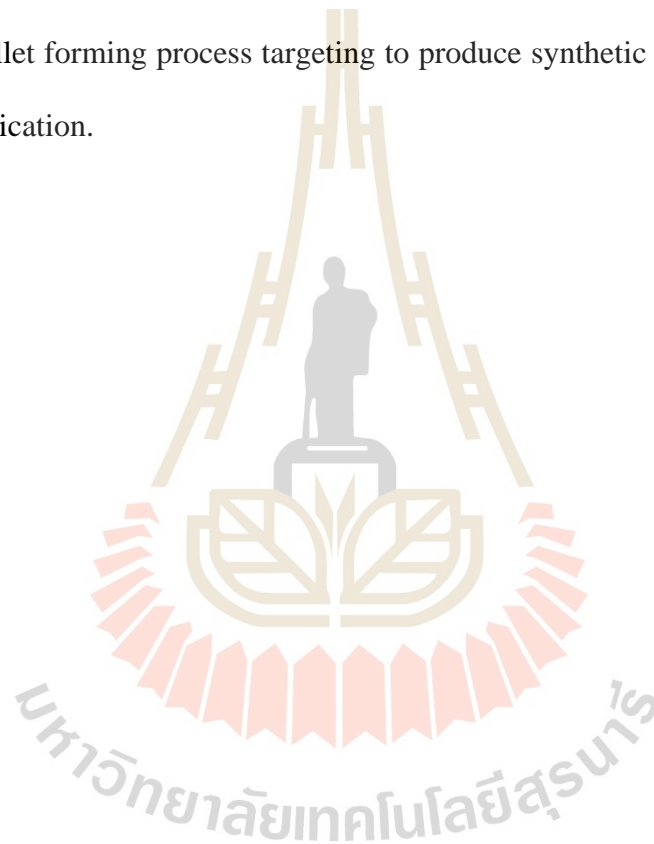
Pellet forming process by extrusion and spheronization is complex as it operates with materials of different phases: solid and liquid. Following issues, therefore, should be considered in future study.

1) Crystal size of the primary synthetic clay appeared to be the most influential factor in properties, such as specific surface area, of the clay powder to be extruded. It was found in this study that the small clay crystal size would lead to final pellet with high porosity and, as a result, lower pellet strength. It was difficult to improve the pellet strength by alternating parameters in pellet forming under this circumstance. Therefore, investigation on how clay forming performed when different primary crystal sizes will give more information about how the pellet strength as well as other properties can be improved.

2) Sizes of agglomerated powder was also found to impact the operation of pellet forming. Studying about effect of mean size distribution of agglomerated powder

on performance of pellet forming will give more technical data that will facilitate the forming process in the future.

3) It was hypothesized in this study that reconstruction of clay structure and clay swelling were the cause of the pellet failure during its utilization as adsorbent for methyl orange adsorption in aqueous solution. Treating process or application of chemical additives that could help decreasing or eliminating this problem will be very useful for pellet forming process targeting to produce synthetic clay pellet with broad range of application.





APPENDIX

LIST OF PUBLICATIONS

มหาวิทยาลัยเทคโนโลยีสุรนารี

LIST OF PUBLICATIONS

International Publications

Julklang, W., Wangriya, A., and Golman, B. 2017. Fabrication of layered double hydroxide microspheres by spray drying of nanoparticles: Effects of process conditions. **Materials Letters** 209 (Supplement C):429-432.

List of Proceedings

W.Julklang, B.Golman, A.Wangriya, and P.Rattanaphanee, Synthetic clay spherical pellet formed by extrusion-spheronization : Effect of spheronization parameter on pellet physical properties, **The 1st Thailand Biorefinery Conference**, July 25-26, 2019: Nakhon Ratchasima, Thailand.

B.Golman, A.Wangriya and W.Julklang, Spray-drying of a Layered Double Hydroxide Nanosuspension, **8th World Congress on Particle Technology**, April 22-26 , 2018: Orlando, USA.

W.Julklang, B.Golman, A.Wangriya, K.Chawong, B.Daengpradab, S.Hasin, and P.Rattanaphanee, Characterization of synthetic clay paste preparation in extrusion process by a modified cone penetration method, **RSCE2017**, November 15-16, 2017: Semarang, Indonesia.

BIOGRAPHY

Mr. Wittaya Julklang was born on September 11, 1985 in Nakhon Ratchasima Province, Thailand. He received his bachelor's degree in Chemical Engineering from Suranaree University of Technology (SUT) in 2010. After graduation, he has been employed under the position of Production Supervisor by Nan Yang Knitting Factory Co., Ltd. He also worked as a Research Assistant under the supervision of Prof. Dr. Chaiyot Tangsathitkulchai at the School of Chemical Engineering, Institute of Engineering, SUT, for one year. He continued with a master's degree at School of Chemical Engineering, at SUT with thesis topic of analysis of slurry drying mechanism in industrial spray dryer for production of high-value particles He received his Master of Engineering in Chemical Engineering.



มหาวิทยาลัยเทคโนโลยีสุรนารี